UNIVERSITEIT VAN PRETORIA
UNIVERSITY OF PRETORIA
YUNIBESITHI YA PRETORIA

FRACTURE IN HIGH PERFORMANCE FIBRE REINFORCED CONCRETE PAVEMENT MATERIALS

ERIK DENNEMAN

A thesis submitted in partial fulfilment of the requirements for the degree of

PHILOSOPHIAE DOCTOR (ENGINEERING)

In the

FACULTY OF ENGINEERING

UNIVERSITY OF PRETORIA

May 2011

UNIVERSITEIT VAN PRETORIA
UNIVERSITY OF PRETORIA
YUNIBESITHI YA PRETORIA

THESIS SUMMARY

FRACTURE IN HIGH PERFORMANCE FIBRE REINFORCED CONCRETE PAVEMENT MATERIALS

ERIK DENNEMAN

Supervisor: Professor Doctor E.P. Kearsley

Co-Supervisor: Professor Doctor A.T. Visser

Department: Civil Engineering

University: University of Pretoria

Degree: Philosophiae Doctor (Engineering)

An innovative pavement system known as Ultra Thin Continuously Reinforced Concrete Pavement (UTCRCP) was recently developed in South Africa. The technology is currently being implemented on some major routes in the country. The system consists of a high performance fibre reinforced concrete pavement slab with a nominal thickness of approximately 50 mm. The material has a significant post crack stress capacity compared to plain concrete. Current design methods for UTCRCP are based on conventional linear elastic concrete pavement design methodology, which does not take into account post crack behaviour. Questions can be raised with regards to the suitability of conventional approaches for the design of this high performance material.

The hypothesis of the study is that the accuracy of design models for UTCRCP can benefit from the adoption of fracture mechanics concepts.

The experimental framework for this study includes fracture experiments under both monotonic and cyclic loading, on specimens of different sizes and geometries and produced from several mix designs. The aim is to quantify size effect in the high performance fibre

reinforced concrete material, to determine fracture mechanics material parameters from monotonic tests, and to investigate the fatigue behaviour of the material.

As part of the study a method is developed to obtain the full work of fracture from three point bending tests by means of extrapolation of the load-displacement tail. This allows the specific fracture energy (G_f) of the material to be determined. An adjusted tensile splitting test method is developed to determine the tensile strength (f_t) of the material.

The values of G_f and f_t are used in the definition of a fracture mechanics based cohesive softening function. The final shape of the softening function combines a crack tip singularity with an exponential tail. The cohesive crack model is implemented in finite element methods to numerically simulate the fracture behaviour observed in the experiments. The numerical simulation provides reliable results for the different mixes, specimen sizes and geometries and predicts the size effect to occur.

Fracture mechanics based models for the prediction of the fatigue performance of the material are proposed. The predictive performance of the models is compared against a model representing the conventional design approach.

It is concluded that the findings of the study support the thesis that design methods for UTCRCP can benefit from the adoption of fracture mechanics concepts. This conclusion is mainly based on the following findings from the study:

- The high performance fibre reinforced concrete material was found to be subject to significant size effect. As a consequence the MOR parameter will not yield reliable predictions of the flexural capacity of full size pavement structures,
- In contrast to the MOR parameter, the fracture mechanics damage models developed as part of this study do provide reliable predictions of the flexural behaviour of the material,
- The fatigue model developed based on fracture mechanics concepts, though not necessarily more precise, is more accurate.

ACKNOWLEDGEMENTS

The author gratefully acknowledges the financial support provided by CSIR and the University of Pretoria (UP), which made this thesis work possible. The author further wishes to thank all those who have contributed to this study, in particular:

- Mr. Derek Mostert of UP for the mix designs and the preparation of specimens tested as part of this study,
- Mr. Derek Mostert, Mr. Herman Booysen and Mr. Johan Scholtz for the production of test fixtures and the execution of the tests on fibre reinforced concrete at UP,
- Dr. Rongzong Wu of the University of California at Davis (UC Davis) for the mentoring provided on the use of the OpenSees finite element software and on the embedded discontinuity method implemented in that software by Dr. Wu,
- Mr. Bill Sluis and Mr. Daret Kehlet, for the support provided during the mix production and testing performed at UC Davis,
- Mr. Benoit Verhaeghe (CSIR), Prof. Wynand Steyn (formerly CSIR) and Prof. John Harvey (UC Davis), for creating a work environment that allowed the author to complete the bulk of the thesis work during office hours,
- Dr. James Maina (CSIR) who acted as a mentor for this study,
- Prof. Elsabe Kearsley and Prof. Alex Visser, for the advice, guidance and valuable input provided to this document and the papers published as part of the study.

TABLE OF CONTENTS

LIST OF FIGURES

LIST OF TABLES

NOMENCLATURE

Abbreviations:

C&CI	South African Cement and Concrete Institute
CMOD	Crack Mouth Opening Displacement
CTOD	Crack Tip Opening Displacement
$CTOD_c$	Critical Crack Tip Opening Displacement
EDM	Embedded Discontinuity Method
FCM	Fictitious Crack Model
FEM	Finite Element Method
FPB	Four Point Bending
FPZ	Fracture Process zone
FRC	Fibre Reinforced Concrete
HVS	Heavy Vehicle Simulator
LE	Linear Elastic
LEFM	Linear Elastic Fracture Mechanics
LVDT	Linear Variable Displacement Transducer
MOR	Modulus of Rupture
SANRAL	South African National Road Agency Limited
SDA	Strong Discontinuity Approach
TPB	Three Point Bending
UTCRCP	Ultra Thin Continuously Reinforced Concrete Pavement
UC Davis	University of California at Davis
UP	University of Pretoria

Symbols:

γ	Specific surface energy	[N/mm]
δ	Deflection	[mm]
ε^f	Fracture strain	
ν	Poisson's ratio	
σ	Stress	[MPa]
σ_1	Major principal stress	[MPa]
σ_I	Stress at base of crack tip singularity	[MPa]
σ_f	Stress at fracture	[MPa]
σ_d	Design value of tensile stress	[MPa]
σ_N	Nominal stress	[MPa]
σ_{Nu}	Ultimate nominal stress	[MPa]
σ_{xx}	Horizontal normal stress	[MPa]
μ	Shear modulus	[MPa]
a	Notch depth or crack length	[mm]
a_1	Calibration constant	
a_2	Distance to corner of slab	[mm]
a_c	Critical crack length	[mm]
a_e	Equivalent effective elastic crack length	[mm]
b	Specimen width	[mm]
b_1	Calibration constant	
f_t	Tensile strength	[MPa]

h	Specimen height or slab thickness	[mm]
h_c	Width of fracture zone	[mm]
k	Subgrade stiffness	[N/mm]
l	Radius of relative stiffness	[mm]
m	Calibration constant	
l_c	Characteristic length	[mm]
n_i	Number of load cycles applied at stress level S_i	
s	Span	[mm]
w	Crack width	[mm]
w_1	Critical crack width	[mm]
w_I	Crack width at base crack tip singularity	[mm]
E	Young's modulus	[MPa]
C	Paris's constant	
E'	Effective Young's modulus in plain strain condition	[MPa]
E_t	Tangent modulus	[MPa]
G_f	Specific fracture energy	[N/m]
I	Moment of inertia	[mm^4]
K	Bulk modulus	[MPa]
K_I	Crack tip stress intensity	[MPa mm$^{1/2}$]
K_{Ic}	Critical crack tip stress intensity	[MPa mm$^{1/2}$]
N	Number of load cycles	
N_i	Number of cycles at stress level S_i	
P	Total of external loads	[N]
P_u	Peak load	[N]
S	Stress level	[MPa]
S_1	Surface energy	[N m]
U^*	Strain energy	[MPa]
W_f	Work of fracture	[N mm]

Entia non sunt multiplicanda praeter necessitate

"Entities must not be multiplied beyond necessity".

William of Ockham
(c. 1288 - c. 1348)

1 Introduction

1 INTRODUCTION

The object of pavement engineering is to design complex pavement structures based on as few assumptions as possible, while eliminating complexities that make little difference to the reliability of the performance prediction. It is vital that the simplifications in the design models are based on a sound understanding of the key mechanisms at play in the pavement system. With time, design models will be replaced by new simplifications that better reflect reality. Also, as innovative pavement solutions are introduced, the suitability of existing models for the design of these solutions needs to be verified.

In this introductory chapter questions are raised regarding the applicability of conventional concrete pavement design approaches to an innovative pavement system developed in South Africa. The high performance fibre reinforced concrete material used in the novel pavement system is known to behave distinctly different in fracture than plain concrete. A need exists to assess the validity of the assumptions in terms of the material behaviour underlying the conventional design methods, for application to this high performance material.

1.1 Background

South Africa boasts an extensive and mature road network. At present, the bulk of pavement design activities in the country are aimed at preserving and upgrading the existing road

infrastructure. Innovative methods of pavement rehabilitation are required to increase the service life of wearing courses and to reduce the need for traffic hampering maintenance activities. To this aim, the South African National Road Agency Limited (SANRAL) has sponsored the development of the so-called Ultra Thin Continuously Reinforced Concrete Pavement (UTCRCP). UTCRCP is intended as an overlay strategy for existing roads. The technology comprises a high performance concrete layer with a nominal thickness of approximately 50 mm. The material incorporates fibres as well as mesh reinforcement and is characterised by its ability to withstand high deflections. The technology is discussed in more detail as part of Chapter 2. During the course of this study the UTCRCP technology progressed from the development phase to the implementation phase. The methodology is now being applied as part of major highway rehabilitation projects in South Africa. The design tools for the innovative UTCRCP system are currently based on conventional concrete pavement design methodologies.

The conventional Mechanistic-Empirical approach to concrete pavement design for fatigue makes use of Linear Elastic (LE) analysis. Both the stress in the pavement slab and the material strength are obtained assuming LE material behaviour. Non-linear, non-elastic post fracture behaviour is not taken into consideration. In these models the material strength is characterised by the Modulus of Rupture (MOR) obtained in monotonic Four Point Bending (FPB) test on beam specimens. The MOR is the stress in the extreme fibre of the specimen, calculated under the assumption of a LE stress distribution at the peak load condition. The ratio between the MOR and the stress in the pavement calculated through LE analysis, is used to predict the fatigue life of the pavement. Researchers have long established that flexural strength for concrete is not a true material property, because its value changes with specimen size (Reagel and Willis, 1931, Kellerman, 1932). The size effect phenomenon is caused by the fact that concrete is a quasi brittle material and at the peak load condition cracks will already have formed in the material. Due to the presence of a crack, the assumed LE stress distribution no longer exists in the beam. In different sizes of specimens, different amounts of energy are released into the crack front, giving rise to the observed size effect. Similarly, a LE stress distribution will not be present in a pavement slab loaded to failure, because it too will have cracked. Size effect in plain concrete has been well documented and can be predicted using fracture mechanics (Bažant and Planas, 1997). Notwithstanding these limitations, LE analysis remains the basis for fatigue prediction in state of the art concrete pavement design methods.

Studies at the University of Pretoria have shown the high performance fibre reinforced concrete material used in UTCRCP to have significantly increased post crack load carrying capacity when compared to plain concrete (Kearsley and Elsaigh, 2003, Elsaigh, 2007). The limitations of linear elastic design assumptions are expected to be magnified when applied to this material, due to its significant post crack stress capacity. The MOR only provides an indication of the peak load capacity of the material, it does not describe the post peak behaviour. The extent to which this impacts on the accuracy and precision of the design models requires investigation. It may also be possible to improve the predictive performance of the fatigue models through the use of size independent, fracture mechanics based approaches.

1.2 Problem statement

Current design methods for Ultra Thin Continuously Reinforced Concrete Pavements (UTCRCP) are based on conventional concrete pavement design theory. However, the fracture behaviour of the high performance fibre reinforced concrete material used in the UTCRCP technology is characterized by a significant post crack stress capacity. A need exists to determine to what extent assumptions with regards to material behaviour, underlying conventional design approaches, are applicable to this high performance material.

Fracture mechanics approaches can be used to simulate the post crack behaviour of both plain and fibre reinforced concrete. An investigation into the possible improvement of the predictive performance of the design methods for UTCRCP through the use of fracture mechanics concepts is required.

A prerequisite for the adoption of fracture mechanics based design approaches by the industry, would be the availability of practical and robust test methods for the determination of the relevant material parameters. The accuracy and precision of fracture mechanics based design models will have to be compared against the results obtained from conventional design methodology.

1.3 Objectives

The study takes a stepwise approach to the problem defined in the previous section. The first objective of the study is to quantify the size effect in the high performance fibre reinforced concrete material used for UTCRCP. The magnitude of the size effect will provide an indication of the suitability of linear elastically derived parameters in the design of UTCRCP.

The second objective is to determine the fracture properties of the material required for the numerical simulation of cracking in the material using a fracture mechanics model. The properties are to be used in fracture mechanics based numerical simulation of the experiments. The aim is to use existing, or develop new test methods that can readily be used by industry on a routine basis.

The final objective is to develop fatigue prediction models based on fracture mechanics concepts. The predictive performance of these models will be compared to the performance of predictive equations calibrated using the conventional design approach.

1.4 Thesis statement

The premise of this study is that current design methods do not include models that accurately describe the mechanisms of fracture damage formation in the UTCRCP material. The main hypothesis of this study is that:

The accuracy of design models for UTCRCP can benefit from the adoption of fracture mechanics concepts.

To build a case to validate or reject the main hypothesis, a set of hypothetical propositions will be tested in this work. These propositions represent the reasoning leading up to the main research hypothesis. These propositions are:

1. *The high performance fibre reinforced concrete material will exhibit a strong size effect due to its high post crack stress capacity. The size effect will limit the reliability of the Modulus of Rupture (MOR) obtained for a specific specimen size and geometry, as a predictor of the peak load of elements of a different size and or geometry.*

2. *In contrast to the MOR, fracture mechanics material parameters can be used to accurately and precisely, predict the peak load and importantly, the post-peak flexural behaviour of elements of a different size and geometry.,*
3. *The accuracy, and possibly the precision, of fatigue prediction models for the material can be improved through the use of fracture mechanics concepts.*

The work in this thesis is aimed at empirically testing each of these propositions and by doing so evaluating the main hypothesis.

1.5 Scope of the work

The scope of the study covers the experimental and numerical simulation work required to test the hypotheses formulated in the previous section. The work will include:

a) A literature survey on the state of the art in the design concrete pavements. The theoretical framework will also cover fracture mechanics theory and practice with regards to concrete,
b) Experiments to determine the fracture mechanics properties of several concrete mixes under monotonic loading using specimens of various geometries and for mix designs prepared with different steel fibre contents,
c) Numerical simulation of the monotonic experimental results using non-linear fracture mechanics,
d) Experiments to determine the fatigue performance of various concrete materials, under cyclic loading and tested in various geometries and at different steel fibre contents,
e) The development of a, fracture mechanics based, predictive model for the fatigue response observed in the experiments. This process will include the comparison of the precision and accuracy of this model against a model akin to conventional concrete design methodology.

The following topics will not be covered in this study:

a) The development of solid mechanics approach that allows for the accumulation of fatigue damage under dynamic loading and can completely replace Miner's linear cumulative damage hypothesis,
b) The calibration of fatigue damage models based on full scale field tests,
c) The evaluation of the predictive performance of existing design methods for UTCRCP.

1.6 Limitations

The experimental work in this thesis is limited to laboratory scale specimens. The assumption is that if the fracture mechanics based design methodologies outperform the conventional type damage models in terms of precision and accuracy with regards to the prediction of behaviour of laboratory specimens of different sizes and geometries, they will also outperform the conventional model for the prediction of fatigue in full size pavement structures.

1.7 Contribution to the state of knowledge

The present study will contribute to the state of knowledge in the following fields:

- Test methods to determine fracture mechanics properties of concrete are well developed. Many of these require advanced equipment. There is a need to develop test methods that can easily be implemented as part of pavement design practice. In addition to this, the test methods need to be adjusted to suit Fibre Reinforced Concrete (FRC). Key methodologies developed as part of the study are an adjusted tensile splitting tests to obtain an accurate measure of the true tensile strength (f_t) of FRC, and a methodology to determine the specific fracture energy (G_f) from flexural tests on beam specimens.
- The MOR of concrete is known to be subject to size-effect, this has been well documented by various researchers. Few studies have been done on the magnitude of the size-effect in fibre reinforced material. For this reason a study of size-effect in the UTCRCP material will contribute to the state of knowledge,

- The suitability of the MOR as a material parameter for use in the design of UTCRCP will be assessed, which is of importance for design practise,
- The development of a suitable fracture mechanics damage model, which can be used to reliably predict the flexural behaviour of UTCRCP under monotonic loading,
- The development of a fatigue prediction model for the high performance fibre reinforced concrete material based on fracture mechanics concepts, and
- As the literature survey in Chapter 2 will indicate, there is a relative limited amount of publications on fatigue behaviour of high performance fibre reinforced concrete. Fatigue tests on the UTCRCP material will therefore expand the available body of knowledge.

1.8 Thesis structure

This introductory chapter is followed by a discussion on the state of knowledge relevant to this study, in Chapter 2. The theoretical framework comprises a description of the UTCRCP technology, the mechanisms of fatigue damage, the state of the art in concrete pavement design and available fracture mechanics approaches.

The research methodology employed to test the hypotheses of the study is discussed in Chapter 3. The selection and development of test methods is also discussed in this chapter, as are the test matrix and the concrete mix designs. The methods used for the numerical simulation of fracture in the study are also introduced.

The results of the experiments and the analysis of the data are presented in Chapter 4. Size effect observations are discussed, as are the methods applied to obtain the fracture parameters for the material from the test data. Finally, the results of tests performed under monotonic loading conditions are compared to the results from cyclic loading (fatigue) tests.

Chapter 5 discusses the development of numerical models. Numerical simulation of the tests under monotonic loading is performed using two different fracture mechanics techniques. Models for fatigue prediction using a fracture mechanics based approaches are also developed in this chapter. The performance of these models is compared to the performance of a calibrated model of the type used in conventional concrete pavement design methods.

The conclusions with regards to the empirical tests of the hypotheses of the study are presented in the final chapter. Recommendations for further work are also provided.

As far as the laws of mathematics refer to reality, they are not certain; and as far as they are certain, they do not refer to reality

Albert Einstein (1922)

2

Theoretical framework

2 THEORETICAL FRAMEWORK

This chapter traces decades of research aimed at describing and predicting the development of fracture in concrete by means of mathematical modelling. As will become evident from the discussion, serious challenges still exist in bringing the mathematical prediction of fatigue fracture closer to the reality observed in concrete pavements.

The chapter starts with a section on the UTCRCP technology and its development. The discussion then shifts to the mechanism of fatigue cracking in concrete from its nucleus at an inherent material flaw to a full size crack. An overview of the current design methodologies for fatigue fracture in concrete pavements and their limitations is given. The advances in the modelling of crack formation in concrete by means of fracture mechanics both under monotonic and cyclic loading conditions are discussed in some detail.

2.1 Ultra Thin Continuously Reinforced Concrete Pavements (UTCRCP)

The South African Ultra Thin Continuously Reinforced Concrete Pavement is a further development of technology used in bridge deck rehabilitation in Europe. The technology comprises a high performance concrete layer with a nominal thickness of approximately 50 mm. A steel mesh is placed at the centre of the layer. The concrete, with an unconfined compressive strength (f_c) in the order of 100 MPa, incorporates both steel and synthetic

fibres. The material is able to withstand high deflections and is intended as an overlay rehabilitation strategy for weakened pavement structures.

The technology was tested extensively under the Heavy Vehicle Simulator (HVS). As part of the test program, the amount of steel fibres, mesh reinforcement, and slab thickness was varied. A description of the development and testing of the technology is contained in Kannemeyer et al. (2008), and Du Plessis and Fisher (2008a, 2008b).

Figure 2-1 shows the typical damage evolution for UTCRCP in HVS experiments. Cracks are indicated with spray paint on the test section.

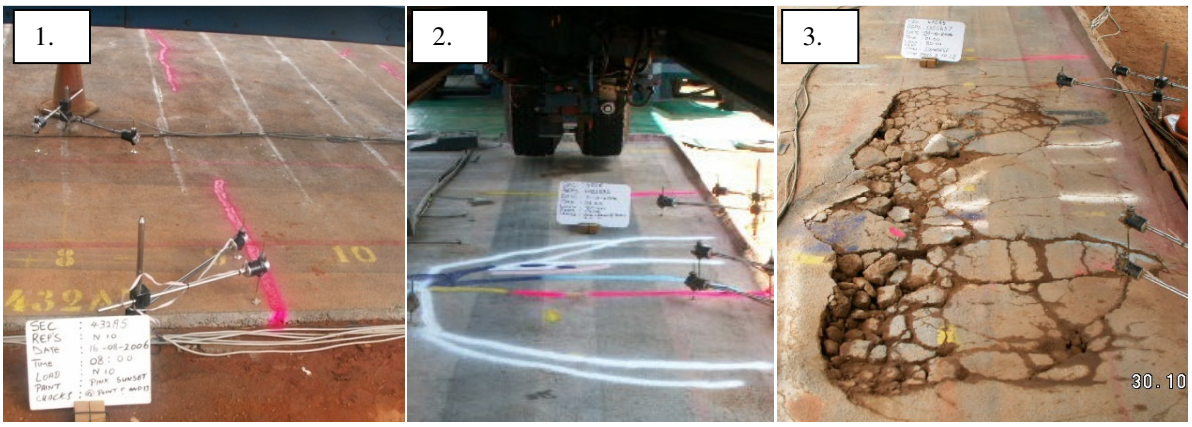

Figure 2-1: Typical damage evolution in UTCRCP under HVS testing (published earlier in Du Plessis and Fisher, 2008a)

The damage propagation in the material as observed during the HVS experiments is understood to occur as follows:

1. Before the start of trafficking, shrinkage cracks will be present as can be seen in the picture on the left. The final failure will always occur at the position of such a shrinkage crack.
2. As the section is being trafficked and water is added to the section, fines of the base material are pumped out through the growing shrinkage crack. Due to the loss of support the bending stresses in the UTCRCP increase in the affected area and at some stage secondary cracks occur as can be seen in the centre picture. These secondary

cracks typically occurred at a distance of approximately 300 mm from the original shrinkage crack (Kannemeyer et al., 2008).

3. Once secondary cracking has occurred the various cracks are able to open wider and the process of water ingress and base erosion is accelerated, finally leading to total collapse of the system, as can be seen from the picture on the right. An observation relevant to the laboratory experiments to be carried out as part of the present study is that the steel mesh reinforcing did not fail during the experiments.

Figure 2-2 shows in schematic form the failure mode of the UTCRCP as observed in the HVS experiments. In the figure it is assumed the maximum stress under trafficking will occur at the top of the slab some distance from the initial shrinkage crack. Linear elastic Finite Element Method (FEM) analysis of the tests by Kannemeyer et al. (2008) indicated that the highest stress under trafficking may in reality occur at the bottom of the slab at a distance of 450 mm from the shrinkage crack. In this case, the mechanism would be similar to what is shown in the figure, with the secondary crack starting at the bottom of the slab.

The HVS results were used to include the UTCRCP design option in cncPAVE (C&CI, 2009) the design software of the South African Cement and Concrete Institute (C&CI). The software and design methods were developed by Strauss et al (2001). The design models for UTCRCP were included in a later version of the software by Strauss et al. (2007). The design method for UTCRCP as implemented in cncPAVE makes use of a conventional approach to concrete pavement design. Stresses in the pavement are calculated using a Westergaard type equation, which is discussed in detail in Section 2.3.2. The ratio of the maximum tensile stress in the pavement to the MOR of the material is then used to predict the life of the pavement by applying Miner's law. Concerns about the MOR as a suitable material property for fatigue prediction are raised in Section 2.4.2, while limitations of Miner's linear damage hypothesis are discussed in Section 2.4.1. The main concern about current concrete pavement design methods is that they do not provide a mechanistic simulation of the fatigue fracture phenomenon discussed in the following section.

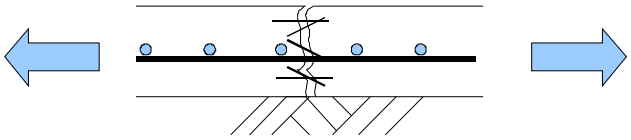

Stage 1: Formation of shrinkage crack shortly after construction

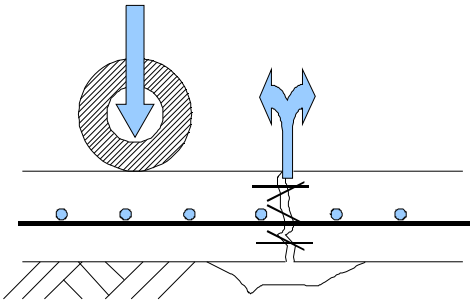

Stage 2: Water penetrates structure through the shrinkage crack, fines pump out under the action of traffic

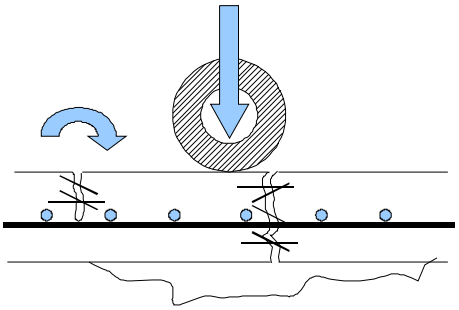

Stage 3: secondary cracking occurs due to tensile strain caused by hogging moment.

Figure 2-2: Schematic representation of failure in UTCRCP

2.2 The mechanisms of fatigue in plain and fibre reinforced concrete

Material fatigue, is the growth of fracture damage in a material as a result of repeated loading at an amplitude lower than the ultimate stress limit of the material. The study of fatigue has its origins in mechanical metallurgy and in this field there is a well established understanding of the fatigue mechanism. In metals, fatigue damage starts at a molecular level with a crystallographic defect, or dislocation, resulting in slip bands followed by micro cracking. Under continued loading a micro crack in the weakest position of the affected area will eventually develop into a macro crack and propagate, resulting in failure.

Concrete is less homogeneous than metal, and rather than microscopic defects it contains relatively large imperfections in the form of air voids, shrinkage cracks and pockets of trapped water. It is at these inherent flaws in the material that micro cracking due to fatigue loading will initiate (Lee and Barr, 2004, Gao and Hsu, 1998). Based on a study of fatigue in

concrete under uniaxial compressive loading, Gao and Hsu (1998) divide the fracture behaviour in three stages. In the first, or linear stage, the pre-existing flaws return to their original condition after loading. In the following non-linear hardening stage micro-cracks start to develop in the mortar and at the interface of mortar and aggregate. In the final stage the micro-cracks propagate to form macro-cracks and the material response shows softening under loading as a result.

Fatigue loading is often classified into low and high cycle fatigue, although various publications provide different brackets for the number of cycles per class. For pavement engineering the relevant fatigue classes are high cycle fatigue which is often used to describe the range from 10^4 to 10^7 load cycles and super high cycle fatigue with more than 10^7 load cycles to failure. Low cycle with less than 10^4 load repetitions is relevant for structures subjected to earthquakes. The loading of airport pavements may also fall within this range. Hsu (1984) points out that there is a difference in the damage mechanism for concrete under low-cycle and high-cycle loading regimes. In low cycle-fatigue cracks form in the mortar, whereas in high cycle fatigue it is the bond between aggregate and mortar that slowly deteriorates. Lee and Barr (2004) indicate that concrete does not appear to have a so-called fatigue limit. The fatigue limit is a stress level below which no fatigue damage occurs and the material is able to withstand an unlimited number of load cycles. This has the important implication that when the stress in a structure is kept lower than the fatigue limit, the structure has infinite life. The fatigue limit is a concept from mechanical metallurgy and has been reported to exist for various metals. With the advent of hypersonic testing however, doubts have been cast around the existence of a fatigue limit for ferrous metals as well (Miller and O'Donnel, 1999, Bathias, 1999).

The material under study is a Fibre Reinforced Concrete (FRC). FRC has a higher post-cracking load carrying capacity than plain concrete (Elsaigh, 2007). The ability of the fibres to transfer stresses across the cracks results in a larger ductile component in failure for FRC compared to plain concrete. The cracking mechanism in fatigue of FRC is determined by crack growth in the concrete matrix, the crack bridging action specific to the type of fibres, and the fatigue damage to bond between fibres and matrix (Li and Matsumoto, 1998, Zhang et al., 1999). Cracking is retarded through the energy dissipation required to fully pull the fibres out of the mastic. For this reason it would be expected that the fatigue performance of FRC in tension is also enhanced by the presence of fibres. The body of knowledge on fatigue behaviour of concrete relatively limited and even less information is available for fatigue in

fibre reinforced concrete. Lee and Barr (2004) compared the fatigue behaviour of plain and fibre reinforced concrete available from literature and found conflicting information. The majority of publications however, were found to indicate that FRC exhibits better fatigue performance in flexure than plain concrete. Published results show that the addition of fibres does not increase the fatigue performance of concrete under compressive cyclic loading.

2.3 Design for fatigue in concrete pavements

Current concrete pavement design methods can be described as supported by three pillars. The first pillar is an empirical relationship for the fatigue performance of the material, which is expressed in terms of number of loading repetitions (N) to failure at a certain stress level (S) using a so-called S-N curve. The second pillar is the calculation of the stresses in the pavement under traffic loading using linear elastic analysis, and the final pillar is the calculation of damage accumulation under traffic loading using a linear cumulative damage hypothesis. The background of each of the pillars will be discussed to some detail in this section as this is key to understanding the need for improvement of design the methodology.

2.3.1 Relating pavement stress condition to fatigue life

Ever since their introduction by Wöhler (1870), S-N curves have been widely applied in different engineering disciplines. In mechanical metallurgy the S-N function is typically derived from a standard test method where a sinusoidal stress is introduced to the specimen. The test is repeated at different stress intensities and the results plotted with the number of repetitions to failure on a log scale. The method is notorious for the statistical scatter of results. The S-N functions in concrete pavement design methods generally are not the result of tests performed on laboratory specimen, but rather a statistical fit to data from full scale field tests or long term pavement performance test sections. The definition of failure may differ between design methods and the results are, amongst others, a function of the material characteristics, the structural support and vehicle types in the area where the method was developed. The number of repetitions to failure is predicted using a ratio between the tensile stresses in the concrete pavement, determined from linear elastic analysis, and the Modulus of Rupture (MOR) of the material. The MOR, also referred to as the flexural strength, is determined from the monotonic peak load in Four Point Bending (FPB) laboratory tests. The

MOR is the ultimate nominal stress (σ_{Nu}) in the extreme fibre of the specimen, calculated assuming a linear elastic stress distribution at failure. The nominal stress (σ_N) (at any load level) is obtained for FPB using Equation 2.1 For Three Point Bending (TPB) testing, a test configuration used extensively as part of this study, σ_N is obtained from using Equation 2.2.

$$\sigma_N = \frac{Ps}{bh^2} \tag{2.1}$$

$$\sigma_N = \frac{3Ps}{2b(h-a)^2} \tag{2.2}$$

Where P is the sum of external loading introduced to a beam, s is the span, b is the width of the beam and h the height, a is the depth of the notch, where applicable. Sketches of the FPB and TPB test configuration are shown in Figure 2-3a and Figure 2-3b respectively.

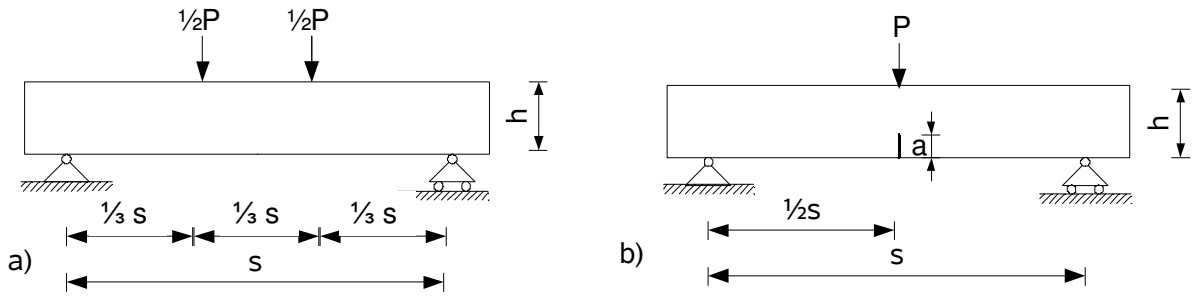

Figure 2-3: a) FPB test configuration, b) TPB test configuration

The calibrated S-N model to predict the fatigue life of a pavement from the results of the MOR tests is known as a transfer function and typically takes the form shown as Equation 2.3.

$$N = a_1\left(\frac{\sigma_d}{MOR}\right)^{b_1} \tag{2.3}$$

Where N is the number of load repetitions to failure, σ_d is the linear elastically derived design tensile stress in the pavement for a defined load condition. Parameters a_1 and b_1 are the calibration constants which form the essence of the transfer function. The calibration constants provide the bridge between the statistical fatigue data from full scale observations on the one side and the ratio between the stress at peak load from monotonic FPB tests and

the calculated tensile stress in the concrete slab on the other side, assuming LE material behaviour. The transfer function for fatigue in continuously reinforced concrete pavements developed as part of the new American Mechanistic Empirical Pavement Design Guide (MEPDG), NCHRP 1-37A (2004) by Selezneva et al. (2004) is plotted in Figure 2-4.

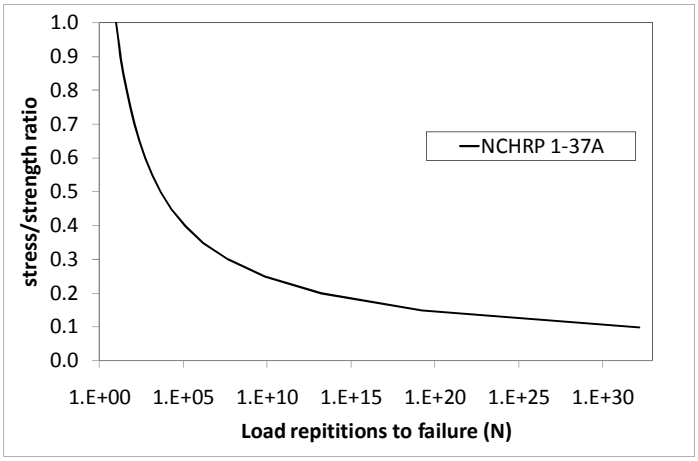

Figure 2-4: Fatigue curve at different stress / strength ratios for continuously reinforced concrete pavements according to NCHRP 1-37A (2004)

2.3.2 Calculation of stress condition in concrete pavements

Traditionally the maximum tensile stresses in the concrete pavement slabs have been calculated using the method introduced by Westergaard in 1923 for a plate on a bed of springs. The theory was first published in English in 1926 (Westergaard, 1926). The number of limiting assumptions of the original method has gradually been decreased over the years by various researchers including Westergaard himself (Ioannides, 2006). Many design methods in use today, including the latest version of the concrete pavement design method developed for South Africa by Strauss et al. (2007), still rely on some of the theory introduced by Westergaard in 1926. Using Westergaard theory, the stresses acting in a concrete slab are calculated based on the relative stiffness of the slab and the support. This linear parameter he named the radius of relative stiffness (l) is determined from the thickness of the slab (h), the modulus of elasticity of the concrete (E), Poisson's ratio (υ) and the linear elastic stiffness of the subgrade (k), using Equation 2.4

$$l = \sqrt[4]{\frac{Eh^3}{12(1-\nu^2)k}} \tag{2.4}$$

Using the factor *l,* Westergaard (1926) approximated LE stresses in the concrete pavement for three typical vertical load cases, i.e. a load at the corner of the slab, a load at an edge of the slab and a load at some distance from the edges of the slab. Examples of combinations of loads to cater for the influence of the different wheels of a truck were also included in the original paper. The equation to calculate the design value of the maximum tensile stress (σ_d) due to a load (P) at a distance (a_2) to the corner of a slab with thickness (h) is provided as an example in Equation 2.5.

$$\sigma_d = \frac{3P}{h^3}\left[1-\left(\frac{a_2}{l}\right)^{0.6}\right] \tag{2.5}$$

The paper by Westergaard did not include failure criteria, but he proposed that critical stresses be calculated in an empirical way, based on existing pavements that performed satisfactory. Before the introduction of suitable computer technology, influence charts developed from the general equations by Westergaard were typically used to calculate stresses under various load configurations (Yoder and Witczak, 1975). The wider use of computer technology made possible the application of Finite Element Method (FEM) in pavement design. Some of the newer design methods, such as the MEPDG (NCHRP 1-37A, 2004) use the results of large sets of pre-run FEM analyses to deduce stresses in the concrete pavement slab by means of neural networks, instead of Westergaard type analysis.

2.3.3 Fatigue damage accumulation

In conventional design methods, the relative damage of each load is calculated based on the calculated stress state in the pavement slab and the number of repetitions to failure at that stress ratio according to the transfer function. In pavement engineering the linear cumulative damage hypothesis first proposed by Palmgren (1924), but best known for the publication by Miner (1945) is generally used to calculate the accumulation of damage. The function shown as Equation 2.6, the hypothesis is that failure occurs when the number of stress cycles (n_i) applied at stress level (S_i) divided by the number of cycles to failure (N_i) at stress level (S_i) equals one.

$$\sum \frac{n_i}{N_i} = 1 \qquad (2.6)$$

The linear cumulative damage concept provides a convenient tool to sum up the proportional damage caused by each load repetition over the life of a pavement.

The methodology described in this section has been widely applied in concrete pavement design. The approach does however contain a number of known limitations and presents scope for improvement.

2.4 Some concerns regarding the conventional concrete pavement design approach

The prediction of fatigue failure in concrete pavements as described in the previous section relies heavily on statistical calibration rather than an accurate model for the failure mechanism. The discussion in this section will highlight some of the limitations in various aspects of the methodology, but all of these may be viewed as consequences of the use of empirical models rather than a mechanistic model for fatigue fracture.

2.4.1 Limitations of Miner's linear cumulative damage hypothesis

Limitations of the cumulative damage hypothesis for prediction of fatigue in concrete are highlighted by a number of authors including Ioannides (1995, 1997a, 2006), Ioannides and Sengupta (2003), Ioannides et al. (2006), Roesler (2006) and Gaedicke et al. (2009). Some of the main limitations are discussed here. The evolution of concrete material response under cyclic loading is distinctly non-linear. The typical development of longitudinal strain of concrete in fatigue tests is schematically shown in Figure 2-5 based on results reported by Holmen (1979). The figure also shows the typical fit allowed by Miner's linear cumulative damage hypothesis, calibrated against empirical *S-N* end of life data. Miner's law will at best accurately forecast the number of load repetitions until the failure threshold is reached, but it cannot be used to reliably predict the state of the material at any other stage during the functional life. An important consequence of this for pavement engineering is that the remaining functional life of a pavement in service cannot be reliably back-calculated from deflection data using these models.

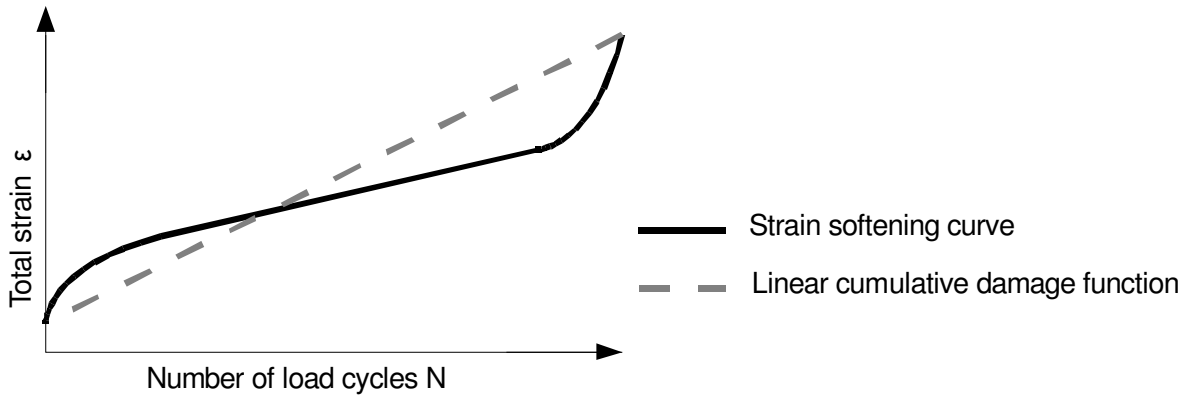

Figure 2-5: The evolution of strain in concrete under cyclic loading (after Holmen, 1979) versus the linear cumulative damage concept.

Another limitation of Miner's law is that it does not take the sequence of loading into account. In reality many small loads followed by a large load can have less of an impact on fracture propagation than the opposite sequence where a large load is followed by smaller loads, or vice-versa, due to the distribution of residual stresses and pre-formed cracks in the material.

A final limitation is that the hypothesis does not cater for the stochastic nature of fatigue damage propagation in concrete. Under Miner's hypothesis every load cycle has a probability of 1 to cause additional damage of a known size, where as in reality there is only a chance of additional damage occurring.

Notwithstanding the limitations, Miner's linear cumulative damage hypothesis has been applied with few adjustments in most concrete design methods. Ioannides (2005) argues that this is done because of practical expediency rather than reliability. Ioannides states that *"Studies to verify Miner's hypothesis often provide adequate information that could justify its abandonment instead. Data reported suggests that predictions of life using Miner can be expected only to approximate reality at best within two or even three orders of magnitude."*

2.4.2 Size-effect

Ioannides (2005) also points out that many of the fatigue relationships for concrete pavements are derived from repeated loading tests on small specimens. In the use of small lab

specimens, typically beams, coupled with linear elastic mechanics for analysis, lies another weakness of current design methods. It has been known at least since the 1930s that the LE derived peak stress (MOR) in beams tested in bending depends on the size of the tested specimen (e.g. Reagel and Willis, 1931, Kellerman, 1932). Ward and Li (1991) showed that this also holds true for fibre reinforced mortars. It follows that the MOR, treated as a material property in concrete design method, is not a true material property as its value depends on the size of the specimen as well as boundary conditions of the test. To illustrate the size effect Figure 2-6 shows the typical load response of two beams with the same geometry, but of different sizes. According to conventional design approaches, these beams, if made from the same material, will have the same σ_{Nu} equal to the MOR determined from a standardized test. However, this is not the case. In general for quasibrittle materials, such as concrete, the smaller sample can be expected to have a higher σ_{Nu}.

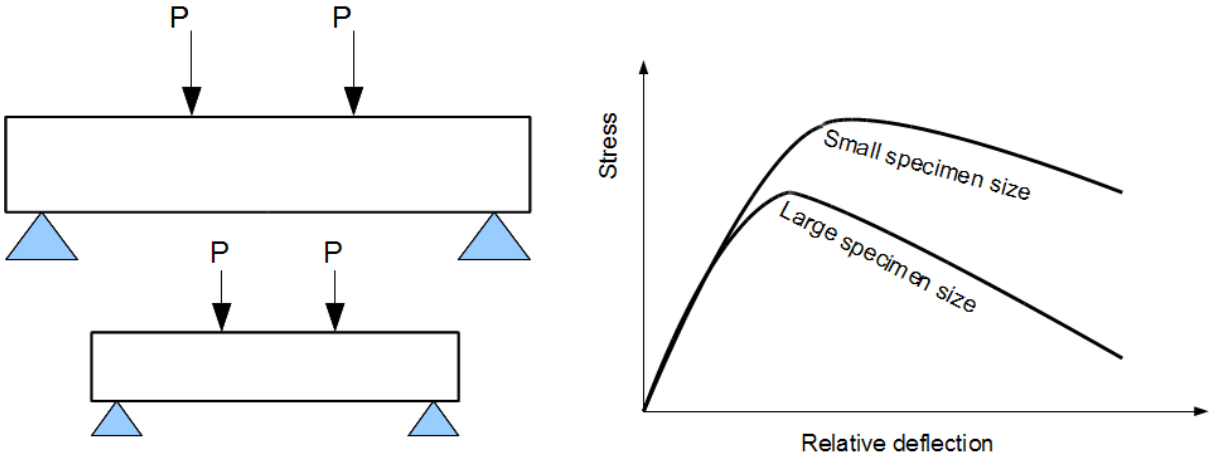

Figure 2-6: Size effect for beams in flexure (after Bažant and Planas, 1997)

There are several known sources of size-effect in concrete. An example is the boundary layer effect, caused by the higher density of fine particles at the side of the beam mould. Other sources are: diffusion phenomena, variation in hydration heat and the statistical size effect (the larger the specimen, the higher the chance of defects) (Bažant and Planas, 1997).

The main source of size-effect however, is the fracture mechanics size effect. The release of stored energy into the fracture front is higher for larger beams and this leads to a relatively lower strength. Ergo, if σ_{Nu} is determined for the small beam in Figure 2-6, it is not possible

to use this parameter and accurately predict the peak load for the larger beam by means of linear elastic beam theory. Much less is it possible to predict the peak load of a slab produced of the same material. Based on this, the suitability of the MOR for the prediction of the fatigue performance of full scale pavements has to be questioned.

To clearly distinguish between the different parameters, the MOR, in this study will refer to the σ_{Nu} determined from a FPB test on a beam with a 150 mm x 150 mm cross section and a span of 450 mm as prescribed in most standard methods.

Roesler (2006) has shown that due to size-effects and boundary conditions, fatigue of full scale concrete slabs cannot be reliably predicted from tests on beam specimens. Slabs exhibit better fatigue performance than beams, which cannot be explained without the use of fracture mechanics. The difference between beam and slab fatigue response is greater for fibre reinforced concrete when compared to plain concrete (Roesler, 2006). The above underlines the necessity for a fracture mechanics based approach to fatigue prediction for concrete pavements in general and fibre reinforced concrete pavements in particular. The mechanics behind the fracture mechanics size effect are explained in more detail in the next section.

2.5 Fracture mechanics and its application to concrete

Fracture mechanics is a specialization within the field of solid mechanics which deals with the formation and growth of cracks in materials. It is increasingly looked upon to mitigate some of the limitations of current pavement design methods. This section contains a discussion on the general principles of fracture mechanics, followed by an introduction of the models most commonly applied to concrete.

2.5.1 Linear elastic fracture mechanics

Griffith (1921) famously introduced the energy balance approach for fracture in glass. His work forms the basis for what is now known as Linear Elastic Fracture Mechanics (LEFM). By studying the energy required to grow a crack by a unit volume he overcame a mathematical problem flowing from the work by Inglis (1913) concerning stress concentrations around elliptical holes. According to the theory developed by Inglis, a perfectly sharp crack in a material would lead to infinitely high stresses at the crack tip and

the material would fail even if a small load was applied. Griffith proposed that energy should be used as a threshold for crack growth rather than stress alone. For a linear elastic material the Griffith equation for the strain energy (U^*) released per unit volume can be written as shown in Equation 2.7 (Roylance, 2001).

$$U^* = \frac{\sigma^2}{2E} \tag{2.7}$$

Where σ is the stress and E is Young's modulus. Griffith studied fracture in glass, a very brittle material, and proposed that the energy required to extend a crack with a unit area is equal to the surface energy that is released. Surface energy quantifies the disruption of intermolecular bonds. In a plane stress state the amount of surface energy (S_1) released in the formation of a crack is calculated using:

$$S_1 = 2\gamma a \tag{2.8}$$

Where γ is the specific surface energy for the material, it is factored by 2 because two surfaces are formed, a is the length of the crack. Figure 2-7a shows the approximately triangular area that is unloaded as a crack progresses. In LEFM the length of the side of the triangle perpendicular to the crack has been found to be π times crack length (a). Griffith's work can be used to determine the critical crack length. Up to the critical crack length an increase in stress is required to grow the crack, after the critical crack length has been reached the system becomes unstable and failure occurs, without additional stress being applied. The stress at fracture σ_f can be obtained from:

$$\sigma_f = \sqrt{\frac{2E\gamma}{\pi a}} \tag{2.9}$$

Surface energy alone is not enough to quantify the energy required to fracture less brittle, more plastic materials. Irwin (1957) argued that for plastic materials such as steels the majority of energy dissipation in crack growth is due to plastic flow at the crack tip. He further classified the two components of fracture energy i.e. the stored elastic strain energy released with crack propagation, and the dissipated energy which includes the surface energy used by Griffiths as well as the plastic flow dissipation and other possible sources. The equation for critical stress can be modified to incorporate the total specific fracture energy (G_f) by simply replacing γ with G_f in Equation 2.9.

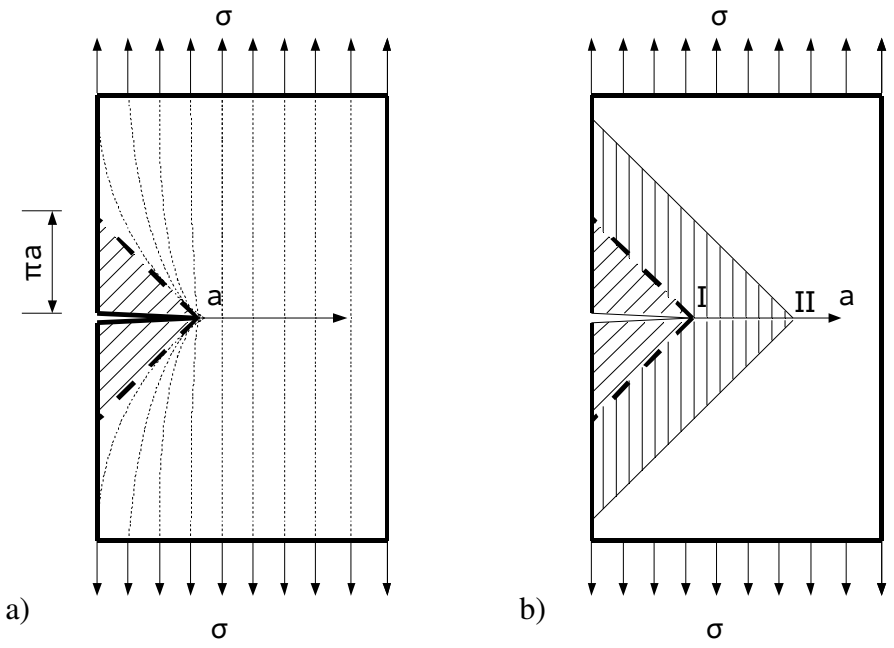

Figure 2-7: a) Approximation of unloaded area due to cracking, b) Change in amount of strain energy released as crack progresses.

2.5.2 The fracture mechanics size effect explained

The theoretical concepts described above can be used to explain the fracture mechanics size effect. Figure 2-7b shows how the amount of strain energy released increases per unit of crack length propagation. More strain energy is released as the crack grows from point I to point II than was initially released when the crack grew over an equal distance to point I. Similarly, if an equal stress state exists in two specimens of the same geometry, but different sizes, the amount of strain energy released into the crack is larger for the larger sized specimen. As a result the smaller specimen will fail at a larger nominal stress.

LEFM has limited applicability to concrete materials as first pointed out by Kaplan (1961). LEFM is suitable for the analysis of brittle or plastic materials where the Fracture Process Zone (FPZ) is small. LEFM is only valid if the size of the FPZ is negligible compared to the size of the specimen (Ioannides, 1997b). Concrete however, is a quasi-brittle material, with a relatively large FPZ. For plain concrete the length of the FPZ is in the order of a meter. LEFM is not the most suitable methodology for crack analysis in this material. The fracture properties determined for the material using LEFM theory would be size dependent (Zhang and Li, 2004). Therefore non-linear fracture mechanics models are typically applied to concrete.

2.5.3 Size effect equations

The size effect in concrete can be predicted without the use of complex fracture mechanics based numerical simulation. Bažant (1984) devised a size effect equation based on non-linear fracture mechanics that can be used to predict the size effect in terms of the value of σ_{Nu} in elements with the same geometry, but different sizes. The Bažant size effect model is shown as Equation 2.10.

$$\sigma_{Nu} = \frac{B_a f_t}{\sqrt{1+\frac{D}{D_0}}} \tag{2.10}$$

Where, B_a is a constant depended on the geometries and fracture properties of the material, as is D_0. The parameter D relates to the size of the specimen, usually the height is used for this parameter. f_t is the tensile strength of the material. This equation can readily be calibrated for a specific material and geometry. A distinct disadvantage of the model is that it cannot be generalized to predict the size effect for specimens with different geometries. Continuum domain based fracture mechanics models are required to be able to use the fracture properties obtained from tests on a certain specimen type and predict the fracture behaviour of structural elements of different geometries.

2.5.4 Cohesive crack model

One method for the analysis of crack propagation in concrete favoured by various researchers for implementation in finite element analysis is the Fictitious Crack Model (FCM). The FCM, nowadays commonly referred to as the cohesive crack model, was introduced by Hillerborg et al. (1976). These authors adapted the Barenblatt cohesive force model so that it would become suitable for concrete. Figure 2-8a provides a sketch of the model as proposed by Hillerborg and co-workers.

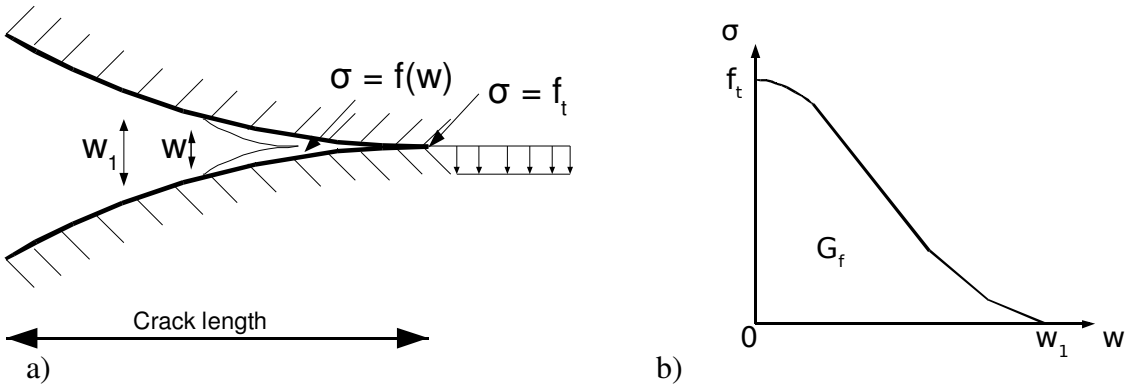

Figure 2-8: a) Sketch of fictitious crack model, b) shape of the softening curve for plain concrete (after Hillerborg et al., 1976)

According to the FCM model, the material behaves linear elastically until the principal stress reaches the tensile strength of the material. At this point a crack is induced. Stresses are transferred over the crack according to a softening function. The shape of the softening behaviour of concrete as put forward by Hillerborg et al. (1976) is shown in Figure 2-8b. The crack bridging stress (σ) is written as a function of the crack width (w):

$$\sigma = \mathrm{f}(w) \tag{2.11}$$

As the crack width approaches w_1 the crack bridging stress gradually falls away. Hillerborg et al., proposed that the zone between the crack tip and the critical crack width (w_1) represents a micro cracked zone where stress transfer is still possible over remaining ligaments, for instance through aggregate interlock. The area underneath the softening curve represents the specific fracture energy (G_f) for the material, therefore:

$$\int_0^{w_1} \mathrm{f}(w)\mathrm{d}w = G_f \tag{2.12}$$

To simplify the softening behaviour of concrete shown in Figure 2-8b, Hillerborg et al. (1976) assumed a linear function in their model. One of the co-authors of that early work later introduced a bi-linear softening function, to better represent the actual behaviour (Petersson, 1981). In literature the shape of the softening function for plain concrete is now often modelled using a bilinear function determined through various methods. For example Guinea et al. (1994), proposed a model using four parameters, i.e.: f_t, G_f and two parameters dependent on the shape of the function determined from experimental results. Recently,

Park et al. (2008) proposed a two parameter model for bilinear softening. Exponential or quasi-exponential curves are used in literature as well. Figure 2-9 shows examples of different shapes of the softening curve. In the construction of the example the specific fracture energy (G_f), i.e. the area underneath the curve, was kept constant.

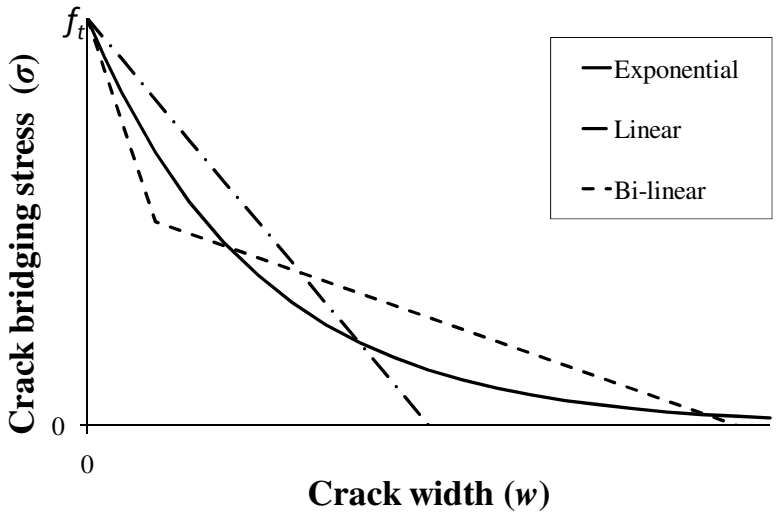

Figure 2-9: Typical assumed shapes of the softening curve

Hillerborg et al. (1976) used the fracture energy (G_f) combined with Young's modulus (E) and the tensile strength (f_t) to calculate a characteristic length (l_c) for the material as per Equation 2.13. Hillerborg (1983) proposed that the characteristic length is a pure material property without a direct physical correspondence, but often proportional to the fracture zone.

$$l_c = \frac{EG_f}{f_t^2} \tag{2.13}$$

Later research has shown that l_c is not a pure material property, it is subject to size-effect which, as discussed earlier, limits the reliability of laboratory testing to predict field performance. Bache and Vinding (1990) introduced the dimensionless brittleness number (B) to factor in the specimen size effect. The brittleness number is an expression of Hillerborg's characteristic length (l_c) in relation to a characteristic dimension usually taken as the thickness of the material (h). Bache and Vinding (1990) propose a model law that the test specimen should have the same brittleness number as the actual structure for which fracture is

predicted. The brittleness number provides an indication of the ductility of the material. The smaller the brittleness number, the more ductile the material. The Brittleness number is defined as:

$$B = \frac{f_t^2 h}{EG_f} = \frac{h}{l_c} \tag{2.14}$$

The FCM as described above has been used to analyse a single discrete crack by means of Finite Element codes. Examples of this approach applied to pavement structures, including the brittleness number refinement, can be found in Ioannides and Sengupta (2003) and Ioannides et al. (2006). The primary factors in the softening behaviour of the concrete, i.e. G_f and f_t are generally determined from beam bending tests and direct or indirect tensile tests on the material.

Some limitations of the FCM highlighted by Bažant (2002) include:

- The FCM is a uniaxial model and is applicable only to elements in bending. The model can not handle tri-axial stresses. The model in its original form also does not include shear stresses transferred across the crack and the influence of parallel compressive stresses,
- The FPZ is not a straight line, as assumed in the FCM, in reality the FPZ is formed by a wider area of material around the crack tip,
- The crack model assumes the fracture energy to be dissipated through micro cracking in the FPZ, while in reality a large part of this energy is dissipated through crack slipping,
- The FCM assumes that the stress at a point is only dependent on the crack width opening at that point and not on the continuum of displacements of the points around it.

Despite these limitations the FCM, often referred to as cohesive crack model remains popular among researchers. A number of the limitations have been addressed by new developments of the model.

2.5.5 Smeared crack or crack band models

A much used alternative to the discrete cohesive crack approach is to model the cracking as tension softening distributed over the material. This approach is known as smeared cracking, a concept introduced by Rashid (1968). The initial methodology had some limitations; it was sensitive to the size of the finite element mesh and allowed the development of volumeless fracture process zones. Bažant and Oh (1983) overcame these limitations by introducing localization limiter which forces the fracture zone to have a certain width (h_c). This width is treated as a material property. Bažant and Planas (1997) show that the response of strain softening crack band can be related to the width of the cohesive crack (w) of the FCM using:

$$w = h_c \varepsilon^f \tag{2.15}$$

where (ε^f) is the fracture strain. The stress-strain behaviour of the crack band model for linear softening is shown in Figure 2-10.

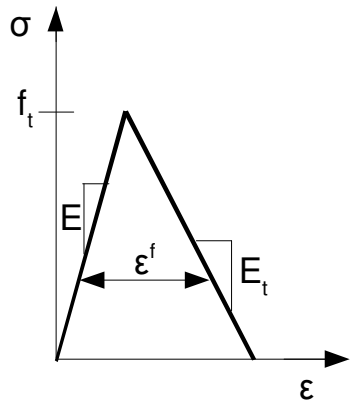

Figure 2-10:Stress-strain behaviour of crack band model after Bažant and Planas, 1997)

Similar to the cohesive crack model, the material response of the material is linear elastic under tensile loading until the tensile strength of the material is reached. The post cracking behaviour is characterized by the strain softening tangent modulus (E_t). For the linear softening behaviour shown in the figure the function defining E_t.is:

$$-\frac{1}{E_t} = \frac{2G_f}{h_c f_t^2} - \frac{1}{E} \tag{2.16}$$

where (E) is Young's modulus of the material in its undamaged state. The crack band model can readily be implemented in finite element software. An advantage over the cohesive crack approach is that tri-axial softening can be accommodated. The smeared crack approach was recently used in local work by Elsaigh (2007) to model the behaviour of steel fibre reinforced concrete pavements.

2.5.6 The Jenq-Shah two parameter fracture model

The last fracture mechanics method for concrete to be discussed in this section is the two parameter fracture model developed by Jenq and Shah (1985). The model has recently been applied extensively to concrete pavement materials by researchers at the University of Illinois (Roesler et al., 2007, Gaedicke et al., 2007, Roesler et al., 2007 and Gaedicke et al., 2009, Gaedicke and Roesler, 2010). The Jenq-Shah model makes use of LEFM in combination with an equivalent elastic crack concept to make the theory applicable to the quasi-brittle fracture behaviour of concrete. The model applies the concept of critical crack length of LEFM. As in LEFM, in the peak loading condition the stress intensity at the crack tip (K_I) is assumed equal to the critical stress intensity at failure (K_{Ic}), and the Crack Tip Opening Displacement (CTOD) is likewise assumed to reach a critical condition $CTOD_c$. These two conditions are formulated as follows:

$$K_I = K_{Ic} \tag{2.17}$$

and,

$$\frac{4K_I}{\pi E'}\sqrt{2\pi\Delta a_e} = CTOD_c \tag{2.18}$$

where a_e is the equivalent effective elastic crack length and E' is the effective modulus of elasticity in a plane strain condition, according to:

$$E' = \frac{E}{1-\nu^2} \tag{2.19}$$

The parameters for the Jenq-Shah model are typically obtained from Three Point Bending tests (TPB) on notched beams. The Crack Mouth Opening Displacement (CMOD) is used to control the test. The beams are loaded past the peak load. Then, as the load starts to drop the beam is unloaded and subsequently reloaded. The fracture parameters are calculated from the loading and unloading compliance.

Various studies have shown that the Jenq-Shah approach yields results equivalent to the cohesive crack method discussed in Section 2.5.4 (Tang et al., 1992, Bažant, 1994, Smith, 1995).

2.5.7 Application of fracture mechanics to conventionally reinforced and fibre reinforced concrete

The cohesive crack, smeared crack and Jenq-Shah models were all originally developed for plain concrete. Fracture simulation of concrete reinforced with steel bars is possible with the models by including the concrete and steel as separate entities in the numerical model (Hillerborg, 1990, Bažant and Planas, 1997). Fracture mechanics modelling of concrete with steel bar reinforcement has only limited application though, as the dominant mode of failure for reinforced concrete is yielding of the steel or compression failure. Quasi-brittle fracture may however, occur in lightly reinforced structures if the tensile capacity of the concrete section is higher than that of the reinforcement.

Importantly for this study, the models can also be applied to model the post crack behaviour of fibre reinforced concrete. In general there are two approaches to the modelling of steel fibre reinforced concrete.

The first involves the modelling of fibres as separate entities within the concrete matrix. This can be done by using a lattice model. Lattice models, also referred to as rigid body spring networks, like smeared crack models, have the advantage over cohesive crack models that they allow triaxial stresses. However, unlike smeared crack models, lattice models can in principle be used to simulate discrete cracks. The concrete material is modelled as consisting of three components, i.e. the mortar matrix (which includes the free water and the fine aggregate fraction embedded in the hardened cement gel), the coarse aggregate, and the Interfacial Transition Zone (ITZ) between the mortar and the coarse aggregate, which is more porous and less stiff than the general mortar matrix. Details of the methodology are contained in Yip et al. (2006), Lilliu and Van Mier (2007) and Schlangen et al. (2010). Because the different components of the concrete mix are modelled separately, their properties and interaction also need to be determined separately through testing. Pull-out tests are required for the fibres. The procedures to obtain the parameters are described by Redon et al. (2001).

The second approach to the modelling of fracture in FRC is by capturing the influence of fibres on the post crack softening material behaviour in cohesive crack, smeared crack or Jenq-Shah models. Hillerborg (1985) proposed the simplified representation of the post crack behaviour of steel fibre reinforced concrete shown in Figure 2-11. In the figure G'_f represents the fracture energy of the concrete matrix without the fibres. The crack needs to open by a certain width before the fibres are activated. Therefore the first part of the softening function is dominated by the softening behaviour of the concrete only. The fracture behaviour of fibre reinforced concrete has also been modelled using bi-linear softening functions e.g. Guo and Li (1999). Due to the extended post crack softening process more complex tri-linear shapes of the softening function have been proposed for fibre reinforced concrete by various researchers e.g. Lim et al. (1987), Pereira et al. (2004), RILEM (2003) and Roesler et al. (2007).

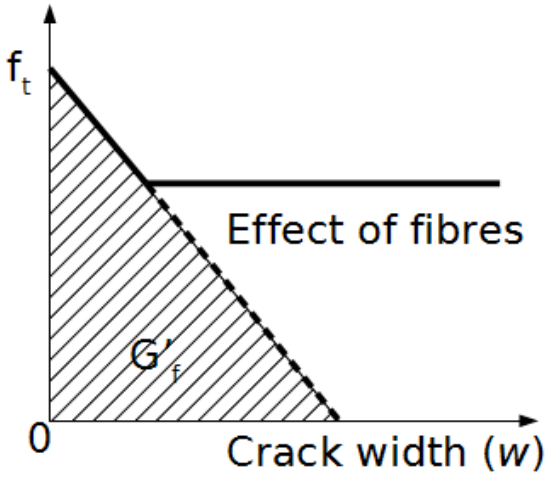

Figure 2-11: Softening function for steel fibre reinforced concrete (after Hillerborg, 1985).

Research on concrete with similar steel fibres from the same producer as used in this study has shown that when a crack forms, the stress transferred across the crack drops rapidly until it stabilizes at a lower stress level. After this, the material softens further at a slower pace (Lim et al., 1987). Based on this work, Lim et al. (1987) proposed a softening function with a crack tip singularity to simulate the behaviour of the material in tension. Such a curve with an initial spike at high strength followed by a long tail at a lower stress is suitable for fibre reinforced composites, as it simulates the initial failure of the matrix followed by the slow pull out of the fibres (Bažant and Planas, 1997).

2.6 Fracture mechanics for fatigue damage prediction

The previous sections described a number of well established methods for the simulation of fracture in concrete under monotonic loading. The models for simulation of fatigue fracture in concrete and in fibre reinforced concrete in particular, are less well developed.

2.6.1 Paris' law

Fatigue crack propagation in metals can be divided into four stages: Crack nucleation, followed by stage I crack growth, during which the crack propagates slowly, when a certain threshold is reached stage II crack growth commences, during this stage the crack propagates in a stable manner, and finally ductile failure. Stage II crack growth is important from a design perspective as it is much longer than the other stages. Fatigue crack growth of metals during phase II can be predicted using a fracture mechanics function shown as Equation 2.20 introduced by Paris and Erdogan (1963), which has become know as Paris' law.

$$\frac{\mathrm{d}a}{\mathrm{d}N} = C(\Delta K)^m \tag{2.20}$$

where da is the change in crack length, dN the change in the number of loading cycles, C and m are empirical material constants, and ΔK the change in amplitude of the stress intensity at the crack tip. The number of load repetitions to failure can be obtained by integrating Equation 2.20 over the domain from the initial crack length (a_0) to the critical crack length (a_c) at which the system collapses.

$$N = \int_{a_0}^{a_c} \frac{1}{C(\Delta K)^m} \mathrm{d}a \tag{2.21}$$

A number of researchers have adapted Paris' LEFM law for the quasi-brittle behaviour of concrete. The early work by Baluch et al. (1987) and Perdikaris and Calomino (1987), recognized the need for a non-linear fracture approach for fatigue in concrete. The studies by Bažant and Xu (1991) and Bažant and Schell (1993) show that the fatigue tests are subject to size effect and that Paris' rule can only be made applicable to a narrow range of sizes. To increase the applicability the models need to be adjusted using a size-effect law (Bažant and Planas, 1997).

Li and Matsumoto (1998) and Carpinteri et al. (2006) developed models based on Paris' law for the prediction of fatigue in fibre reinforced concrete. These models include additional factors to accommodate the crack bridging action of the fibres.

Slowik et al. (1996) devised the model for fatigue softening behaviour of concrete under variable amplitude loading shown in Equation 2.22. The model is rather complex to cater for loading history and size effect. Besides the fracture toughness (K_{Ic}) and the change in amplitude of the stress intensity (ΔK_I), the model includes the maximum stress intensity for the load cycle (K_{Imax}) and the maximum stress intensity reached during the life of the material (K_{Isup}). Factors m,n,p are calibration constants. F is a function that accounts for overloading of the system. The final parameter is Paris' constant (C) which is calibrated for the non-linear quasi-brittle crack growth per load cycle.

$$\frac{\mathrm{d}a}{\mathrm{d}N} = C\frac{K_{\mathrm{Im}ax}^{m}\Delta K_I^{n}}{(K_{Ic} - K_{I\,\mathrm{sup}})^{p}} + F(a,\Delta\sigma) \qquad (2.22)$$

The model by Slowik et al. (1996) was recently developed further in work by Sain and Chandrakishen (2007, 2008).

Gaedicke et al. (2009) made use of a Paris' law related non-linear fracture mechanics model originally developed by Subramaniam and co-workers (Subramaniam et al., 1998), (Subramaniam et al., 1999), (Subramaniam et al., 2000), to predict the fatigue response of concrete ground slabs. The model by Subramaniam et al., differs from Paris' approach in that it covers different stages of fatigue crack propagation. Where Paris' law was developed only for the stable phase II fatigue growth in metals, Subramaniam et al., proposed seperate equations for deceleration stage crack propagation and acceleration stage crack propagation. Figure 2-12 shows the deceleration and acceleration stages of the crack growth in concrete under cyclic loading.

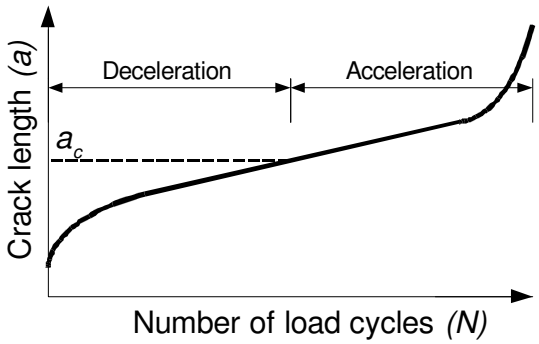

Figure 2-12: Stages of fatigue crack growth Subramaniam model

The crack growth per cycle is decelerating until the critical crack length (a_c) is reached, after this point crack growth starts to accelerate again. The crack growth in the deceleration stage is described by Equation 2.23, crack growth in the acceleration phase can be described using Equation 2.24.

$$\frac{da}{dN} = C_1(a - a_0)^{n_1} \qquad \text{for } a < a_c \tag{2.23}$$

$$\frac{da}{dN} = C_2(\Delta K)^{n_2} \qquad \text{for } a \geq a_c \tag{2.24}$$

where a_0 is the initial crack length, and C_1, C_2, n_1, n_2 are calibration constants.

Note that all fracture mechanics models based on Paris' law are valid only in situations with a pre-existing crack. The approach does not provide a threshold for crack nucleation. An additional limitation is that the calibrated models provide a prediction of fatigue crack growth, which is hard to implement in numerical software. The models can be used to predict the length of a fatigue crack after a certain number of load repetitions which can then be used to calculate the residual strength of the material as shown by Sain and Chandrakishen (2007). However, without numerical implementation the analysis of structures with more than one crack developing will be cumbersome.

2.6.2 Fatigue softening behaviour in cohesive crack model

Hordijk (1992) proposed a model for fatigue in concrete in which the load displacement curve under static loading represents the envelope within which evolution of the load displacement curve in fatigue takes place. Figure 2-13a shows a sketch of the concept. The

cyclic load level is set at a percentage of the monotonic peak load. The material softens with every loading cycle until a cyclic load-displacement loop crosses the monotonic envelope, at which time unstable failure takes place. Hordijk used the focal points model, proposed by Yankelevsky and Reinhardt (1987), for the softening behaviour of the material in fatigue. A rather simplified sketch of the softening curve after crack induction for the cyclic model used by Hordijk is shown in Figure 2-13b.

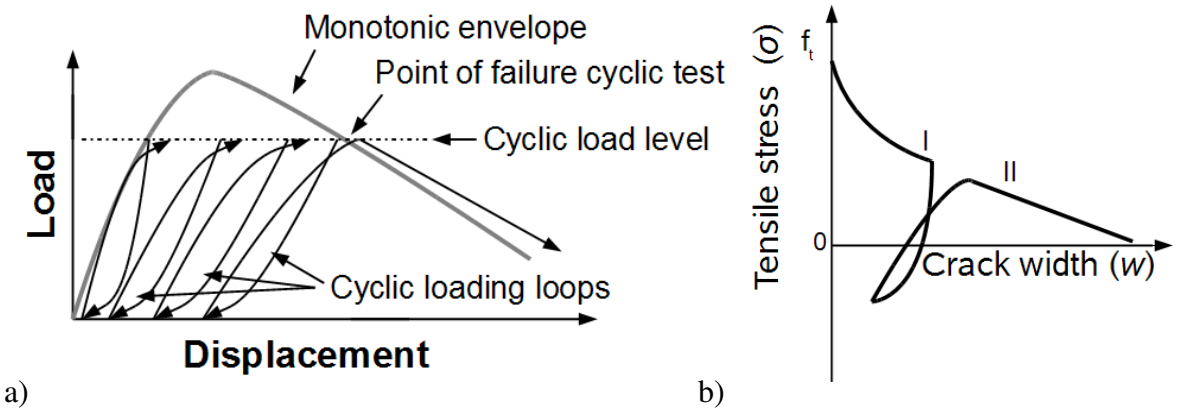

Figure 2-13: a) Load-displacement evolution according to Hordijk model, b) Sketch of cyclic cohesive softening function.

The figure shows that when the material is unloaded at point I and subsequently reloaded the function does not return to point I but joins the original softening curve at point II. The difference between point I and II is the fatigue damage. The softening function with damage degradation can be calibrated for a specific material and used to model the fatigue behaviour using FEM. The experimental study by Hordijk included direct tensile and Three Point Bending (TPB) tests on beam specimens. Although the model showed promise, the data obtained from the experiments to validate the simulation method showed considerable scatter.

Hordijk (1992) reported a better fit of the model to low cycle fatigue situations compared to high cycle fatigue situations. Other researchers later established that the monotonic curve does not provide a good fit for high cycle fatigue situations (Subramaniam et al., 2000), (Lappa et al., 2006). Lappa et al. (2006) propose that this difference is due to the fact that a single crack is formed in high cycle fatigue situations, while multiple cracks are formed under monotonic loading and low cycle fatigue.

Subramaniam et al. (2000) show that unlike the deflection, the crack length recorded in the monotonic tests on plain concrete does provide a suitable envelope for fatigue tests. There is some published research available that indicates that the monotonic load displacement curve does provide a suitable envelope for fibre reinforced concrete (Otter and Naaman, 1988, Zhang and Stang, 1998).

2.7 Discussion on theoretical framework

The aim of this chapter was to provide a concise overview of the state of the art in the prediction of fracture in concrete pavement materials. There is a sizeable body of previous knowledge available to take direction from in this study.

One of the limitations of conventional concrete pavement design methods is the assumption of LE material behaviour. Both the material strength and the stress in the pavement are characterized based on LE analysis. Concrete is known to have a distinctly non-linear, non-elastic component in fracture, giving rise to the size effect observed in experiments. The size effect phenomenon has been studied extensively for plain concrete by various researchers. From literature it is known that the MOR parameter, currently used in concrete pavement design to characterize the material in terms of fatigue performance, is subject to considerable size-effect. As a consequence of size effect the MOR obtained for a specimen of a certain size cannot be used to predict the peak load of a specimen with the same geometry, but a different size. This raises questions on the suitability of the MOR parameter obtained for a beam under monotonic loading to be used as an indicator of the fatigue performance of a full size concrete pavement under cyclic loading.

Compared to plain concrete, few studies on size effect in fibre reinforced concrete are available. It would be valuable to quantify the size effect in the high performance fibre reinforced concrete material used for UTCRCP.

Studies have indicated that fibre reinforced concrete has an improved resistance to fatigue fracture propagation in tension due to the post crack stress transfer capacity of the fibres. It is not known however whether the MOR is a suitable design parameter for this effect, as the MOR only provides an indication of the peak load capacity of a specimen. The available literature indicates that the there is a larger difference in the fatigue behaviour of FRC beams and slabs then there is for plain concrete beams and slabs.

The flexural behaviour of both plain and fibre reinforced concrete can be predicted using fracture mechanics models. Concrete pavement design approaches could benefit from the introduction of size independent fracture parameters.

Probably the most significant limitation to conventional design methods is the use of Miner's cumulative linear damage hypothesis. The hypothesis has been shown to be unsuitable for the prediction of fatigue damage evolution in concrete pavements. In future it may be possible to replace Miner's law with fracture mechanics based fatigue models.

A range of methods based on Paris' law are available, but they have found limited application. The challenge is to develop a model that can readily be adopted in general pavement engineering practice. This would require the model to use parameters that are easily determined from routine testing preferably under monotonic loading conditions. The relationship between the monotonic load displacement curve and the behaviour under cyclic loading should be explored.

Based on the findings of the literature survey, it is proposed that fracture mechanics properties obtained from monotonic tests are less susceptible to size effect and better capture the fracture toughness of the material, compared to the MOR parameter currently used in concrete pavement design. These parameters would allow a more accurate prediction of fracture propagation, both under monotonic and cyclic loading.

If a man will begin with certainties, he shall end in doubts; but if he will be content to begin with doubts he shall end in certainties.

Francis Bacon (1605)

3

Methodology

3 METHODOLOGY

In this chapter a methodology is formulated to test the main research hypothesis that the accuracy of design models for UTCRCP can benefit from the adoption of fracture mechanics concepts. The methodology is developed taking cognizance of the state of existing knowledge presented in Chapter 2.

The methodology chapter comprises three main sections. The first section on the research design delineates the approaches used to test the hypothetical propositions of this work. In Section 3.2, the structure of the experimental work is discussed as well. The selection of test methods and the experimental setup used for the study is described. To obtain a reliable estimate of the tensile strength of the fibre reinforced material, an adjusted tensile splitting procedure was developed. The FEM based numerical methodologies used in the study are discussed in Section 3.3.

3.1 Research design

The test of the main hypothesis, formulated in Chapter 1, lies in the validation of the set of three hypothetical sub-propositions.

The first of the propositions is that the high performance fibre reinforced concrete material will exhibit a strong size effect due to its distinctly non-linear behaviour in fracture. This is tested by means of laboratory experiments on specimens of different sizes. The results will be

compared to published size effect data for plain concrete. Bažant and Planas (1997) have summarized the results of size effect studies on plain concrete. A range of different test methods have been used by various researchers. The most common test configurations are the Three Point Bending (TPB) and Four Point Bending (FPB) flexural beam setup. The TPB and FPB tests are the main approaches used to explore size effect of the UTCRCP as part of this study. Testing on different sized circular panels is done as well to compare the size effect results for different geometries.

If the first proposition is supported by the experimental data, this will imply that the reliability of MOR, obtained for a specific specimen size and geometry, as a predictor of the peak load of elements of a different size and or geometry, is limited.

The second proposition states that, in contrast to the MOR, fracture mechanics can be used to more accurately and precisely predict the peak load and flexural behaviour of elements of a different size and geometry. This hypothesis is tested by numerically simulating the flexural experiments using fracture mechanics. The fracture mechanics parameters are determined for a certain specimen size and geometry and based on this a fracture mechanics model is defined for the material. The validation of the hypothesis depends on the predictive performance of the fracture mechanics model for the fracture behaviour of different sizes and geometry, in comparison to the performance of a MOR based design approach.

The final proposition pertains to the prediction of the fatigue performance of the material. It states that the accuracy, and possibly the precision, of fatigue prediction models can be improved through the use of fracture mechanics concepts. To test this hypothesis, prediction models are calibrated based on cyclic flexural tests on beams. These models are then applied to predict the fatigue performance of beams of different sizes and of centrally loaded circular panels. The precision of the models developed using the conventional approach is compared to the performance of models developed based on fracture mechanics concepts.

A requirement for the envisaged methodology is that the parameters can be determined using robust test methods that can be applied by the industry on a routine basis.

3.2 Experimental program and methods

The experimental work for this study took place in four consecutive phases. Three of the test phases were conducted at the University of Pretoria (UP). These phases focussed on the material behaviour of fibre reinforced concrete. One phase of testing took place at the University of California at Davis (UC Davis). In this phase an initial exploration of the relationship between the behaviour of plain concrete under monotonic and dynamic fatigue loading was conducted. The timeline, test configuration and objectives of the different phases are shown in Figure 3-1.

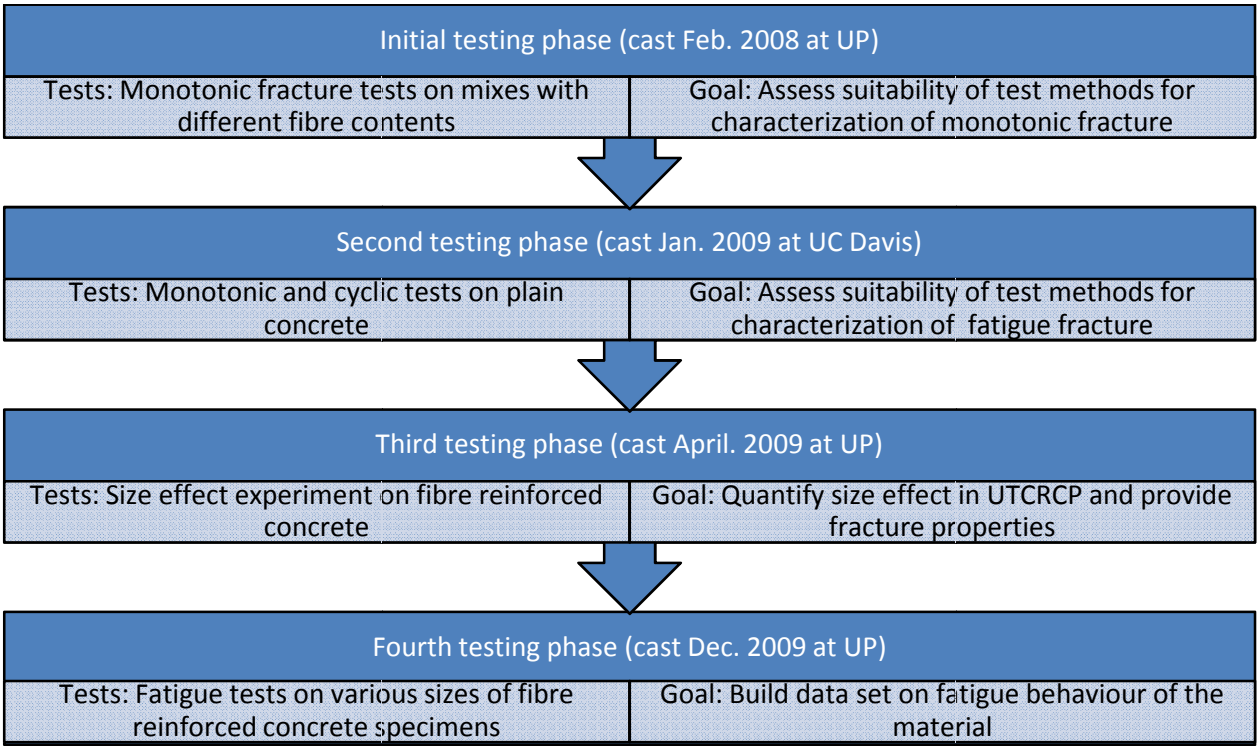

Figure 3-1: Timeline and objectives of experimental phases

The first two phases were aimed at identifying suitable test methods for the characterization of the fracture behaviour of the material under monotonic and cyclic loading. The focus in these phases was on the determination of fracture properties from the monotonic tests which could be used in fracture mechanics models.

After the test and analysis methods were developed, a size effect study on the high performance fibre reinforced material was performed in phase three.

Finally, in phase four, cyclic testing was performed in conjunction with monotonic experiments. The aim was to build a data set against which the fatigue models could be calibrated.

Each phase contains a different set of flexural tests to suit the specific objectives of that phase. The flexural test setup and mix designs are discussed per phase in the following sections. In every phase further experiments were performed as part of quality control, to determine general engineering properties and the tensile strength of the materials. These tests, reoccurring in every phase, are discussed in separate sections.

3.2.1 Phase I determining fracture properties of fibre reinforced concrete

The first mixes were cast in February 2008 at the University of Pretoria. The aim of the initial testing phase was to obtain and compare the fracture properties of two mixes. In terms of the propositions of this study, the results from this round of testing were used to develop fracture mechanics models and to show that these models can be used to predict the flexural behaviour of the material.

One mix was prepared with 80 kg/m^3 steel fibres, the other with a steel fibre content of 120 kg/m^3. The components by mass for the mix designs are shown in Table 3-1. The designs are typical for the designs used in the construction of UTCRCP.

The first round of testing was in many ways an explorative study to determine the optimum test methods for the determination of fracture properties. Beams of various sizes and geometry were tested in TPB and FPB test configurations. To investigate fracture in a three dimensional test, a centrally loaded panel circular panel on three support points was used. Table 3.2 and Table 3.3 show the dimensions of the specimens cast as part the first phase for Mixes A and B respectively. The table lists the mix type, the dimensions of the specimen and the identifier per specimen type. Individual specimens would be numbered TPB1-A-1,2,3, etc.

Table 3-1: Mix components by mass first round of testing

Component	**Type**	**Mix A [kg/m^3]**	**Mix B [kg/m^3]**
Cement	Cem I 42.5 R	450.3	448.0
Coarse aggregate	Quartzite [4.75 mm - 6.7 mm]	930.6	925.9
Fine aggregate	Quartzite [0.00 mm - 4.75 mm]	725.5	721.8
Water		170.7	169.8
Steel Fibres	Bekaert Dramix [30 mm x 0.5 mm]	80.1	119.5
Polypropylene Fibre	[12 mm]	2.0	2.0
Admixture	P100	4.0	4.0
Admixture	O100	2.5	2.5
Silica Fume (CSF)	Witbank	65.0	64.7
Fly ash	Lethabo	80.1	79.6

Table 3-2: Specimen dimensions mix A

Identifier (ID)	Type	Length (L) / Diameter (D) [mm]	Height (h) [mm]	Width (b) [mm]	Span (s) [mm]	Notch (a) [mm]	Rebar	Number cast
TPB1-A	TPB	550	150	150	500	25	-	3
TPB2-A	TPB	550	125	150	500	-	-	3
TPB3-A	TPB	550	75	150	500	25	-	3
TPB4-A	TPB	550	50	150	500	-	-	3
TPB5-A	TPB	550	150	150	500	25	3Y5.6	3
TPB6-A	TPB	550	125	150	500	-	3Y5.6	3
TPB7-A	TPB	550	75	150	500	25	3Y5.6	3
TPB8-A	TPB	550	50	150	500	-	3Y5.6	3
FPB1-A	FPB	750	150	150	600	-	-	3
FPB2-A	FPB	750	150	150	600	-	3Y5.6	3
Cu-A	Cube	100	100	100	-	-	-	12
Cyl1-A	Cylinder	150	300	-	-	-	-	3
Cyl2-A	Cylinder	75	300	-	-	-	-	3
Disk1-A	Disk	600	55	-	-	-	-	3
Disk2-A	Disk	800	70	-	-	-	-	3
Disk3-A	Disk	600	55	-	-	-	50x50x5.6 [1]	3
Disk4-A	Disk	800	70	-	-	-	50x50x5.6 [1]	3

Notes: [1] mesh reinforcement

Table 3-3: Specimen dimensions mix B

Identifier (ID)	Type	Length (L) / Diameter (D) [mm]	Height (h) [mm]	Width (b) [mm]	Span (s) [mm]	Notch (a) [mm]	Rebar	Number cast
TPB1-B	TPB	550	125	150	500	-	-	3
TPB2-B	TPB	550	75	150	500	25	-	3
TPB3-B	TPB	550	50	150	500	-	-	3
TPB4-B	TPB	550	125	150	500	-	3Y5.6	3
TPB5-B	TPB	550	75	150	500	25	3Y5.6	3
TPB6-B	TPB	550	50	150	500	-	3Y5.6	3
FPB1-B	FPB	750	150	150	600	-	-	3
FPB1-B	FPB	750	150	150	600	-	3Y5.6	3
Cu-B	Cube	100	100	100	-	-	-	12
Cyl1-B	Cylinder	150	300	-	-	-	-	3
Cyl2-B	Cylinder	75	300	-	-	-	-	3
Disk1-B	Disk	600	55	-	-	-	-	3
Disk2-B	Disk	800	70	-	-	-	-	3

The procedure for TPB to determine fracture properties as recommended by RILEM technical committee 162-TDF (RILEM, 2002) was used as the point of departure for the TPB tests. Besides the standard recommended beams of 150 mm x 150 mm cross section with a 550 mm length and a 25 mm notch, a number of other specimen sizes and geometries were used. The reason for using different cross-sections is that the typical application thickness of the UTCRCP is 50 mm. Samples with and without a notch were also included to investigate the suitability of the eventual numerical models for fracture simulation for cases with and without a pre-formed crack. A schematic representation of the TPB test setup can be found in Figure 3-2a. A picture of the TPB test setup used at the University of Pretoria is shown in Figure 3-3a.

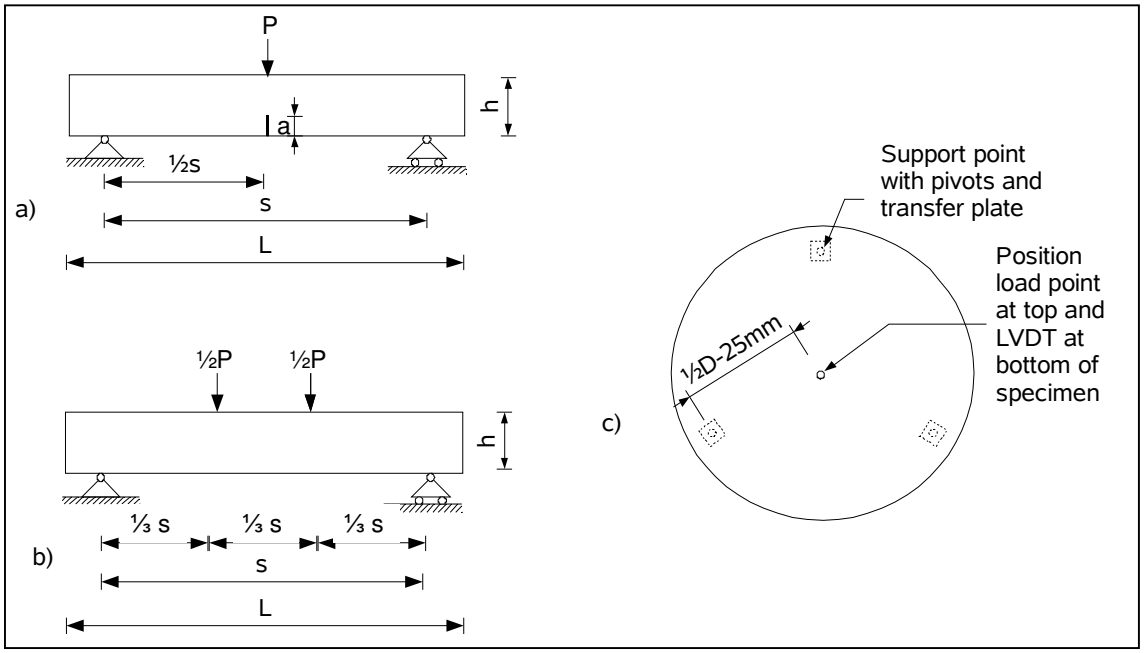

Figure 3-2a) TPB test setup, b) FPB test setup, c) Disk test configuration

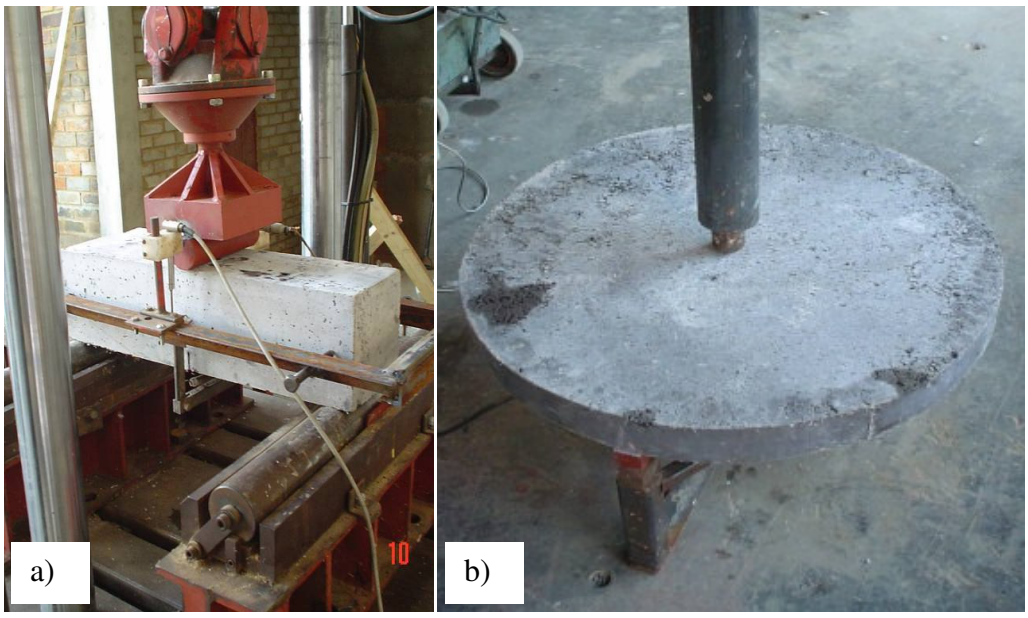

Figure 3-3a) Picture of TPB setup, b) picture of disk test setup

The FPB tests were performed on specimens without notch in accordance with Japanese test method JCI SF 4 (JCI, 1983). This test method had been used previously by Elsaigh (2007) at the University of Pretoria to successfully describe the post cracking behaviour of fibre reinforced concrete. The FPB test configuration is shown in Figure 3-2b.

In both the TPB and FPB tests the vertical displacement at mid-span was recorded by means of Linear Variable Displacement Transducers (LVDT) at either side of the beam. The reference frame for the displacement was mounted at half height of the beam specimen and mid-span displacement was measured relative to reference points above the supports. The reference frame can be seen in Figure 3-3a.

The test method for the centrally loaded concrete disks was performed in accordance with ASTM standard test method C 1550 – 05 (ASTM, 2005). Apart from the standard 800 mm diameter, 70 mm thick specimen dimension as prescribed by the standard, smaller 600 mm diameter, 55 mm thick specimens were also tested. In this test the flexural response of a centrally loaded concrete disk supported on three pivot points is measured. Figure 3-2c shows the test setup. A picture of the test is shown in Figure 3-3b. The vertical displacement is measured with an LVDT placed under the disk in line with the position of the loading point at the top of the disk. The test method is used routinely at the University of Pretoria to characterize the flexural strength of UTCRCP material (Kearsley and Mostert, 2010).

Half of the beam samples prepared at each steel fibre content contained three 5.6 mm diameter reinforcement bars. Half of the disk specimens contained a 50 mm x 50 mm x 5.6 mm mesh. The tensile yield strength (f_t) of the bars was determined in direct tensile tests as 550 MPa. The rebar was included to capture the effect of the mesh reinforcement built-in at half depth in the UTCRCP layer. The reinforcement bars were placed with 25 mm cover to either, the bottom of the specimen or, for notched specimen, the top of the notch.

All tests were run in displacement control, at the loading rates prescribed by the respective standard test methods.

An important finding from this round of testing for the subsequent experimental phases, was that fracture properties are best determined from notched TPB specimens in tests run up to high displacements.

3.2.2 Phase II fracture properties of concrete under monotonic and cyclic loading

The second phase of testing took place at the University of California, Davis (UC Davis), during an eight month work visit of the author to this university. The aim of the tests at UC Davis was to compare the fracture behaviour of concrete cyclic loading with the behaviour

under monotonic loading. During this phase the methodology to study the fatigue behaviour of concrete in flexural experiments was developed. The monotonic test results were used to further developed the fracture mechanics models and the TPB test procedure.

A plain concrete mix was used for this purpose. The mix design shown in Table 3-4 is a typical design for Portland Cement Concrete (PCC) pavements in the state of California. The specimens were cast in January 2009.

The specimen dimensions are shown in Table 3.5. To ensure stability of the TPB tests up to high displacements, a self-weight corrected geometry was used. The length of the specimens is twice the size of the span, thus ensuring that no collapse under self-weight occurs near the end of the test. The test setup at UC Davis is shown Figure 3-4a and b.

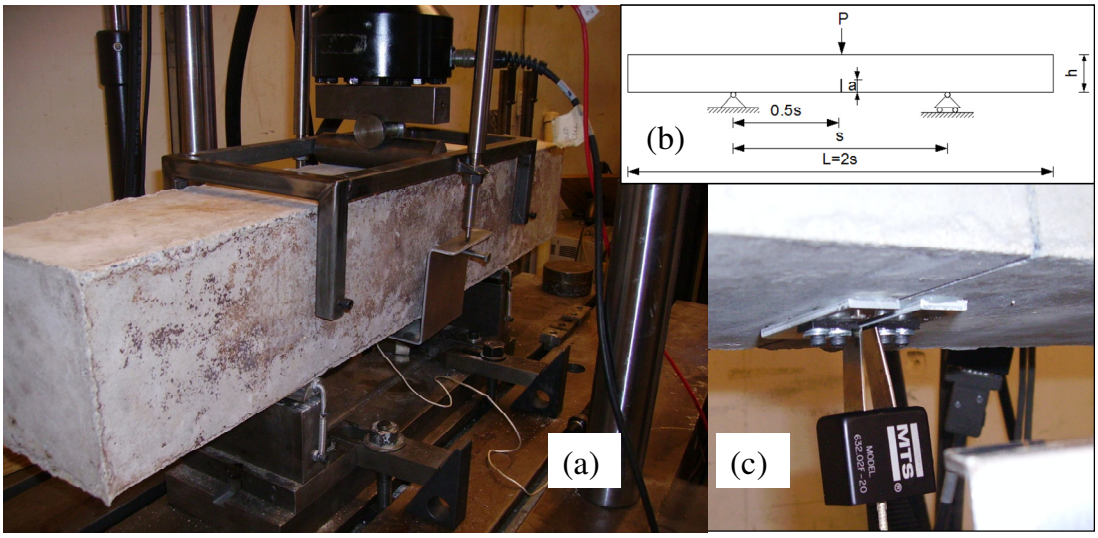

Figure 3-4a and b) TPB test configuration at UC Davis, c) Detail of the knife edges and clip gauge.

The vertical displacement was measured using LVDTs on either side of the beam in a similar fashion as was done earlier during the tests at UP. In addition to the vertical displacement, the opening of the crack was measured by means of a clip gauge mounted to knife edges on either side of the notch. A detail of the clip gauge measuring the Crack Mouth Opening Displacement (CMOD) is shown in Figure 3-4c. The clip gauge allows a more sensitive measurement of the fracture behaviour of the specimens. The range of the clip gauge is

however, limited to about 5 mm, therefore the vertical LVDTs are relied upon to measure the behaviour at larger displacements.

The loading rate for the monotonic tests was set to 0.5 mm per minute, which is equal to the loading rate used during the experiments at UP. The fatigue tests were performed in load control. A haversine loading was applied at a frequency of 4 Hz. The loading amplitude was set to various percentages of the peak load obtained in the monotonic tests. The load-displacement response in terms of vertical displacement and CMOD was recorded at sampling rates of at least 10 Hz.

Table 3-4: Mix components by mass testing at UC Davis

Component	Type	[kg/m^3]
Cement	Type II-V	306.9
Coarse aggregate	Granite [19 mm- 38 mm]	593.7
Coarse aggregate	Granite [4.75 mm – 25 mm]	593.7
Fine aggregate	Granite [0.00 mm -4.75 mm]	768.8
Water		168.0

Table 3-5: Specimen dimensions mix C

Identifier (ID)	Type	Length (L) / Diameter (D) [mm]	Height (h) [mm]	Width (b) [mm]	Span (s) [mm]	Notch (a) [mm]	Number cast
TPB1-C	TPB	914.4	152.4	152.4	457.2	50.8	3
TPBF1-C	TPB fatigue	914.4	152.4	152.4	457.2	50.8	9
Cyl1-C	Cylinder	150	300	-	-	-	14

The results showed that the use of weight corrected specimens in the TPB test allows for stable tests up to high deflections. This approach was used in the subsequent test phases to obtain a better measure of the fracture properties of the materials.

3.2.3 Phase III Size-effect in fibre reinforced concrete

In April 2009 specimens were cast at UP cast for a third round of testing. The objective was to investigate size-effect in fibre reinforced concrete. Weight corrected TPB specimens were cast, using the mix design shown in Table 3-6. The mix contained 120 kg/m^3 steel fibres. Beam specimens of three different sizes were cast while maintaining the geometry. In other words, the depth to span and notch to depth ratios were kept constant for all sizes. The beam

geometry is as shown in Figure 3-4c. In this round of testing the combination of a frame with LVDTs to monitor vertical displacement and a clip gauge to measure the CMOD was again used. Once the specimens were broken in the TPB tests, the halves were tested again in FPB test configuration (as shown in Figure 3-2b), thus providing an indication of size effect in both TPB and FPB. The smallest, 50 mm deep, specimens could not be tested in FPB due to the fact that their span was too short for the testing equipment. Since the FPB test specimens do not contain a notch vertical displacement only was measured during the tests. All tests were run in displacement control at a constant displacement rate of 0.5 mm per minute.

Table 3-6: Mix components by mass mix D

Component	Type	[kg/m^3]
Cement	Cem I 42.5R	464.5
Coarse aggregate	Quartzite [4.75 mm - 6.7 mm]	865.9
Fine aggregate	Quartzite [0.00 mm - 4.75 mm]	750.5
Water		176.1
Steel Fibres	Bekaert Dramix [30 mm x 0.5 mm]	120.2
Polypropylene Fibre	[12 mm]	2.0
Admixture	O100	4.4
Admixture	P100	3.0
Silica Fume (CSF)	Witbank	63.8
Fly ash	Lethabo	78.5

Table 3-7: Specimen dimensions mix D

Identifier (ID)	Type	Length (L) / Diameter (D) [mm]	Height (h) [mm]	Width (b) [mm]	Span (s) [mm]	Notch (a) [mm]	Number cast
TPB1-D	TPB	330	50	150	165	16.5	3
TPB2-D	TPB	1000	150	150	500	50	3
TPB3-D	TPB	1500	225	150	750	75	3
FPB1-D	FPB	500	150	150	450	-	3
FPB2-D	FPB	750	225	150	675	-	3
Cu-D	Cube	100	100	100	-	-	9
Cyl1-D	Cylinder	150	300	-	-	-	9

3.2.4 Phase IV fatigue in fibre reinforced concrete.

The final set of specimens were cast in December 2009 at UP. The main aim of this experimental phase was to explore the fatigue behaviour of the high performance fibre reinforced concrete under cyclic loading. Specimens of various sizes were cast to investigate the occurrence of size effect in fatigue. For each size a set of specimens was cast for

monotonic testing as well. The monotonic testing was included to further explore size effect, to determine the static fracture properties and to compare the fracture results from monotonic experiments to the fatigue behaviour of the material. The test results from this phase provided the data set for the development of conventional and fracture mechanics based fatigue models. The mix design containing 80 kg/m^3 steel fibres is shown in Table 3-8.

Table 3-8: Mix components by mass mix E

Component	**Type**	**[kg/m^3]**
Cement	Cem II 52.5 N	450.0
Coarse aggregate	Dolomite [4.75 mm – 9.5 mm]	950.0
Fine aggregate	Dolomite [0.00 mm - 4.75 mm]	900.0
Water		165.0
Steel Fibres	Bekaert Dramix [30 mm x 0.5 mm]	80.0
Polypropylene Fibre	[12 mm]	2.0
Admixture	O100	4.0
Admixture	P100	4.0
Silica Fume (CSF)	Witbank	50.0

TPB, FPB and disk specimens were cast as part of this experimental phase. An overview of the specimen types is provided in Table 3-9. TPB samples were produced with the weight corrected geometry shown in Figure 3-4c. TPB specimens were tested under monotonic loading only to obtain fracture mechanics properties for the mix. Both the vertical displacement and the CMOD were measured during the tests using the same procedure as in the previous two phases. The FPB and centrally loaded disk specimens were tested under both monotonic and cyclic loading. The peak load was obtained from the monotonic tests and the cyclic loads and the cyclic test were run at different ratios of the average monotonic peak load.

Table 3-9: Specimen dimensions mix E

Identifier (ID)	Type	Length (L) / Diameter (D) [mm]	Height (h) [mm]	Width (b) [mm]	Span (s) [mm]	Notch (a) [mm]	Number cast
TPB1-E	TPB	900	150	150	450	50	10
FPB1-E	FPB	500	150	150	450	-	10
FPB2-E	FPB	350	100	100	300	-	5
FPB3-E	FPB	200	50	50	150	-	5
FPBF1-E	FPB fatigue	500	150	150	450	-	20
FPBF2-E	FPB fatigue	350	100	100	300	-	20
FPBF3-E	FPB fatigue	200	50	50	150	-	20
Disk1-E	Disk	600	55	-	-	-	3
DiskF1-E	Disk fatigue	600	55	-	-	-	18
Cu-E	Cube	100	100	100	-	-	12
Cyl1-E	Cylinder	150	300	-	-	-	12

The vertical displacement was measured at a sampling rate of 10 Hz during both monotonic and cyclic FPB tests. The monotonic tests in both TPB and FPB setup were run in displacement control at a constant displacement rate of 0.5 mm per minute. The cyclic tests were run in load control, the haversine loading was applied at a frequency of 2 Hz. Figure 3-5 shows the test setup for the smallest of the FPB specimen types.

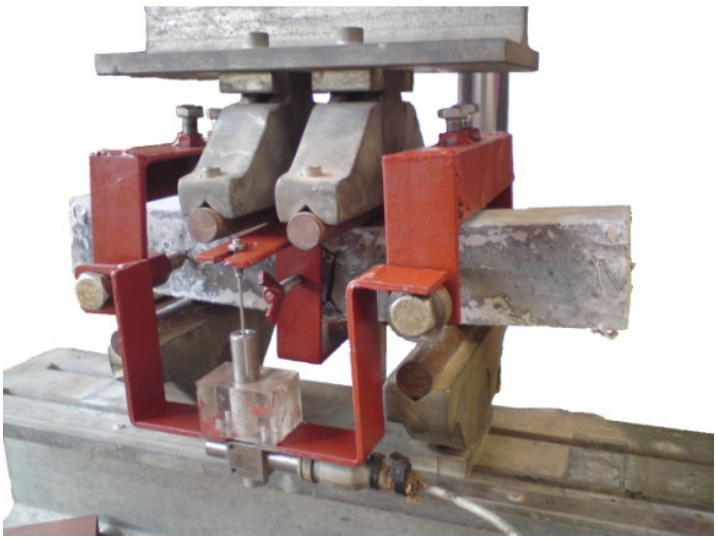

Figure 3-5: Picture of test setup for FPB3-E and FPB3F-E

The monotonic load experiments on the disk specimens were performed using the procedures as discussed for the first testing phase. The cyclic loading tests were conducted using a haversine load wave at a frequency of 2 Hz.

3.2.5 Determining engineering properties

In each test phase, specimens were cast to determine the compressive strength (f_c) as a quality control measure. Specimens were also produced to determine static modulus of elasticity E and Poisson's ratio υ. The static E and υ are used as material properties for the linear elastic part of the material behaviour in the numerical simulations performed as part of this study. The tests were performed in accordance with local test methods. At the University of Pretoria the compressive strength tests were performed on cubes (denoted "Cu" in the specimen tables of the previous section) in accordance with British Standard BS 1881 (BSI, 1983). Cylindrical specimens (denoted "Cyl1-C" in Table 3-5) were used to determine the compressive strength at UC Davis in accordance with ASTM C 39 (ASTM, 2008a) At both universities the tests to determine E and υ were performed in accordance with the standard procedures contained in ASTM C469-02 (ASTM, 2008b).

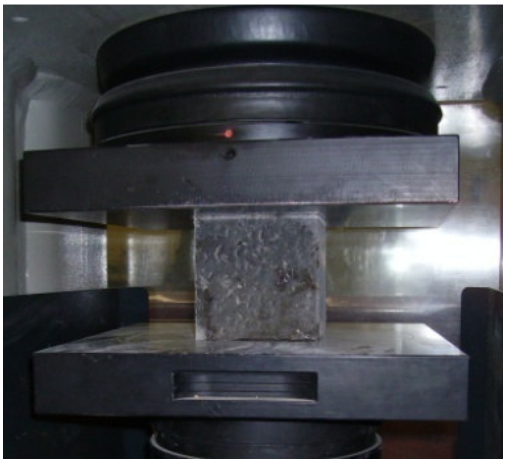

Figure 3-6: Compressive strength test setup at UP

3.2.6 Determining tensile strength

The tensile strength (f_t) is a key material parameter for fracture mechanics based analysis of concrete structures. It is generally determined using either a direct tensile test or splitting

tensile test setup. Both tests are simple in concept, but have proven quite complicated to run in such a way that reliable results, independent of specimen size and boundary conditions, are obtained. Additional challenges occur when the aim is to obtain a reliable measure of f_t for FRC, as is the case in this study.

The complexity of the direct tensile test concerns mainly the selection of specimen size. Bažant (2002) points out that if a small specimen size is selected the development of the fracture process zone is hindered by the boundary conditions. If on the other hand, a large specimen size is selected the crack does not form uniformly over the cross-section causing the sample to flex sideways, in which case the load condition at fracture is no longer purely uniaxial. This poses a problem for concrete mixes containing large fibres, such as steel fibres. For these mixes relatively large tensile specimens are required to ensure a fibre dispersion in the ligament area representative of the dispersion found in full-size structures. Direct tension tests on 300 mm long, 100 mm diameter cylinders were attempted as part of this study, but had to be abandoned. The specimens without exception cracked at the interface between the fixture and the cylinder. This indicated that the specimens did not fail in direct tension, but due to a stress concentration at the boundary. The results were therefore invalid and are not reported.

The splitting tensile test, also known as the Brazilian test, is typically performed on 150 mm diameter by 300 mm length cylindrical specimens. These dimensions are appropriate to create representative samples for most fibre reinforced concrete mixtures. Like the direct tension test though, the splitting tensile test is known to have a number of limitations. For normal strength concrete the empirically obtained split tensile strength can be expected to be 10 to 40 per cent higher than the actual uniaxial strength of the material (Olesen et al., 2006). Importantly for this study, Olesen et al. (2006) have shown that in the standard configuration the test cannot be used to obtain the tensile strength of FRC due to the ductility of the material.

The challenges in using the split cylinder test for both plain and fibre reinforced concrete are caused by the difference between the simple boundary conditions and linear elastic material behaviour assumed in the continuum mechanics model of the test, and the actual boundary conditions of the test and the non-linear material response. As part of this study an adjusted tensile splitting test procedure was developed to obtain a close estimate of the true tensile strength of fibre reinforced concrete. The methodology addresses the shortcomings of the

tensile splitting test for this purpose, by combining concepts introduced by various researchers in this field. The method can be summarized as follows: The linear elastic tensile stress calculation for the test is corrected for the influence of the width of the load strip by using the equation Tang (1994) recommended. The fracture mechanics size-effect, which is due to the quasi-brittle material behaviour of concrete, is reduced to acceptable proportions based on the recommendations by Rocco et al. (1999a, 1999b). Finally, the limit between linear elastic pre-crack behaviour and the ductile post crack behaviour of FRC is identified by monitoring transversal deformation perpendicular to the load direction during the test.

The calculation of the maximum principal stress in the splitting test is based on the two dimensional problem shown in Figure 3-7a.

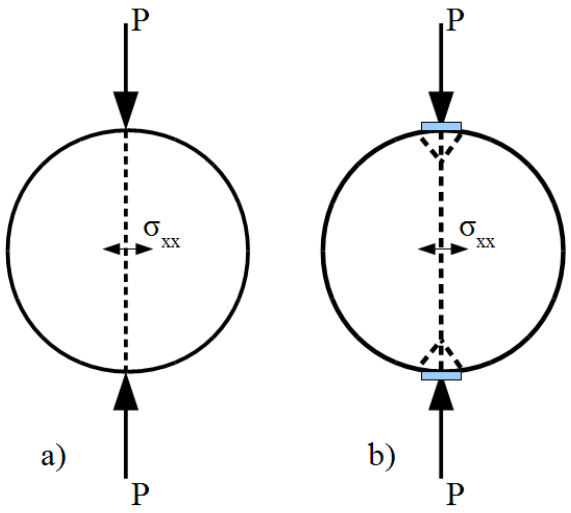

Figure 3-7a: Assumed load condition tensile splitting test, b: Actual load condition

The plane stress continuum mechanics solution for this problem provided by Timoshenko and Goodier (1970) allows calculation of the horizontal normal stress (σ_{xx}) along the loading axis of two equal and opposed point loads using Equation 3.1.

$$\sigma_{xx} = \frac{2P}{\pi D} \tag{3.1}$$

Where D is the specimen diameter and P is the magnitude of the point loads. A point load in the plane stress problem corresponds to a load per unit length of the specimen in the three

dimensional situation, which is how P is used throughout this section on tensile splitting tests. The load causes a uniform tensile stress state along the loading axis of the specimen. The actual loading condition in the splitting test setup (shown in Figure 3-7b) differs from the assumed situation of Figure 3-7a.

In reality the loads are introduced to the specimen by means of a loading strip with a certain width and not as point loads. The loading strip results in a non-uniform distribution of the normal stress along the loading axis of the specimen, with a compressive zone in the material near the contact area of the load strip. The size of the compressive zone depends on the size of the load strip and the condition leads to an overestimation of f_t obtained from Equation 3.1 (Rocco et al., 1999b). Tang (1994) corrected the linear elastic plane stress solution for the presence of a load strip with a finite width. Based on the correction by Tang (1994) the horizontal normal stress at the centre of the cylinder may be calculated using:

$$\sigma_{xx} = \frac{2P}{\pi D}\left[1-\left(\frac{b_1}{D}\right)^2\right]^{\frac{2}{3}} \tag{3.2}$$

Where b_1 is the width of the load strip. This correction results in a downward adjustment of the maximum stress of 4 % if the size of the load strip is within the specifications of ASTM 496 (ASTM, 2008b). The correction of the linear elastic load condition therefore accounts only for a small portion of the overestimation of f_t reported for splitting tensile tests.

A larger proportion of the difference between the splitting tensile strength and the true tensile strength is due to the quasi-brittle material behaviour of concrete and the related fracture mechanics size effect. Rocco et al. (1999a, 1999b) investigated the influence of the fracture mechanics size effect on the results of the tensile splitting test. Their analysis indicates that differences of up to 40 per cent in tensile strength can be found depending on the width of the load strip and the applied loading speed. In a later publication, Rocco et al. (2001) reported a 30 per cent difference in tensile strength values between much used international standards, i.e. ASTM C-469, ISO 4105 and BS 1881-117. They proposed that the split cylinder test can yield a true indication of the tensile strength as long as the width of the loading strip does not exceed 8 per cent of the diameter of the specimen and the speed of loading does not exceed 1.0 MPa/min (Rocco et al., 1999a).

The assumed fracture mode in the calculation of the tensile stress in current standard methods, using Equation 3.1, is rupture starting at the centre of the specimen. The crack would grow in the direction of the highest stress, i.e. towards the loading strips. In a study on mechanisms of rupture in the splitting test, Rocco et al. (1999c) found that this primary mode of failure, schematically shown in Figure 3-8a, is followed by secondary cracking, as shown in Figure 3-8b. This implies that after the tensile strength of the material is reached and a crack has formed in the centre of the specimen along the loading axis, the stresses redistribute and new highly stressed areas appear. By measuring the transversal deformation during the test, Rocco et al. (1999c) found that both the principal crack formation and secondary crack formation have a peak as shown in Figure 3-8c. The relative position of the peaks varies depending on material type and specimen geometry. In a situation where the secondary peak load exceeds the principal peak load, the tensile strength calculated using Equation 3.1 would be invalid.

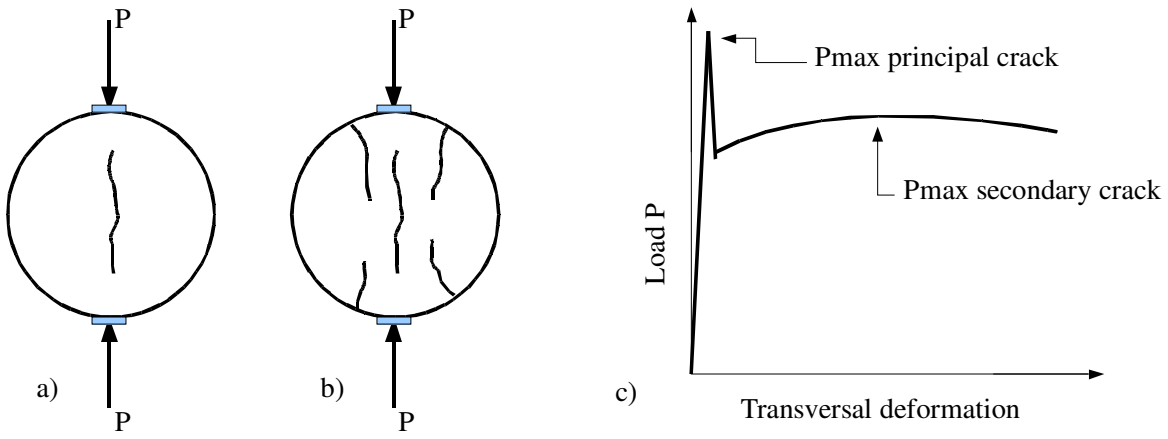

Figure 3-8: a: Principal crack formation, b: Secondary crack formation, c: schematic load-deformation curve (after Rocco et al., 1999c).

Adjusted split cylinder tests were performed to obtain the tensile strength for the high performance fibre reinforced concrete mixes under study. The test configurations used for the study are shown in Figure 3-9. For the experiments on mixes A, B and D the spring loaded LVDTs were held by fixtures mounted to the base plate in the test machine as shown in Figure 3-9a.

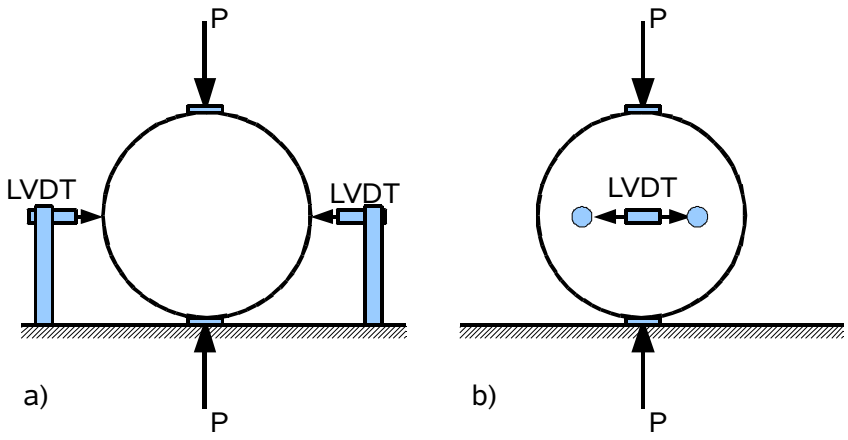

Figure 3-9: a: Initial test configuration, b: Improved test setup

The LVDTs were positioned at centre line of the specimen and at the centre of its length. A more advanced measuring system was developed for the tests performed on mix E. For this last mix the transversal deformation was measured using LVDTs mounted to datum points which were glued to the specimens. Measurements were taken on both sides of the cylinder.

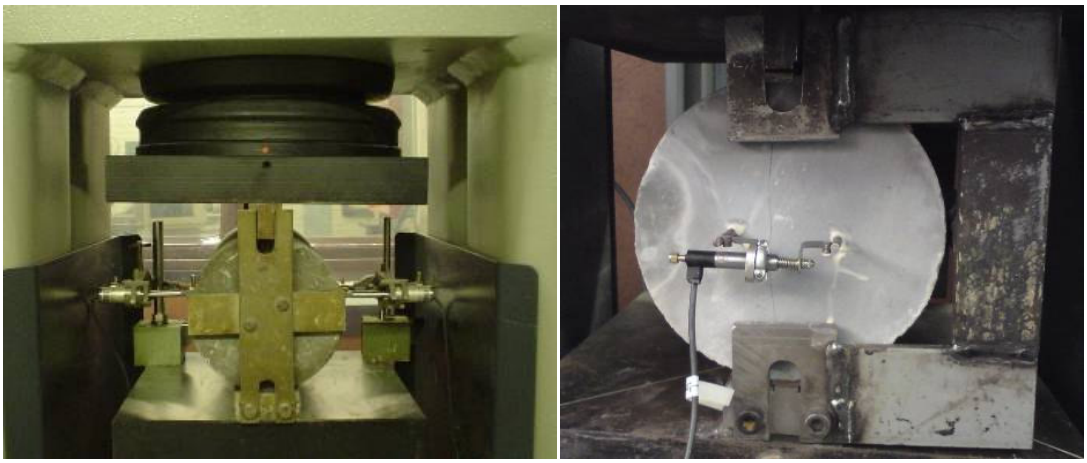

Figure 3-10: Photos of split cylinder test setup

The setup is shown schematically in Figure 3-9b. Photos of both test configurations are shown in Figure 3-10. In accordance with the recommendations for reduction of size effect

by Rocco et al. (1999a), a loading strip of 12mm width (8 % of the diameter) was used and the loading rate was kept at 1 MPa per minute for all tests.

The measurement of transversal deformation using LVDTs has a limited precision, especially when the fixtures are mounted to the base plate as was done for the first mixes. The objective however is to identify the point at which the linear elastic stress distribution ceases to exist, for which purpose the method was found to be adequate.

For the plain concrete (Mix D), measurement of the transversal displacement was deemed unnecessary to obtain reliable results. Therefore, the standard test configuration in accordance with ASTM C-469 was used.

3.3 Selection of numerical simulation methods

An overview of relevant fracture mechanics approaches was provided in Section 2.5 of this document. Importantly, Elsaigh (2007) had previously used a smeared crack approach to model fracture in similar materials as part of his PhD studies at the University of Pretoria. Elsaigh reported considerable difficulty in implementing the highly non-linear fracture behaviour of the material in the MSC.Marc (Mentat, 2003) finite element software.

The selection of the numerical methods for this study was largely dictated by the availability of suitable methods. The study employs both discrete and smeared crack approaches to simulate fracture. Two software platforms were used at different stages of the study. Initially, the open source FEM framework OpenSees (OpenSees, 2008) was used for the modelling of fracture in beams. In OpenSees software discrete fracture was modelled in two dimensional space by means of the Embedded Discontinuity Method (EDM). When, at a later stage in the study, modelling of fracture in three dimensional space became required, the commercial FEM code Abaqus (Abaqus, 2009) was acquired. In Abaqus, a cohesive fracture approach was used for the simulation of cracking in the three dimensional flexural disk tests as well as two dimensional simulation of the tensile split cylinder test. Earlier attempts to simulate the splitting test using the EDM approach had been unsuccessful. Due to the large “snap back” in the response of the cylinder when a crack is formed the calculation using OpenSees software failed to converge. Abaqus can be set to automatically adjust the number of iterations per load step and this made simulation of the split cylinder test possible. A simplified model of a

pavement structure is also analysed in Abaqus, using a cohesive crack damage model for the concrete slab.

3.3.1 Modelling of flexural beam tests with EDM in OpenSees

As part of a work visit to the University of California at Davis, the author assisted in the validation of the EDM code implemented in Opensees as later published by Wu et al. (2009). The EDM is based on work by Simo et al. (1993), Oliver (1996a, 1996b) and Sancho et al. (2007).

The EDM takes its name from embedding the Strong Discontinuity Approach (SDA) within finite elements. A strong discontinuity is typified by *"the occurrence jumps in the displacement field appearing at a certain time, in general unknown before the analysis, of the loading history and developing across paths of the solid which are material (fixed) surfaces"* (Oliver, 1996b). Essentially, EDM adds internal nodes to cracked elements. The extra degrees of freedom associated with these internal nodes are used to describe the displacement jumps (both in shear and opening) across crack faces. Internal nodes do not show up in the global stiffness matrix for finite element analysis, allowing the flexibility of adding them or removing them in any element without affecting the overall analysis. An advantage of SDA and therefore EDM over more conventional discrete crack models, such as cohesive crack interface element models, is that it allows cracks to propagate through elements, in other words, independent of nodal positions and element boundaries. EDM differs from so-called smeared crack or crack band approaches in that it forms a discontinuous cracked surface. The use of displacement rather than strain to enforce softening has as important advantage that EDM does not suffer from mesh size dependencies. The constitutive equations of the EDM formulation used for the present study are as published in Wu et al. (2009). The methodology uses the efficient crack adaptation technique to prevent crack locking developed by Sancho et al. (2007).

The cracking function in the EDM is based on the principles of the cohesive crack model introduced by Hillerborg et al. (1976), discussed in Section 2.5. According to the cohesive crack approach a crack is induced when the stress in the material reaches the tensile strength (f_t) of the material. After the crack has formed, stresses will still be transferred over the crack, however, the amount of stress transferred reduces as the crack width increases.

In the flexural beam tests, crack growth due to shear stress should be negligible. The characterization of shear damage evolution requires specialized testing, not undertaken as part of this study. The EDM code used in this study does however allow for tension, shear and mixed mode fracture to occur where applicable. In the implementation, the shear softening curve is exactly the same as tension softening curves. The traction across the crack faces is the vector sum of the crack opening (tension) and crack sliding (shear) traction. The total traction vector has the same direction as the relative opening movement. The magnitude of the traction vector is determined by the softening function using the magnitude of the total crack opening displacement.

The EDM was implemented in OpenSees using three-node triangular elements. The model geometry and meshes were created using Gmsh (Geuzaine and Remacle, 2009) pre- and post-processor software. Routines in this opensource software were adjusted by the author to allow the creation of mesh definitions that are compatible with the OpenSees code.

A typical example of a two dimensional mesh used in the simulation of a TPB test on a notched specimen is shown in Figure 3-11. In principle it is possible to use embedded discontinuity elements for the entire geometric model. This will allow the crack to form at the position in the specimen with the highest tensile stress. In simulation of the notched TPB tests however, the crack will always form directly above the notch. To make the calculation more efficient, the elements with embedded discontinuity were arranged in a vertical band above the notch as shown in Figure 3-11. A characteristic length of 1.0 mm was used for the EDM elements in the analysis of all specimens. The remainder of the material is modelled using LE bulk elements.

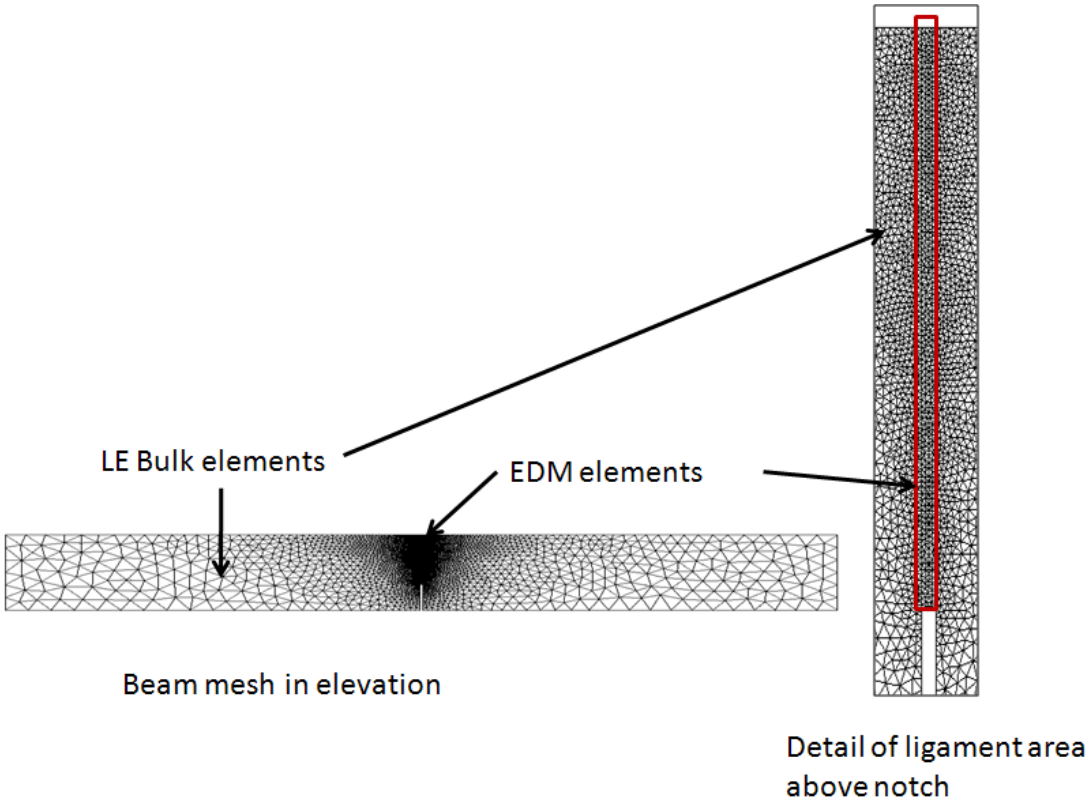

Figure 3-11: Example of TPB finite element mesh

3.3.2 Modelling of centrally loaded panels and split cylinder tests using Abaqus

The commercial FEM software package Abaqus includes a number of fracture mechanics models that can be applied to concrete. Amongst these is a brittle cracking model intended specifically for the simulation of fracture in concrete. The approach follows the smeared cracking assumption as discussed in Section 2.5.5. Damage evolution however, takes place using the cohesive crack model by Hillerborg et al. (1976) rather than strain softening. This to remedy the mesh size sensitivity problem of conventional smeared crack approaches (Dassault Systèmes, 2009). Because the Abaqus brittle crack model uses the cohesive crack principle for damage evolution in the principal tensile stress direction, the same softening functions can be used for the numerical simulation in both Abaqus and OpenSees.

In contrast to the EDM in which both shear and tension are handled using a crack width softening function, the brittle cracking model in Abaqus has a separate strain softening function for shear. The reason for the combination of a mode II strain softening model with a mode I displacement softening model, instead of displacement softening for both modes is not clear from the documentation. To ensure that the response of the Abaqus model in shear

was similar to that in the EDM simulation, the shear strain softening function was defined in accordance with the function in Equation 2.15. This equation relates the strain softening in smeared crack models to the softening as function of crack width in cohesive crack models.

Figure 3-12 shows the geometry of the numerical model for the tensile splitting test. Owing to symmetry, only a quarter of the cylinder test needs to be modelled.

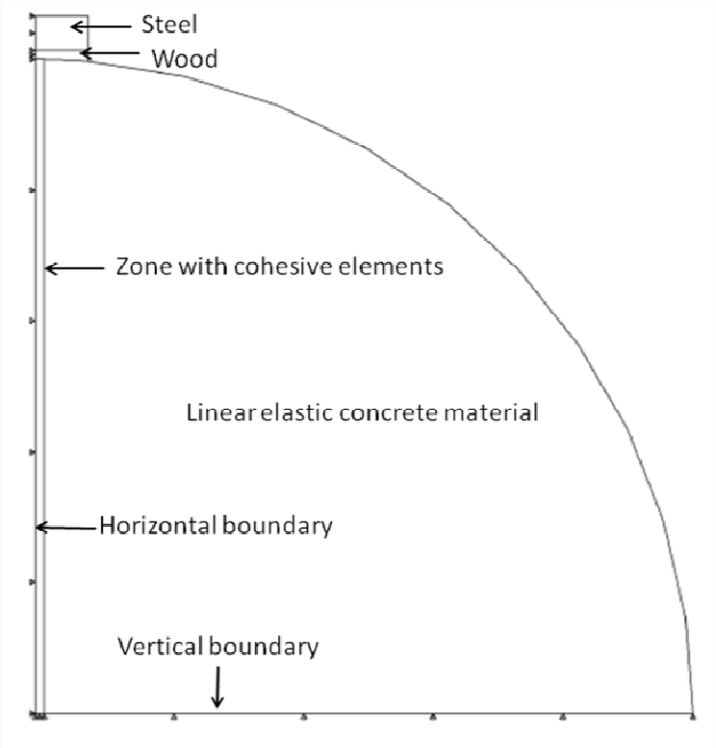

Figure 3-12: Geometry of numerical model for splitting test

A vertical zone of 1 mm x 1 mm sized, standard Abaqus plane stress cohesive elements with the brittle fracture model was provided along the loading axis. The brittle fracture elements behave linear elastically based on the values for E and υ obtained for the material until the tensile strength is reached, after which damage evolves as defined by a cohesive crack model to be developed for the material in Chapter 5. The behaviour of the remainder of the concrete section is simulated using plain stress linear elastic bulk elements. To accurately simulate the load introduction to the specimen, the steel loading strip and the plywood interface strip are also modelled. An E value of 210 GPa and υ value of 0.25 were assumed for the steel. Values of E= 5 GPa and υ= 0.3 were assumed for the plywood.

Numerical simulation of the centrally loaded disk test was also performed using Abaqus. The layout of the test is shown schematically in Figure 3-13a. Owing to symmetry, only one sixth of the disk needs to be modelled. The geometry and boundary conditions are shown in Figure 3-13b. This simplification considerably increases the efficiency of the numerical simulation. The disks are analysed both using LE material properties and a fracture mechanics damage model. For the LE analysis all elements used for the model were LE bulk elements. For the fracture mechanics analysis, the LE bulk elements in the areas indicated in Figure 3-13b were replaced by elements with a fracture mechanics damage definition. The support point is connected to a surface corresponding to the area of the transfer plate under the panel using a kinematic rigid coupling. Standard Abaqus 8 node brick elements of the C3D8R type were used for the mesh. The characteristic size of the elements throughout the model is 5 mm, with exception of the area around the support, away from the highly stressed areas, where a size of 15 mm was used.

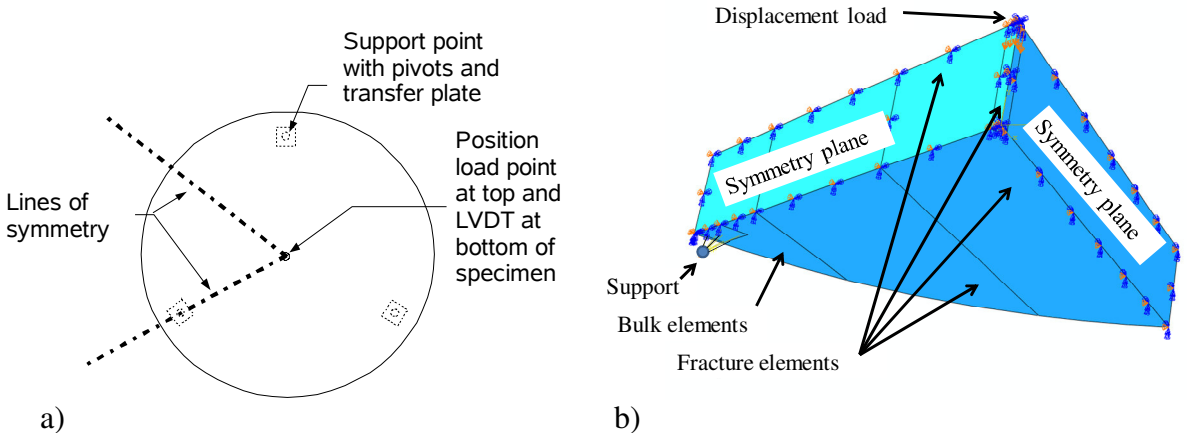

Figure 3-13a: Geometry of test, b: Geometry and boundary conditions of model

3.4 Discussion on the methodology

The research methodology was developed to test the different hypotheses of this work. The first proposition is that high performance fibre reinforced concrete material will exhibit a strong size effect due to its distinctly non-linear behaviour in fracture. The size effect for the high performance fibre reinforced concrete material under monotonic and cyclic loading is quantified using a FPB tests on beams of different sizes, but of a constant geometry. Tests on

centrally loaded disks of different sizes under monotonic loading are included in the experimental matrix for size effect as well,

According to the second proposition, fracture mechanics can be used to more accurately and precisely predict the peak load and flexural behaviour of elements of a different size and geometry. To test this hypothesis, fracture properties are determined from TPB tests on weight corrected beam specimens with a notch. The tensile strength is obtained from an adjusted tensile splitting test procedure. The fracture mechanics properties obtained from these tests are then used in the definition of a cohesive crack function for the material. The cohesive crack model, or softening function, is implemented in finite element software to simulate the fracture behaviour observed in the experiments for specimens of different sizes and geometries.

The third proposition states that the accuracy, and possibly the precision, of fatigue prediction models can be improved through the use of fracture mechanics concepts. To test this hypothesis, cyclic tests are performed on FPB beam and centrally loaded disk specimens. The behaviour of the material in the cyclic loading tests is compared to the behaviour in the monotonic loading experiments. The aim is to calibrate a conventional and a fracture mechanics based prediction model against the fatigue results of the FPB beam tests. These models will then be used to predict the fatigue life of the centrally loaded disks and of beams of different sizes.

The results for the tests of the three propositions will be used to evaluate the main hypothesis of the study that the accuracy of design models for the high performance fibre reinforced concrete used in UTCRCP can benefit from the inclusion of fracture mechanics concepts.

Meten is weten

"To measure is to know"

Dutch proverb

4

Fracture experiments

4 FRACTURE EXPERIMENTS

This chapter contains the results and analysis of the experimental work performed according to the research methodology presented in the previous chapter. The main objectives of the chapter are to determine the fracture properties, to study size effect, and to explore the fatigue behaviour of the high performance fibre reinforced material.

The general engineering properties determined for the materials tested in the different phases are presented in Section 4.1. The data processing and presentation techniques used for the flexural test are discussed in Section 4.2. The outcomes of the size effect study on the high performance fibre reinforced material are presented in Section 4.3. In Section 4.4, a method is developed to determine the specific fracture energy G_f from TPB experiments. Another key fracture property of the material, the tensile strength (f_t), is determined from an adjusted tensile splitting procedure in Section 4.5. The results of the cyclic flexural tests are analysed in Section 4.6, followed by a discussion on the main findings of the experimental work in Section 4.7.

4.1 Engineering properties

The average results for the compressive strength (f_c), Young's modulus (E) and Poisson's ratio (υ) for all mixes are shown in Table 4-1. These general engineering properties were obtained using the procedures discussed in Section 3.2.5. The results for the f_c, are based on six specimens per mix type, the results for E and υ are based on three tests per mix types.

The results for the high performance concrete mix designs (A, B, D, E) show an upward trend in the values of the f_c and E with time. This was unintentional. The mix designs did not change significantly for the different phases. The increase of the f_c is believed to be a function of changes in cement quality over the course of the project. During this time period similar trends were observed in experiments on concrete at the UP laboratory unrelated to this project.

Table 4-1: Average engineering properties for all studied mixes

	f_c [MPa]	Std.dev. [MPa]	E [GPa]	Std.dev. [GPa]	υ	Std.dev.
Mix A	108.9	7.4	49.6	0.5	0.14	0.023
Mix B	115.5	4.9	46.3	0.3	0.16	0.012
Mix C	40.8	4.4	31.2	6.4	0.20	0.040
Mix D	125.5	4.7	49.7	0.7	0.17	0.005
Mix E	137.2	6.0	62.9	0.7	0.15	0.005

4.2 Presentation of monotonic flexural test results

The results of all flexural tests under monotonic loading conducted as part of this study are presented in Appendix A. The results are plotted in terms of load versus vertical displacement as measured during the test using LVDTs. A typical example of such a curve is shown in Figure 4-1a. In the later experimental phases, the CMOD was recorded in addition to the vertical displacement for the notched TPB specimens. An example of a load-CMOD curve is shown in Figure 4-1b.

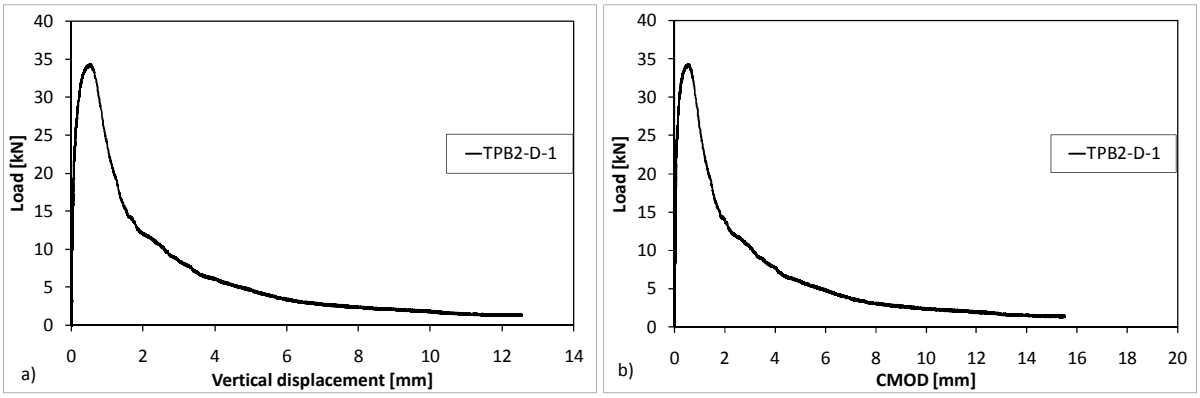

Figure 4-1: Example of load-displacement curve, b: Example of load-CMOD curve

The test matrix contains specimens with and without weight correction. A weight corrected specimen has a length of twice the size of the span thus, the initial moment due to self weight at the centre of the span is approximately zero. If a specimen is tested without weight correction, a load due to self weight is introduced when the specimen is placed in the test rig. The influence of this offset in load on the flexural capacity of the beam will not be captured in the load-deflection curve of the subsequent bending test unless a correction is made. To take the initial load P_0 due to self-weight into account, the load-displacement curve for these tests is shifted up by:

$$P_0 = \frac{4M_0}{s} \tag{4.1}$$

Where M_0 is the bending moment at centre span due to self weight, calculated assuming a density of 2500 kg/m^3 for the material. Where required, the results for flexural tests on beams presented in this document have been corrected for self weight using this procedure. The corrected load-displacement curves are used to evaluate the flexural results for size effect in Section 4.3 and from them the specific fracture energy is determined in Section 4.4.

4.3 Size effect

According to linear elastic limit state design theory, failure will occur when a certain critical level of stress or strain is reached in a structural element, regardless of the size of the element. Under this assumption it should be possible to use the elastic limit determined for a flexural beam test, to for example predict the peak load of a slab in flexure. As discussed in Chapter 2, this approach is known to have limitations for application to concrete, due to the occurrence of size effect. In this section, size effect in the UTCRCP material is quantified. To this aim, beam and disk specimens of different sizes were tested while maintaining geometry.

4.3.1 Size effect in flexural beam tests

Table 4-2 shows the ultimate nominal stress (σ_{Nu}) results per specimen type for the different mixes. The nominal stress (σ_N) (at any load level) is calculated for FPB tests using Equation 2.1 and for TPB tests using Equation 2.2 introduced earlier in the document. The table shows that for each mix type the average value of σ_{Nu} varies for the different sizes and

test configurations (i.e. TPB, FPB). To investigate the size dependency of σ_{Nu}, specimens of different sizes were tested while maintaining the geometry. These series of specimens tested as part of phase three and four (Mixes D and E) have different heights, but a constant span to height (*s/h*) and notch dept to height (*s/a*) ratios. For the tests on Mix E specimens geometry was maintained in all three dimensions, i.e. the width to height ratio (*b/h*) was also kept constant. The results of the size effect investigation discussed below were published as part of this study in Denneman et al. (2010a) and Denneman et al. (2010b).

Table 4-2: σ_{Nu} results flexural beam tests

Specimen type	*s/h*	*a/h*	*b/h*	σ_{Nu} [MPa]	Std.dev. [MPa]	Number of specimens
Mix A						
TPB1-A	3 1/3	1/6	1	13.3	1.08	3
TPB2-A	4		1	13.5	1.27	3
TPB3-A	6 2/3	1/3	2	11.3	1.76	3
TPB4-A	10		2	13.9	0.89	3
FPB1-A	4		1	10.9	0.84	3
Mix B						
TPB1-B	4		1	13.9	1.45	3
TPB2-B	6 2/3	1/3	2	13.4	1.83	3
TPB3-B	10		2	14.7	1.43	3
FPB1-B	4		1	11.7	0.84	3
Mix C						
TPB1-C	4	1/3	1	4.7	0.18	3
Mix D						
TPB1-D	3 1/3	1/3	3	17.9	2.30	2
TPB2-D	3 1/3	1/3	1	15.2	0.43	3
TPB3-D	3 1/3	1/3	2/3	13.1	1.45	3
FPB1-D	3		1	14.0	0.56	3
FPB2-D	3		2/3	12.0	0.85	3
Mix E						
TPB1-E	3	1/3	1	10.9	0.81	5
FPB1-E	3		1	12.9	1.35	5
FPB2-E	3		1	14.3	0.66	5
FPB3-E	3		1	14.5	1.49	5

Figure 4-2a shows the average load displacement curves for TPB tests on mix D specimens. The figure shows the large post-peak bearing capacity of fibre reinforced concrete. The peak load required to break the specimen increases with the size of the beam as expected. When the nominal stress (σ_N) for the beams is plotted against the deflection (δ) as a ratio of the effective beam height (h-a), a clear size effect as discussed in Section 2.4.2 appears. This is shown in Figure 4-2b. The graphs show the effect of size on the peak load as well as the post peak load capacity of the material. In the figure, the nominal strength of the material

increases with a decrease in size. This is of course not related to a real increase in strength of the material, but rather a manifestation of the limitations to LE calculation of the stress condition in the beam specimens.

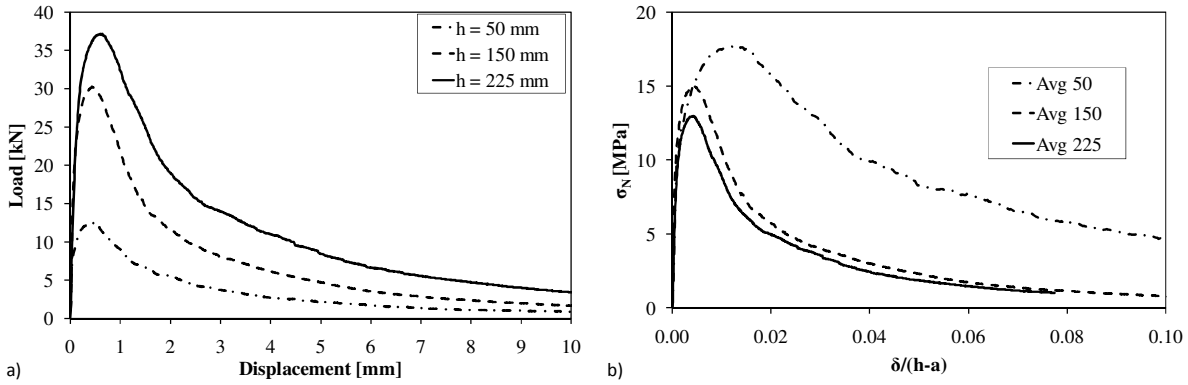

Figure 4-2a) Average load displacement curves for monotonic TPB tests mix D, b) Nominal stress versus relative displacement Mix D specimens.

A comparison of the σ_{Nu} values for TPB and FPB specimens of different sizes is plotted in Figure 4-3a for Mix D and in Figure 4-3b for mix E. The Mix D specimens show similar size effect trends in σ_{Nu} for the TPB and FPB. The results indicate a statistically significant (95% confidence) size effect in σ_{Nu} for both test configurations. The results for the FPB tests on Mix E specimens, shown in Figure 4-3b, also show a statistically significant size effect. The trend is however less steep, in particular between the 50 mm and 100 mm specimens. One of the reasons for this phenomenon may lie in the geometry of the specimens. In the first phase of the size effect experiment (Mix D) the width of the specimen was kept constant for the different beam heights. In the second phase (Mix E) the width was scaled as well in accordance to the span to depth ratio. The fracture mechanics size effect for Mix E may have become obscured due to the boundary layer effect. As the boundary layer contains mainly small sized material it will contain less steel fibres. Furthermore the steel fibres need a certain cover to function properly. Due to the limited width, the 50x50 specimens will have a relatively larger boundary layer than the larger 100x100 mm and 150x150 mm specimens.

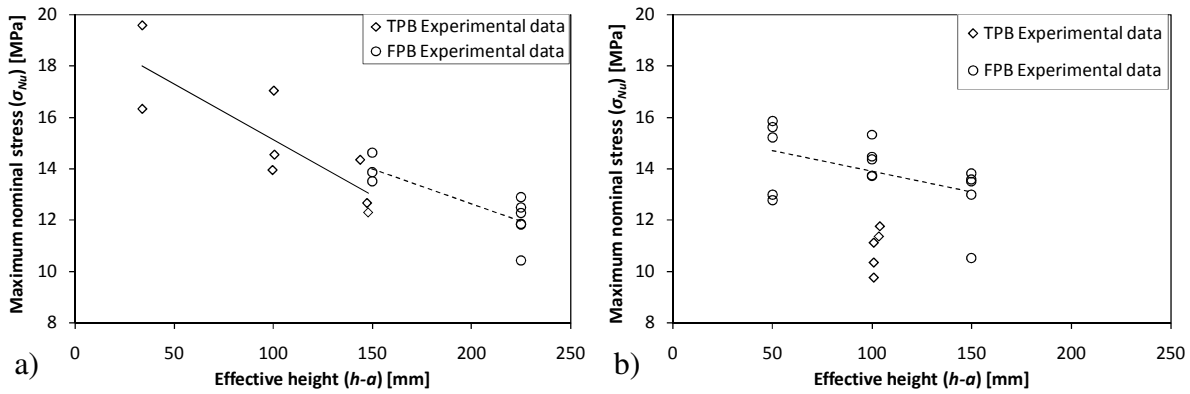

Figure 4-3a) Size effect in σ_{Nu} results for mix D, b) Size effect in σ_{Nu} results for mix E

4.3.2 Comparison of size effect results against published data for plain concrete

In the previous section it was shown that the σ_{Nu} for the high performance fibre reinforced concrete is subject to considerable size effects. The material differs from plain concrete in terms of its high compressive strength and substantial post crack stress transfer capacity. These characteristics may influence the magnitude of the size effect in the material compared to plain concrete. The size effect in the high performance material will be compared to the size effect of plain concrete recorded in literature. The relative magnitude of the size effect will determine whether LE design approaches are more or less applicable to the high performance concrete material than to plain concrete.

Bažant and Li (1995) collated the results of a number of size effect studies on plain concrete. In this publication a linear regression was fitted to the size effect results from the historic data.

$$\sigma_{Nu(I)} = c_1\left(1+\frac{c_2}{h_I}\right) \qquad (4.2)$$

Where $\sigma_{Nu(I)}$ is the nominal maximum stress in pounds per square inch, c_1 and c_2 are regression constants, h_I is the height of the specimen in inches. For a number of studies with specimen sizes in the range used for this study, the regression equations, converted to SI units are shown in Figure 4-4. Also plotted in the figure is a regression for the data produced by this study. The curve was fitted using the Microsoft excel solver. The plot allows a comparison of size effect in plain concrete and the high performance fibre reinforced concrete used for this work. To be able to compare the size effect relative to the σ_{Nu} value for the standard 150 mm MOR test, the ratio of σ_{Nu}/MOR is shown in Figure 4-5.

The figures show that in absolute terms the size effect of the UTCRCP material is higher than that of plain concrete. The size effect in the UTCRCP material relative to the value of the standard MOR test is comparable to what can be expected in plain concrete.

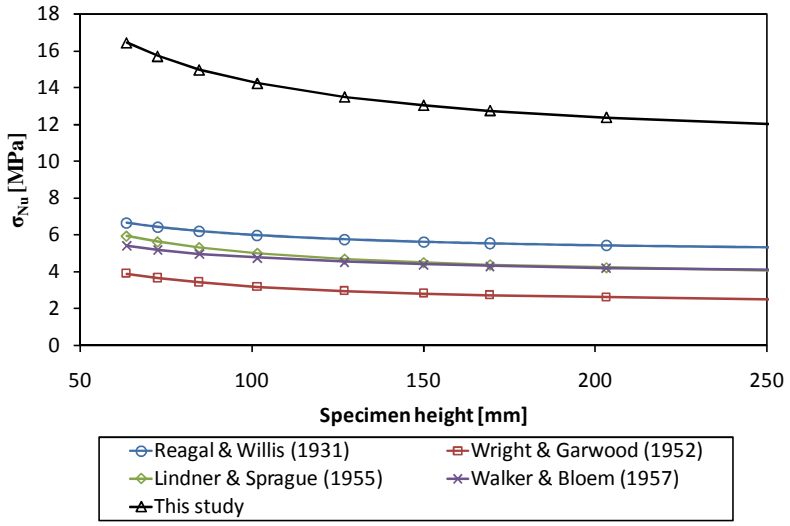

Figure 4-4: Linear regression for size effect in this and other studies.

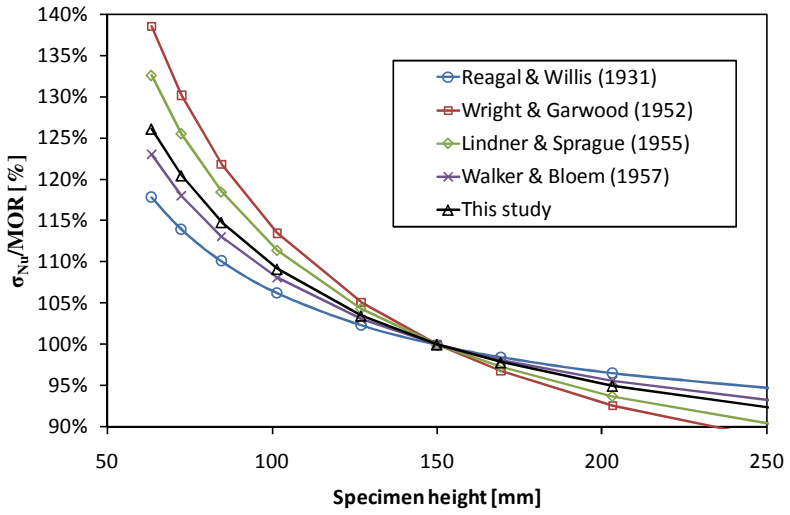

Figure 4-5: Relative size effect in studies normalized for MOR standard size specimen

4.3.3 Size effect in flexural disk tests

As discussed in Chapter 2, size effect has been linked to the underestimation of the carrying capacity of slabs when the calculation is based on beam MOR results and linear elastic analysis. This phenomenon becomes apparent in the analysis of the flexural disks tested as

part of experimental phase one and four. The load-displacement curves for the disks are contained in Appendix A.

The typical mode of failure for the disk specimens is cracking at midspan between the supports, forming the pattern shown in Figure 4-6. As the cracking pattern is instrumental to the analysis, test results were rejected in cases where the cracks formed elsewhere. Dupont and Vandewalle (2004) showed that yield line analysis can be used to relate the loading of the disks to the moment capacity of the specimens.

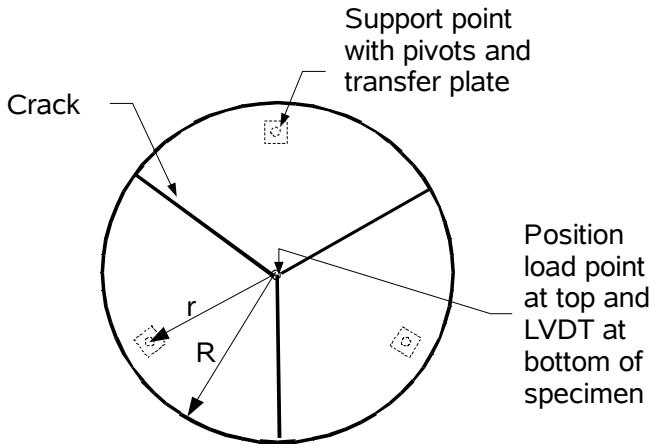

Figure 4-6: Typical crack pattern in disk experiments

Assuming that yielding takes place at the same time along the full length and depth of the lines shown in the sketch, the moment capacity (M_u) is given by:

$$M_u = \frac{P_u r}{6R\cos 30°} \tag{4.3}$$

Where P_u is the peak load, r and R are the radii from the centre of the disk centre to the centre of the support and from the centre of the disk to the edge of the disk, respectively. Assuming a linear elastic stress distribution at failure Barnett et al. (2010) equate the stress distribution disk to that in a beam of the same height by stating:

$$M_u = \frac{P_u r}{6R\cos 30°} = \frac{\sigma_{Nu} h^2}{6} \tag{4.4}$$

Which allows:

$$\sigma_{Nu} = \frac{P_u r}{h^2 R \cos 30°} \tag{4.5}$$

The ultimate nominal stress (σ_{Nu}) values calculated for the disks using the above equations are shown in Table 4-3. The 55 mm and 70 mm high specimens are geometrically similar as there is only slight difference in the radius to height (r/h) ratio. The σ_{Nu} values are consistent for the different sizes and mix types. The results do not show a statistically significant size effect between the 50 and 70 mm high disk specimens for either mix. The reason for this may be the relatively small difference in specimen size. The test matrix for the disk specimens was not designed with a size effect study in mind. Comparison of the σ_{Nu} for the disks in Table 4-3 to the σ_{Nu} values from flexural tests on beams in Table 4-2 shows that the values for σ_{Nu} for the disks are on the high side of the result spectrum for Mix A and B.

Table 4-3: σ_{Nu} results flexural disk tests

Specimen type	r/h	σ_{Nu} [MPa]	Std. dev. [MPa]
Disk1-A	0.20	13.8	0.2
Disk2-A	0.19	13.9	1.0
Disk1-B	0.20	14.1	1.0
Disk2-B	0.19	13.7	1.3

Note here however, that the stresses in the disks were calculated using plastic yield line theory instead of the LE analysis applied to concrete pavements. In LE analysis of the disks stresses are not distributed evenly along the eventual yield lines. Consequently, the stresses in LE analysis may be expected to be significantly higher than the σ_{Nu} values shown in Table 4-2. To get a full appreciation of the size effect between the LE analysis of beams and disks, numerical simulation is required, which will be performed in the next chapter.

4.4 Fracture energy

The specific fracture energy G_f is a key fracture mechanics parameter to be determined for use in numerical simulation of crack propagation. As part of this study, a detailed analysis

method was developed to determine G_f for FRC. The fracture energy is determined from TPB flexural tests performed in the different phases as described in Section 3.2.

4.4.1 Work of fracture and fracture energy

The work of fracture W_f required to completely break a specimen in a flexural test is represented by the area under the load-displacement or load-CMOD curve. Figure 4-7 shows the load-displacement curves obtained for the first group of specimens tested as part of this study, i.e. TPB1-A. An important assumption of this study is that the effect of the synthetic and steel fibres is distributed equally over the fracture area. The composite fibre concrete material behaves as a homogeneous material and the fibres do not need to be handled as separate entities. The energy required to produce a unit of fractured area is G_f, which is calculated for the concrete-fibres composite material using Equation 4.6:

$$G_f = \frac{W_f}{b(h-a)} \tag{4.6}$$

where b is the width of the sample, h the total sample height and a the notch depth.

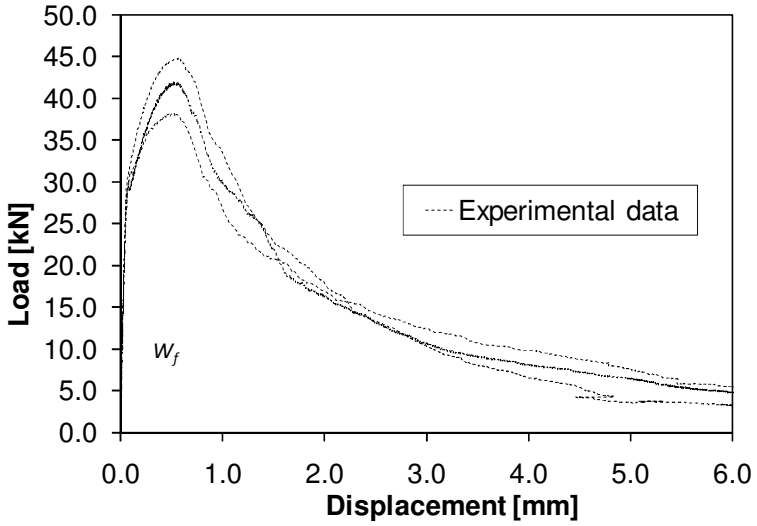

Figure 4-7: Load-displacement curves for specimens type TPB1-A

Some of the specimen tested in phase I contained reinforcement in the form of steel bars (rebar) in addition to steel fibres. The influence of the inclusion of the reinforcement bars on the work required to break the sample is shown in Figure 4-8. The additional work W_{rebar}

required, at a specific fibre content, to break the samples with steel bars can be calculated from the average value $W_{f(rebar)}$ for samples with both fibres and rebar, and the average value W_f for samples with fibres only:

$$W_{rebar} = W_{f(rebar)} - W_f \tag{4.7}$$

It is of course impossible to express the additional work required to break specimen with reinforcement bars in terms of G_f, as the bars are not homogeneously distributed over the cross-sectional area.

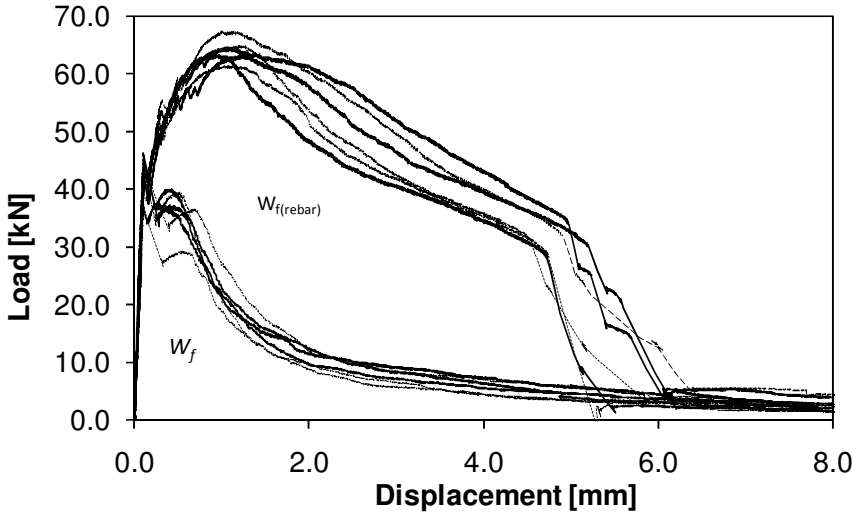

Figure 4-8: TPB on results on samples with and without rebar

4.4.2 Modelling of the load-displacement tail

The fibre reinforced concrete under study behaves ductile when compared to plain concrete. To obtain the full work of fracture from the TPB test, the specimen needs to be broken completely. This requires all steel fibres over the ligament area to be pulled out right to the top of the beam. For the 30 mm long steel fibres used in this study this would require a theoretical crack width of 15 mm at the top of the beam. The large rotation of the two beam halves needed to achieve this cannot be reached in the normal TPB test setup.

TPB tests on fibre reinforced concrete will therefore generally be stopped before the beam is fully broken. As a result a part of the tail of the load-deflection curve will be missing, as can

be observed in Figure 4-1 and Figure 4-8. The figure shows that after the peak, the load moves asymptotically to zero. At the final stage of the experiment the load has reduced significantly, but the specimens have not broken into two halves completely and the full work of fracture has not been recorded. If the results have been corrected for self weight, the upwards shift of the load displacement curve adds to the portion of the load-displacement tail that is missing from the recorded data.

To calculate the full work of fracture and get a precise measure of G_f, it will be necessary to model the missing part of the load deflection curve. A methodology is proposed that draws from the work on plain concrete published in Elices et al. (1992), Elices et al. (1997), Bažant and Planas (1997) and Rosselló et al. (2006).

Near the end of the test, the crack has propagated to the top of the beam and the crack mouth has opened considerably. The neutral axis of the stress distribution shifts ever closer to top of the beam as the size of the compressive zone reduces during the test. In this situation, the beam can be modelled as two ridged parts rotating around a point at the top of the beam at centre span, as shown in Figure 4-9a.

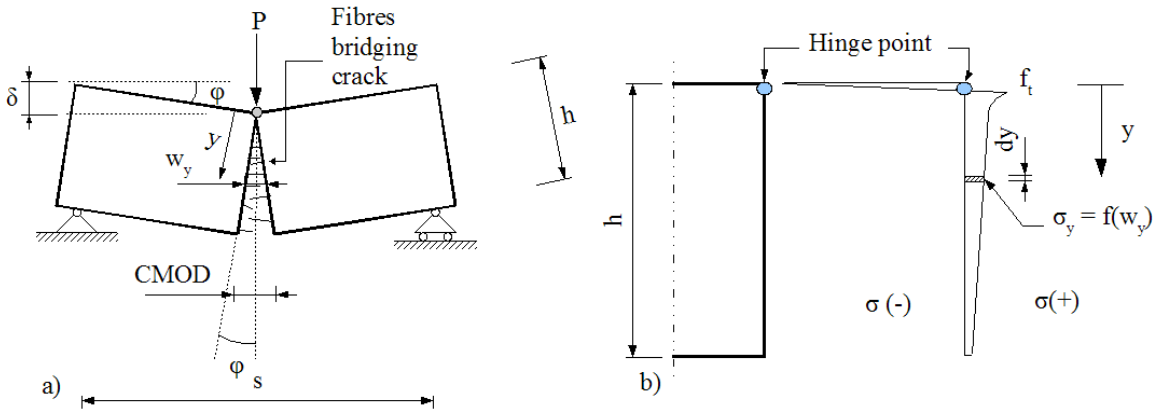

Figure 4-9a: Kinematic model of TPB test at large deflections, b: Stress distribution in kinematic model (not to scale)

For fibre reinforced concrete this situation will exists for a considerable longer period than for plain concrete, while the fibres bridging the crack are being pulled out. The angle of

rotation (φ) around the hinge point at the top of the beam at any value of deflection (δ) is obtained from:

$$\tan\varphi = \frac{2\delta}{s} \Rightarrow \varphi \approx \frac{2\delta}{s} \tag{4.8}$$

The crack width at any depth (y) of the beam near the end of the test is calculated from:

$$w_y = 2y\sin\varphi \approx 2y\varphi \tag{4.9}$$

It can be shown that the kinematic model of the beam in Figure 4-9a is accurate, by comparing the horizontal crack opening displacement at the mouth of the notch calculated using the model, to the CMOD measured with a clip gauge for tests in which both the CMOD and vertical displacement were recorded. At large rotations the recorded CMOD and the crack mouth opening calculated using the kinematic model in Figure 4-9a reach unity, i.e.:

$$\frac{2h\sin\varphi}{CMOD} = 1 \tag{4.10}$$

For the beam data shown in Figure 3, unity is reached at approximately 2 mm deflection, implying that after 2 mm the kinematic model is valid for the data.

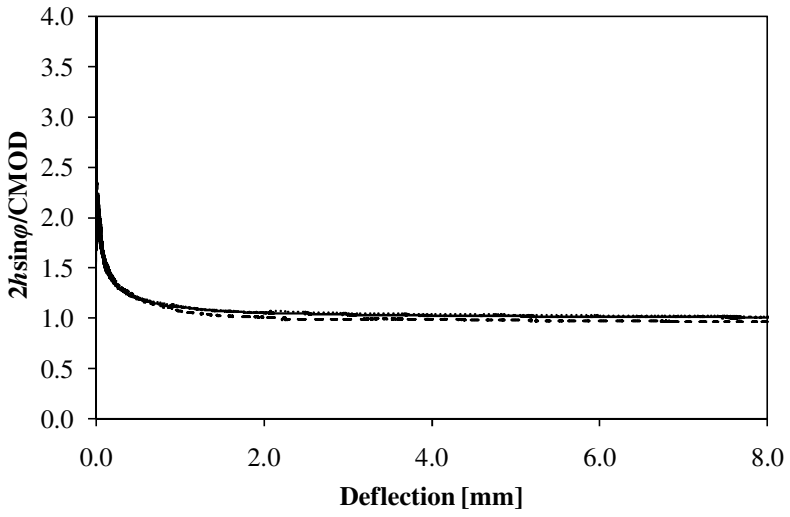

Figure 4-10: Comparison of recorded CMOD and crack mouth opening calculated using the kinematic model in Figure 4-9a.

The stress distribution in the beam at large rotations may be approximated by assuming that the depth of the compressive zone is negligible and concentrated at the hinge point (Elices et al., 1992). The post crack softening behaviour of the material can be described using a cohesive crack approach as introduced for concrete by Hillerborg et al. (1976). Under the assumption of a cohesive crack, the material behaves elastically until the stress reaches the tensile strength (f_t) of the material. At this point a crack is formed. Stresses are transferred over the crack according to a softening function. The crack bridging tensile stress (σ_y) at any point (y) along the depth of the cracked beam shown in Figure 4-9b is written as a function of the crack width (w_y) at that position

$$\sigma_y = \mathrm{f}(w_y) \tag{4.11}$$

Regardless of the shape of the softening function, the moment capacity in the kinematic model can be written as the integral of the softening function times the lever arm to the top of the beam:

$$M = \int_0^h \sigma(w_y) b y \, \mathrm{d}y \tag{4.12}$$

Substituting w_y in Equation (4.12) by the function in Equation (4.9) results in:

$$M = \frac{b}{(2\varphi)^2} \int_0^{w_c} \sigma(w_y) w_y \, \mathrm{d}w \tag{4.13}$$

where w_c is the crack width opening position at which the softening is complete and $\sigma = 0$. Note that for exponential softening $w_c = \infty$. Following Elices et al. (1992), the integral in Equation (4.13) is defined as parameter A:

$$A = \int_0^{w_c} \sigma(w_y) w_y \mathrm{d}w \tag{4.14}$$

With this, Equation (4.13) may be written as:

$$\frac{M}{b} = \frac{A}{(2\varphi)^2} \tag{4.15}$$

This defines a relationship between the remaining moment capacity (M) in the beam at large displacements, and the angle of rotation (φ). Parameter A can be calculated without having to define the shape of the softening curve, as A corresponds to the slope of a graph plotting M/b against $(2\varphi)^{-2}$. The behaviour of parameter A at large rotations (small values of $(2\varphi)^{-2}$), where it becomes a constant, is shown in Figure 4-11a for data obtained from TPB tests performed as part of this study. A was determined per specimen type using least squares fitting. Bažant and Planas (1997) propose that A is a size independent material property for plain concrete. This would imply that the fracture energy G_f is a true material property as well. Figure 4-11b shows the behaviour of A for the different specimen sizes tested for mix B. Parameter A has a similar value for different specimen sizes of the same material. It is possible that A is size independent for fibre reinforced concrete. The limited number of specimens tested per size and mix type in this study does however not allow a statistical test of the hypothesis that A is size independent.

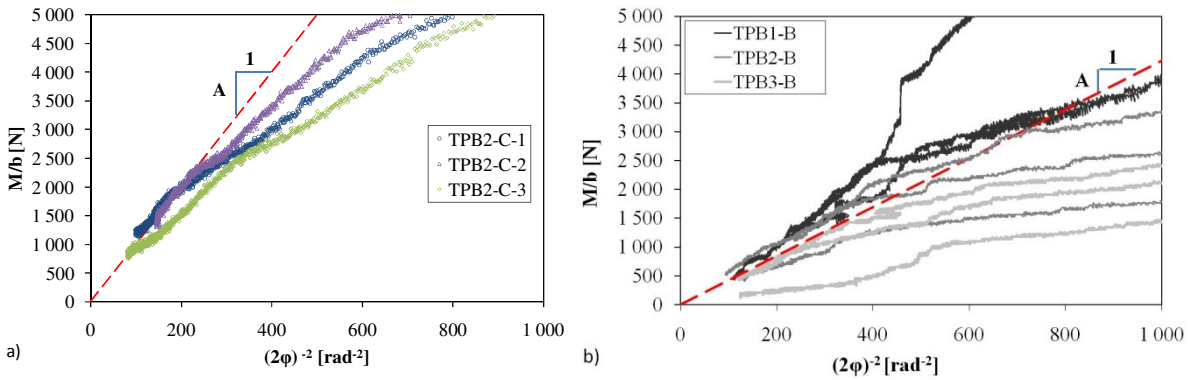

Figure 4-11a: Determination of A for single specimen type, b: Determination of A for different sizes of Mix B specimens.

Once A has been determined the missing part of the asymptotic tail of the displacement curve can be modelled by combining Equations (4.8) and (4.16) which allows calculation of P_{tail} for any δ.

$$P_{tail} = \frac{bsA}{4\delta^2} \quad , \tag{4.16}$$

An example of a load-deflection curve with a modelled tail end is shown in Figure 4-12. The modelled tail provides a close fit to the path of the experimental tail. The curve can now be extrapolated to infinity. The total work of fracture is calculated by adding the area under the modelled tail of the curve to the area under the known part of the curve. The work under the modelled tail is determined from:

$$W_{tail} = \int_{\delta_{end}}^{\infty} P\mathrm{d}(\delta) = \frac{bsA}{4\delta_{end}} \tag{4.17}$$

Where, δ_{end} is the deflection at the last available experimental data point. The total W_f can be calculated by adding W_{tail} to the area under the experimental load-deflection curve. G_f can be obtained using Equation 4.6.

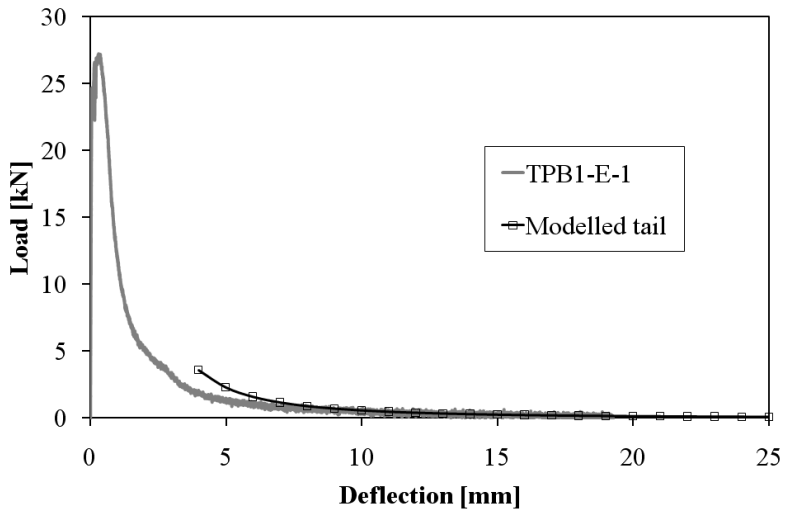

Figure 4-12: Load-displacement curve with modelled tail

The average values for A, W_f, W_{tail}, W_{rebar} and G_f for the TPB experiments on the different mixes are shown in Table 4-4. According to the proposed model, approximately 18 per cent (on average) of the work of fracture was still available under the missing part of the tail when the tests were stopped (for beams without rebar).

The results obtained in this study do not indicate a statistical size-effect in the value of G_f. Due to the variability inherent to the material and TPB results, a large number of specimens would have to be tested in order to verify whether any size effect in G_f occurs.

The differences in the fracture energy of mixes produced at different fibre contents is evident from the results. Mixes B and D, produced at 120 kg/m^3 steel fibre content have a significantly higher specific fracture energy than mixes A and E, produced with 80 kg/m^3 steel fibres.

The methodology developed in this study to determine the fracture energy was published in Denneman et al (2011a).

Table 4-4: Summary of work of fracture results

Specimen type	A [Nmm rad^2]	W_f [Nmm]	W_{tail} [%]	W_{rebar} [Nmm]	G_f [N/mm]	Std.dev. [N/mm]	Number of specimens
Mix A							
TPB1-A	9.74	1.23E+05	17.6%		6.57	0.96	3
TPB2-A	4.96	8.54E+04	12.0%		4.56	0.69	3
TPB3-A	4.59	3.70E+04	22.2%		4.93	1.10	3
TPB4-A	2.97	2.86E+04	16.5%		3.82	0.88	3
TPB5-A		3.26E+05	8.49%	1.98E+05			3
TPB6-A		2.71E+05	8.47%	1.96E+05			3
TPB7-A		1.86E+05	30.4%	9.00E+04			3
TPB8-A		2.00E+05	44.9%	2.33E+01			3
Mix B							
TPB1-B	8.36	9.97E+04	15.7%		5.32	0.31	3
TPB2-B	4.34	4.13E+04	21.0%		5.51	1.21	3
TPB3-B	5.22	4.23E+04	21.2%		5.64	1.37	3
TPB4-B		2.70E+05	6.7%	1.68E+05			3
TPB5-B		2.26E+05	41.5%	9.98E+04			3
TPB6-B		2.19E+05	43.8%	9.02E+04			3
Mix C							
TPB1-C	0.10	3.21E+03	22.4%		0.211	0.033	3
Mix D							
TPB1-D	13.99	4.26E+04	19.2%		8.34	0.24	3
TPB2-D	11.38	9.66E+04	15.0%		6.41	0.63	3
TPB3-D	15.23	1.62E+05	17.8%		7.41	0.86	3
Mix E							
TPB1-E	11.61	5.43E+04	19.0%		3.53	0.50	5

4.4.3 Tensile splitting results

The split cylinder tests were performed using the adjusted test procedure as discussed in Section 3.2.6. The load-transversal deformation curves obtained for the cylinder splitting tests performed as part of this study are shown in Figure 4-13. The observed material behaviour is comparable to the graph shown in Figure 3-8c. Two separate peak load conditions are reached during the test. An important finding for the tensile splitting tests performed on FRC as part of the study is that with the second peak is higher than the first peak.

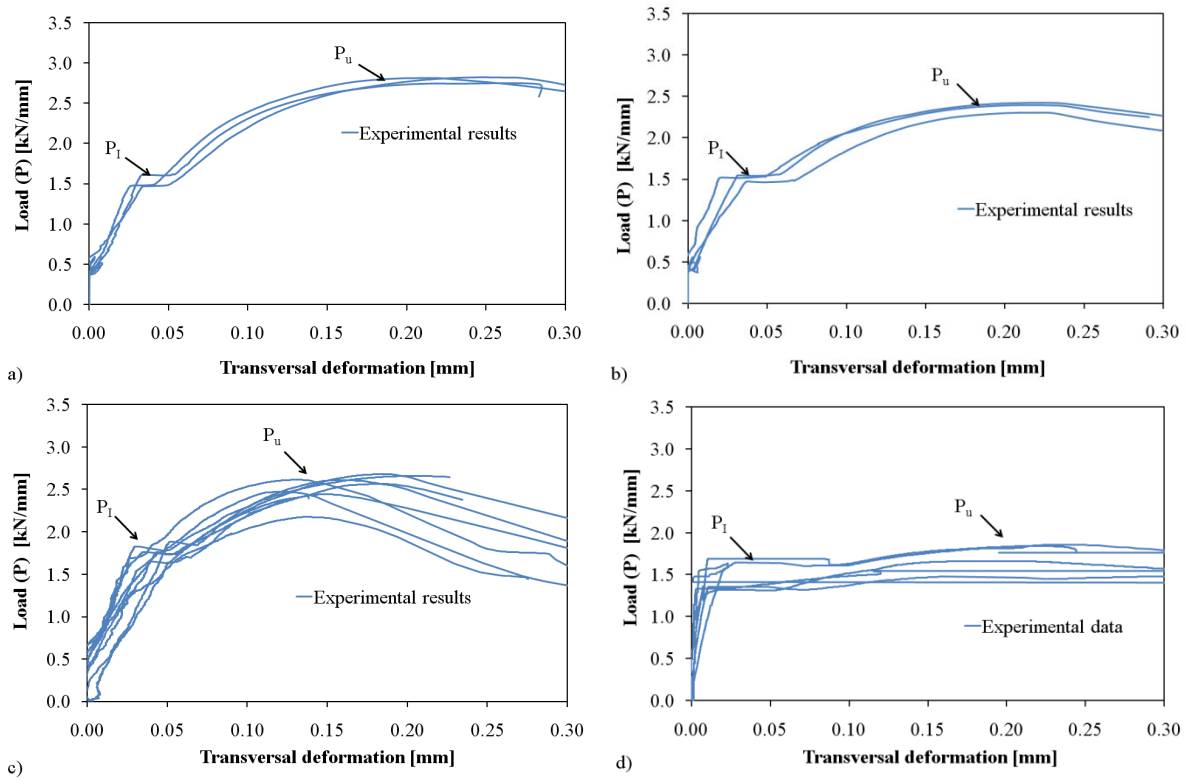

Figure 4-13: Load-transversal deformation curves for cylinder splitting tests on: a: Mix A specimens, b: Mix B specimens, c: Mix D specimen and d: Mix E specimens,

The figures indicate that the material behaves linear elastically until a first peak is reached at load level (P_I). At this point a crack is introduced. The load stabilizes at this level before increasing again with an increase deformation. Eventually a second and higher peak load (P_u) is reached. In conventional splitting tests, this second, ultimate peak load is the only value that would be recorded. Using the approach in conventional test methods, the nominal ultimate tensile stress σ_{Nu} would be calculated using the relationship in Equation 3.1:

$$\sigma_{Nu} = \frac{2P_u}{\pi D} \tag{4.18}$$

The results of this study, indicate that P_u is related to a secondary cracking mechanism in the tests and not to linear elastic tensile stress distribution in the cylinder.

It is proposed, based on the discussion in Section 3.2.6, that a close estimate of the true tensile strength (f_t) may be obtained from the linear elastic limit state at load level P_I, while also taking into account the correction for the width of the load strip proposed by Tang (1994):

$$f_t = \frac{2P_I}{\pi D}\left[1-\left(\frac{b_1}{D}\right)^2\right]^{\frac{2}{3}} \tag{4.19}$$

The values obtained for σ_{Nu} and f_t after correction for statistical outliers are shown in Table 4-5. The values for σ_{Nu} are up to 45 per cent higher than the values for f_t. The correction proposed by Tang (1994) is constant for all results and accounts for only 4 percent of this difference. For the mixes of which enough samples were tested to allow such an analysis, the results of a statistical boxplot test for outliers is shown in Figure 4-14. Based on this analysis a single outlier for D was excluded from the results in the table.

Table 4-5: Tensile splitting test results

Mix ID	Number of specimens	Peak load [kN]	Std.dev. [kN]	σ_{Nu} [MPa]	f_t [MPa]	Std.dev. [MPa]
Mix A	3	708	18.9	10.01	6.29	0.25
Mix B	3	833	12.5	11.78	6.39	0.33
Mix C	12	164	46.4	2.25	2.23	0.59
Mix D	9	767	29.8	10.86*	7.28*	0.51
Mix E	6	510	42.2	7.21	6.56	0.73

* Outlier omitted

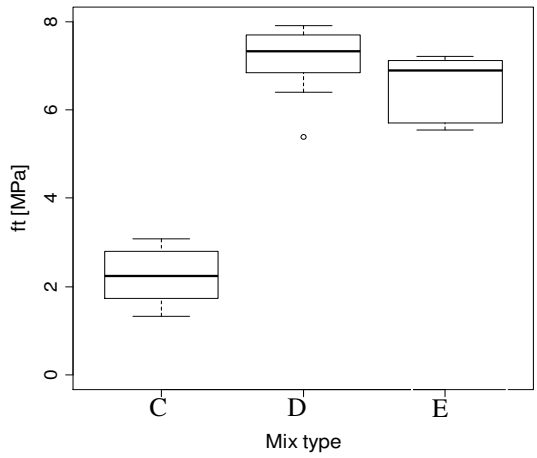

Figure 4-14: Box plot of cylinder splitting results

The adjusted tensile splitting test methodology to determine the tensile strength of fibre reinforced concrete developed as part of this study was published in Denneman et al (2011b).

The fracture mechanism and stress redistribution that leads to the occurrence of the two peaks require further evaluation. As part of the numerical simulation in Chapter 5, the tensile splitting test is modelled in a finite element framework using a fracture mechanics approach.

With both the fracture energy and the tensile strength known, it is possible to create a model of the fracture behaviour of the material. A crack will be induced when the tensile stress reaches the tensile strength of the material. The fracture energy represents the amount of energy that needs to be dissipated to reduce the stress transfer between the cracked faces to zero.

4.5 Analysis of fatigue tests

Cyclic loading tests were performed as part of experimental Phase 2 and 4. In Phase 2 cyclic testing with limited scope was performed on plain concrete beams at UC Davis. The fatigue testing performed in Phase 4 had a wider scope and includes a size effect study on beams as well as tests on disk specimens. The results are presented in terms of the evolution of vertical displacement or CMOD with the increase in number of cycles. Figure 4-15 shows the evolution of the load-CMOD response of a test run at 80 per cent of the monotonic peak load for specimen type TPBF1-C. The results indicate that secant stiffness of the beam reduces with each stress cycle, even at this lower stress level. The displacement consequently increases with every cycle. The results of the cyclic tests, where displacement was successfully recorded are contained in Appendix B. Note that a limited number of data points are recorded per load cycle as result, the peak and minimum load levels are often not visible in the graphs.

4.5.1 Repetitions to failure and size-effect

Fatigue tests are run in load control at a percentage of the monotonic peak load. The number of cycles to failure for the various specimen types tested at the different load levels is shown in Figure 4-16. The results shown are for the plain concrete beams tested as part of phase II, and the different specimen types (beams and disks) tested as part of phase IV. The results

show considerable scatter and only a limited number of tests were performed on the plain concrete samples.

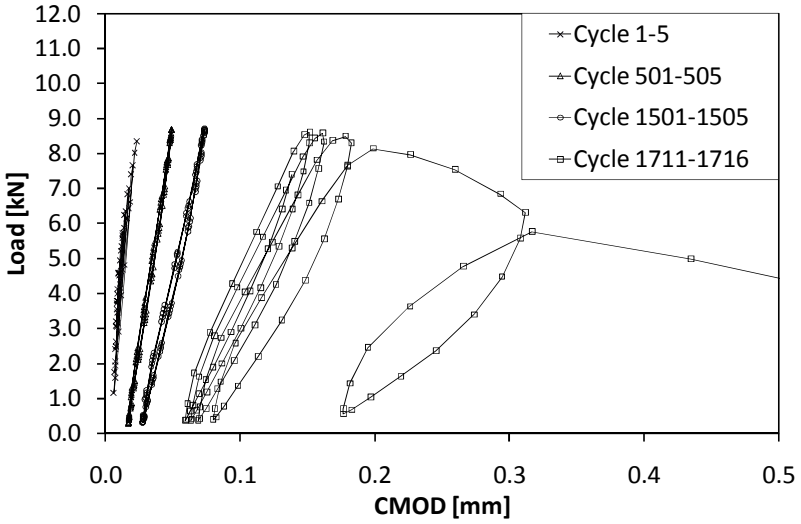

Figure 4-15: Evolution of CMOD in fatigue test on TPBF1-C specimen

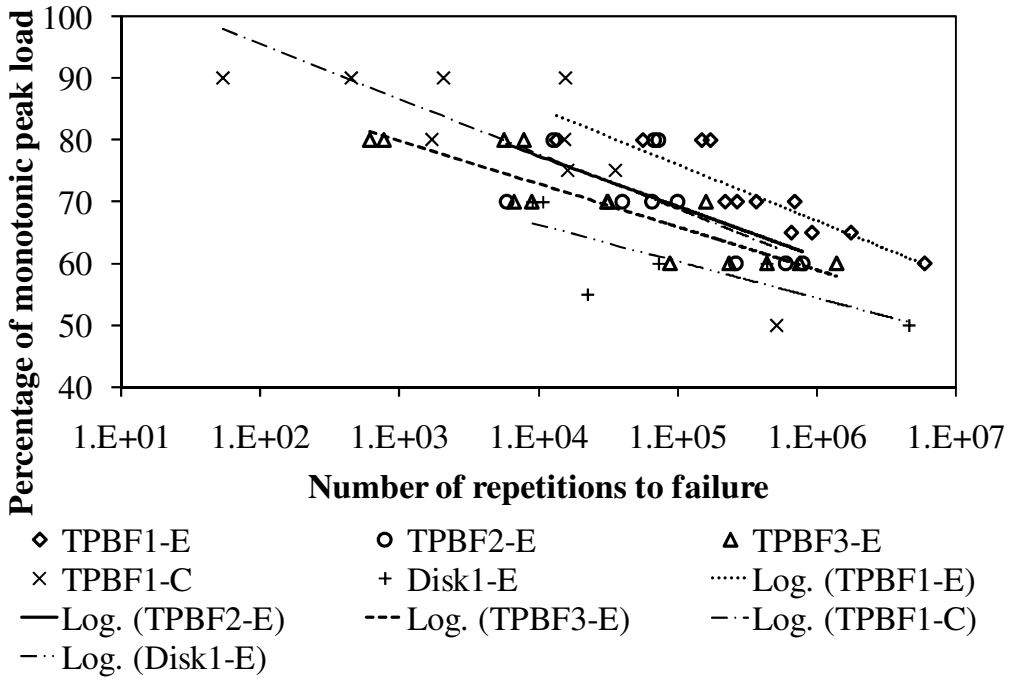

Figure 4-16: Number of repetitions to failure versus percentage peak load

The individual difference in performance between the 50, 100 and 150 mm high beam specimens (TPBF1-E and TPBF2-E) and the disks Disk1-E in Figure 4-16 are caused indirectly by size effect. The MOR for the smaller specimens is relatively higher and these are therefore tested at a higher stress level. If plotted in terms of nominal stress, as shown in Figure 4-17, the difference between the 100 and 150 mm high samples disappears. The trend line for the 50 mm high TPBF3-E specimens still plot below the results for the other sizes. The 50 mm beams may have been weaker due to the small dimensions of the beam cross-section with may have given rise to other sources of size effect as discussed in Section 4.3.

The results in Figure 4-17 do not indicate any significant size effect in the fatigue performance of the fibre concrete material between the beam specimens. The absence of size effect in fatigue would imply a model for fatigue life prediction based on the ratio of MOR approach would yield reliable predictions. Figure 4-17 also shows the results for the disk specimens however. The stresses shown for the disk were calculated using finite element method under the assumption of linear elastic material behaviour. The FEM model is presented in the next chapter. The results show that the disk specimens have superior fatigue performance, if analysed in terms of LE stress condition. These results indicate that the use of the beam results to predict the fatigue performance of slabs using the conventional LE approach would not yield reliable results. This will be discussed in more detail in Chapter 5.

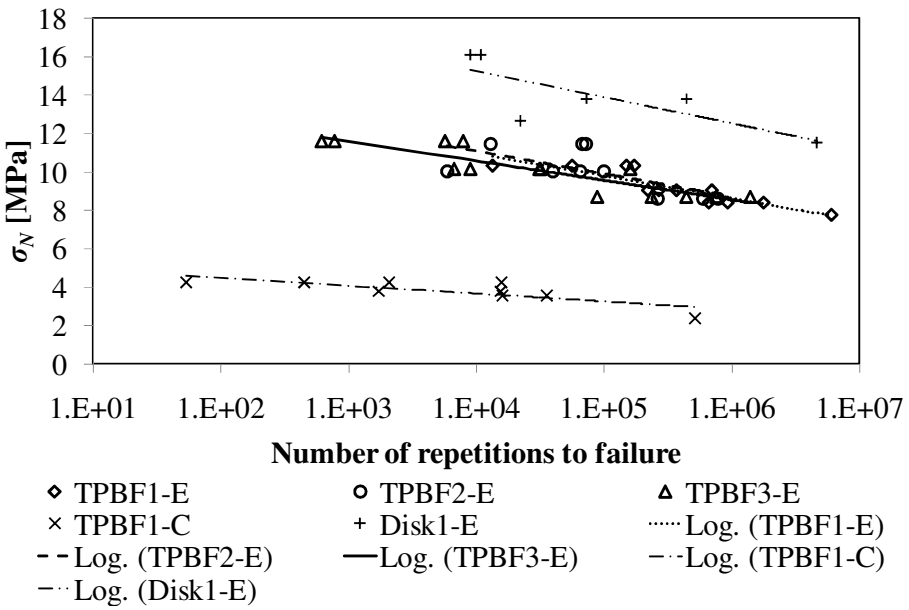

Figure 4-17: Number of repetitions to failure versus nominal stress

The graph in Figure 4-17 shows that the fatigue experiments on both the plain and fibre reinforced concrete, although run at a percentage of the peak load, were performed at a stress level well above the tensile strength values for the material in Table 4-2. This implies that the linear elastic limit state for the specimens is reached in the first load cycle. According to fracture mechanics theory, cracking is induced when the tensile strength is reached. Implying that in these tests fatigue damage was present from the time of the first load application.

4.5.2 Exploring the relationship between monotonic and cyclic tests

As mentioned in Section 2.6.2, the notion proposed by Hordijk (1992), that the monotonic load-displacement curve provides an envelope for fatigue tests has been opposed by later research. There is some evidence from literature that the monotonic curve as an envelope for cyclic tests is a workable model for fibre reinforced concrete. For this reason, the relationship between monotonic and cyclic tests is explored in this section. Figure 4-18 shows a comparison between the monotonic experimental data and the cyclic loading results for TPB tests on plain concrete performed at UC Davis. The results shown in the figure are typical, for both the tests on plain and fibre reinforced concrete performed as part of this study, in that the softening process under cyclic loading continues until the displacement at the peak of the cycle approximately coincides with the envelope of the monotonic load-CMOD curve.

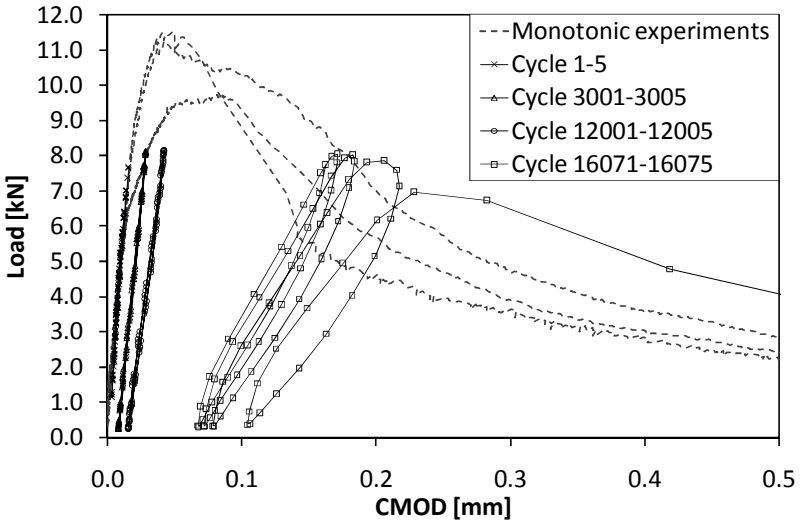

Figure 4-18: Comparison between monotonic and cyclic load-CMOD curves.

Figure 4-19 schematically shows a method which was developed to determine the displacement at which unstable collapse follows in the cyclic experiments. It is necessary to make an approximation of the displacement due to the limited number of data points recorded for each load cycle. As a rule, no data point will be available for the peak of the load cycle. To determine the location of point C in Figure 4-19, representing the displacement at the last cyclic peak load, the secant modulus of the final cycle is estimated. This is then used to obtain the approximate position of point C.

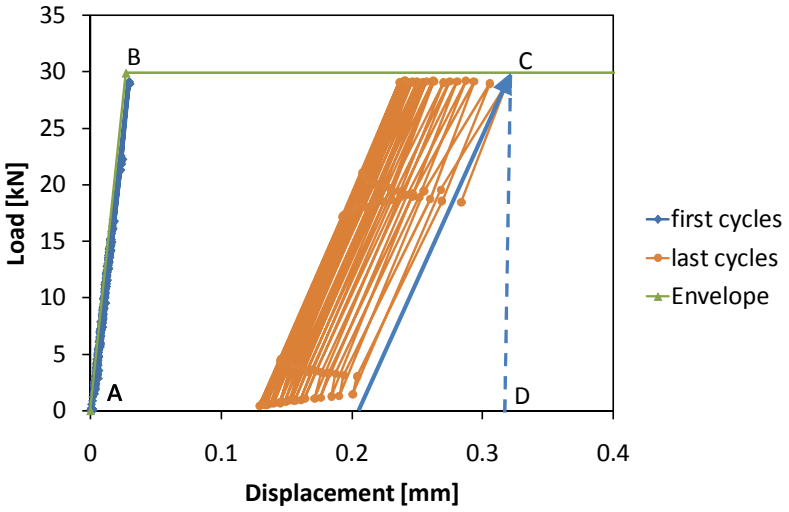

Figure 4-19: Determining displacement at point C and dissipated work of fracture

With point C known, the work of fracture applied in the cyclic loading experiments under stable loading can also be estimated. The work of fracture delivered in the test is obtained from calculating the area ABCD in Figure 4-19. The work of fracture applied up to the induction of unstable failure shall be denoted W_{ff}. The line A-B representing the load-displacement behaviour in the first load cycle is constructed using linear elastic beam theory. The deflection (δ) at the centre of a simply supported beam with two equal loads is obtained from:

$$\delta = \frac{Wx}{24EI}\left(3s^2 - 4x^2\right) \qquad (4.20)$$

Where in the case of the FPB experiments W is $P/2$, x is $s/3$ and I is the moment of inertia. Using this equation the deflection at the peak of the first load cycle can be calculated. To

demonstrate that the linear elastic solution approximates the initial response, the load displacement curve for the first five cycles is included in the figure.

Drawing a horizontal line from point B provides an envelope for the load displacement behaviour of the cyclic tests. This envelope is included in the cyclic loading results in Appendix B.

By drawing a vertical line from point C down to the horizontal axis, the area ABCD is completed. This area is W_{ff}, i.e. the work applied from the first load cycle to the last cycle in which the cyclic peak load was reached before unstable failure occurred.

Figure 4-20a shows the position of point C for cyclic tests on plain concrete TPB1-C performed at different stress levels. Figure 4-20b and Figure 4-20c. show similar data for the tests on fibre reinforced concrete FPB3-E and disk1-E specimens.

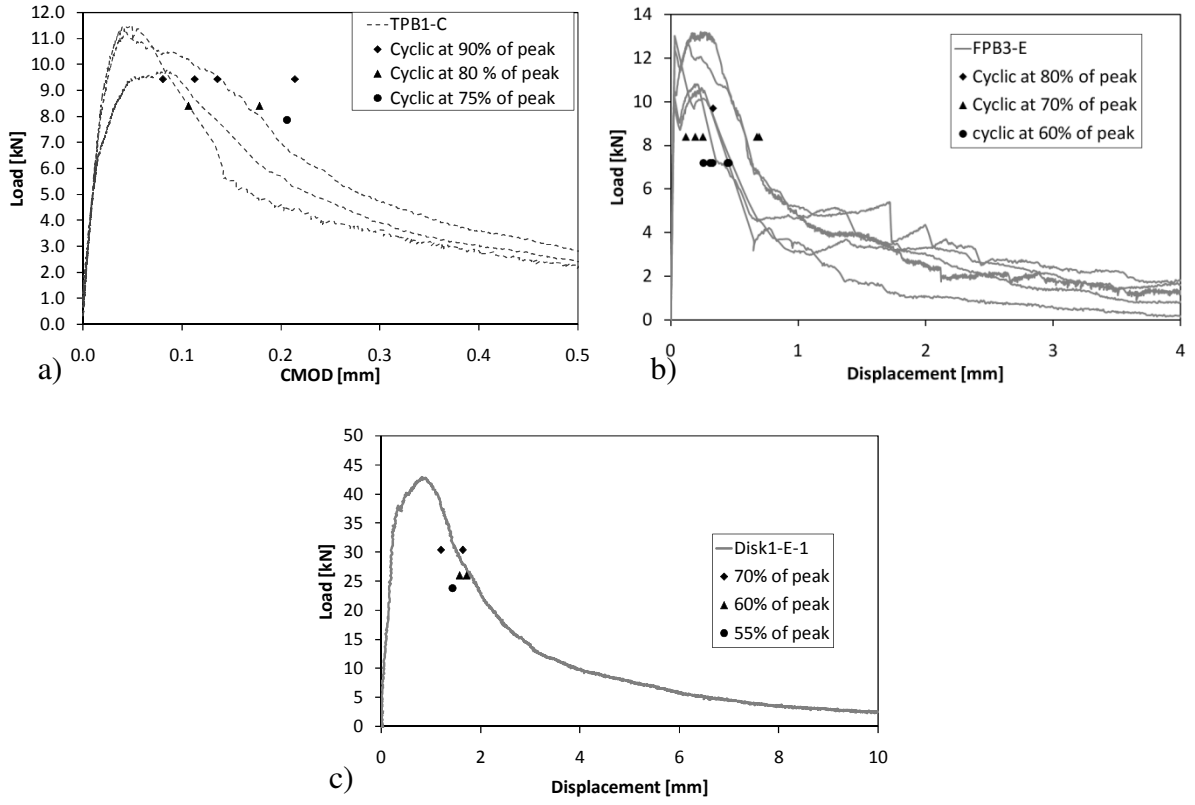

Figure 4-20a: Position of point C for plain concrete TPB1-C specimens, b: position point C for FRC FPB3-E specimens, c: position point C for FRC disk1-E specimens

Unfortunately, a comparison between the monotonic and cyclic results for other Mix E specimen types is not possible, because the monotonic tests failed in a brittle manner just after the peak was reached. Therefore, no reliable load-displacement data is available for the post peak behaviour of the specimens.

The available results are insufficient to reach a conclusion on whether the monotonic curves provide an envelope for the cyclic data. The data does indicate that the spread of the displacement at which unstable fracture is initiated (the spread in the position of point C) is wider than the spread of the monotonic load-displacement curve trajectories. As the combined data for all tests on Mix E beam specimens in Figure 4-21 shows, there is also no clear trend that the unstable failure is initiated at higher deflections for lower stress levels.

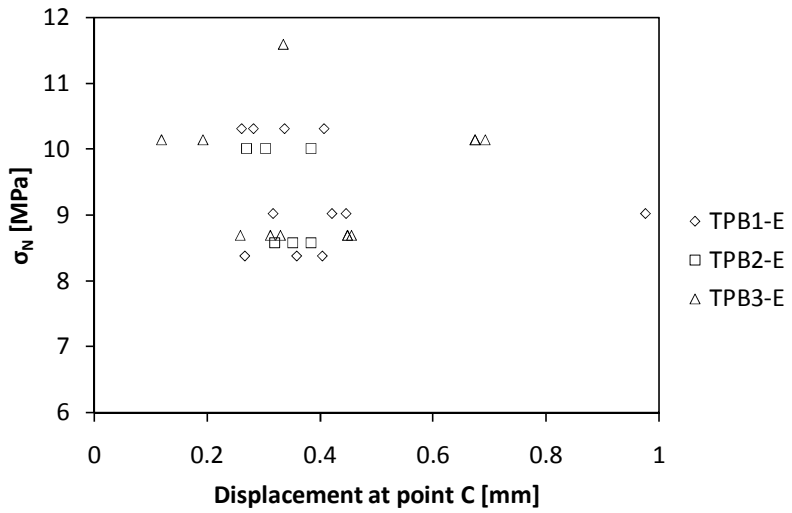

Figure 4-21: Position of point C for cyclic tests on mix E

The work of fracture applied at the induction of unstable failure (W_{ff}) for the different Mix E specimen types is shown in Figure 4-22a. W_{ff} is calculated using the methodology described above and plotted against the nominal maximum stress at which the test was run. The results show that, as expected, the amount of W_{ff} depends on the size of the specimen and geometry. The results can be normalized for the size of the fracture ligament. W_{ff} is divided by the area of the fracture plane in the test yielding an energy equivalent (G_E). Therefore, for the FPB tests G_E is calculated using:

$$G_E = \frac{W_{ff}}{bh} \tag{4.21}$$

For the disk specimens G_E is obtained from:

$$G_E = \frac{W_{ff}}{3Rh} \tag{4.22}$$

Note that the dissipated W_{ff} divided by the area of the fracture ligament does not equate to dissipated fracture energy (G_f) as the specimen is only partially cracked and the softening is unevenly distributed. When the results are normalized for size as shown in Figure 4-22b, the average dissipated work is more or less consistent. In Figure 4-23 the values for G_E at different stress levels are combined in box plots for the different specimen types. The figure shows that the mean value for the mixes is around 1 N/mm for the specimen types tested at various stress levels.

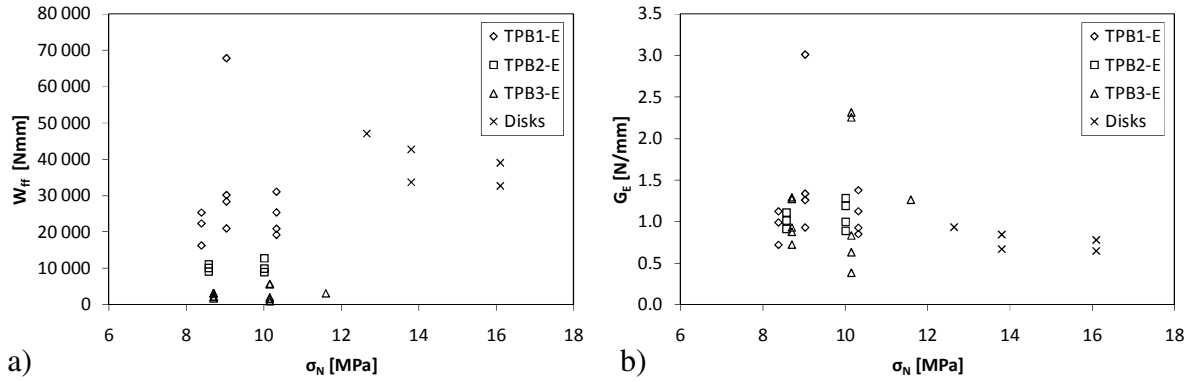

Figure 4-22a: W_{ff} for cyclic tests on Mix E specimens, b: G_E for cyclic tests on Mix E specimens

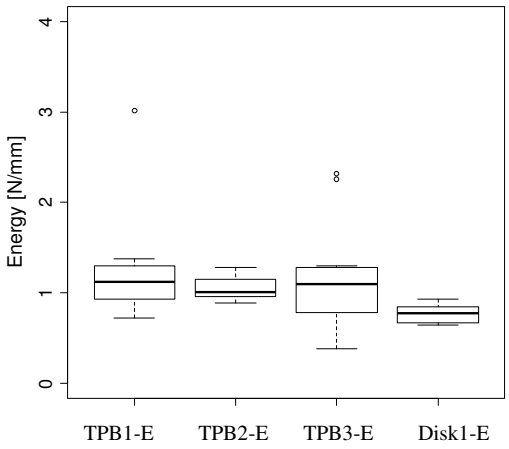

Figure 4-23: Box plot G_E results

In Figure 4-24 the values for G_E are plotted against the number of repetitions to failure. This was done to investigate whether more energy is dissipated in tests ran up to a higher number of repetitions. The outliers identified from the box plot in Figure 4-23 are excluded from this plot. The results indicate that if there is a trend for a higher G_E at higher numbers of repetitions, it is a weak one.

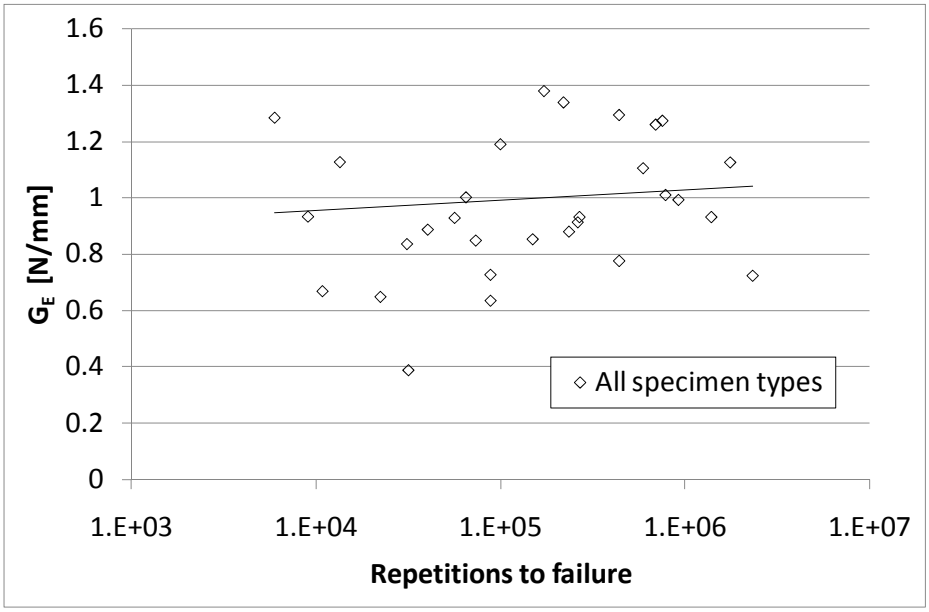

Figure 4-24: Trend of G_E with repetitions to failure

4.6 Discussion of fracture experiments

The testing performed as part of this study had three main aims. The first was to explore the magnitude of the size effect for the material. The second aim was to determine the fracture mechanics material properties required to numerically simulate cracking in the material. The final objective was to compare behaviour of the material under monotonic and cyclic loading, and further to determine fracture properties from the cyclic loading tests that can be used in the prediction of the fatigue performance of the material.

The monotonic testing showed that the material is subject to significant size effect. The implication is that σ_{Nu} or MOR is unsuitable as a design parameter, as the results obtained for a certain specimen size cannot be used to predict the peak load of a specimen with the same geometry, but a different size. σ_{Nu} can therefore not be expected to yield reliable predictions of the bending capacity of a full size pavement. To illustrate this further, a comparison between the LE derived stresses for the beams and the stresses in the centrally loaded disks obtained through LE numerical simulation will be provided in the next chapter.

The magnitude of the size effect in the high performance fibre reinforced concrete was found to be comparable to published values for plain concrete. This highlights the known limitations of the assumption of linear elastic material behaviour in the design of plain concrete pavements, as raised by other researchers and discussed in Chapter 2. For fibre reinforced concrete material under study σ_{Nu} has the added limitation that it does not distinguish between mixes at different fibre contents. The parameter provides an indicator of the nominal peak stress for the material only. It does not provide much indication of the post peak stress capacity of the material. Post peak stress capacity is a key property for fibre reinforced concrete. For fibre reinforced concrete it is important to optimize mixes for post peak toughness rather than for peak strength alone. The post cracking material response needs to be described using a suitable fracture mechanics based parameter, to capture the influence of fibres on the material behaviour under monotonic and cyclic loading.

The above builds a case for the use of a non-linear, fracture mechanics based approach to predict the bending capacity of high performance fibre reinforced structures. Fracture properties that can be used as input to fracture mechanics simulation were determined in this chapter. A method was introduced to model the tail of the load displacement curve in TPB test, in order to obtain the full work of fracture required to completely break the beam. From this, the specific fracture energy for the material was determined. The tensile splitting test

was adjusted to allow the determination of the tensile strength of the fibre reinforced material. It is proposed that a close estimate of the true tensile strength of high performance fibre reinforced concrete may be determined from cylinder splitting tests provided that: measures to reduce size effect are observed, the calculation is corrected for the influence of boundary conditions, and the transversal deformation is measured.

The fracture energy and tensile strength parameters can be used in the definition of a fracture mechanics damage function for the material. The numerical modelling exercise will also serve to further validate the methods of deriving fracture energy and tensile strength introduced in this chapter.

The comparison of results from the monotonic and cyclic flexural tests seems to indicate that the monotonic load-displacement curve may provide an envelope for the evolution of the load-displacement curve under cyclic loading at least at the relatively high stress levels applied as part of this study. The experiments have provided valuable data for the comparison of material response under monotonic and cyclic loading. There is little evidence of size effect in the cyclic test results for beams. The results for the disks however, do indicate that the use of a fatigue function based on the MOR obtained from the beam specimens, will not lead to reliable prediction of the fatigue performance of the disks.

The analysis of the load displacement curves for the fatigue tests resulted in the identification of one parameter that may prove useful in the development of fatigue prediction models. The equivalent energy (G_E) dissipated per unit ligament area is largely consistent regardless of specimen shape and size. The value of this parameter in the prediction of fatigue will be assessed in the next chapter.

Essentially, all models are wrong, but some are useful

George E.P. Box,

(Box and Draper, 1987)

5

Advanced fracture models

5 ADVANCED FRACTURE MODELS

In the previous chapter it was shown that the MOR parameter cannot be relied upon to predict the peak load and post crack behaviour of different sized structural elements in flexure. In this chapter, the aim is to devise a fracture mechanics damage model for the material. The damage function will be based on the specific fracture energy (G_f) and tensile strength (f_t) parameters determined for the high performance fibre reinforced concrete in the previous chapter. The hypothesis is that such a model would allow better prediction of the flexural capacity of the material. A further purpose of the numerical modelling is to validate the methodology used to determine the fracture parameters as presented in the previous chapter.

The second aim of this chapter is to test the hypothesis that the accuracy, and possibly the precision, of fatigue prediction models for the material can be improved through the use of fracture mechanics concepts. The findings of the monotonic and cyclic loading experiments are combined in order to devise a model for the prediction of fatigue in UTCRCP material.

The development and validation of the fracture mechanics damage models for the material are discussed in Section 5.1. The work in Section 5.2 demonstrates that the numerical models allow the numerical simulation of fracture in beam and centrally loaded disk specimens. The models can be used to predict size effect observed in the experiments. In Section 5.3 the numerical models are adjusted to allow the simulation of flexural behaviour of beams containing rebar. The results of the numerical simulation of the cylinder splitting tests are presented in Section 5.4. In Section 5.5 the numerical models developed in the study are used to simulate fracture in examples of full size pavement structures. Models for the prediction of fatigue using conventional methods and fracture mechanics based approaches are developed

in Section 5.6. The final section of this chapter contains a discussion on the numerical fracture models put forward by this study.

5.1 Development of fracture models

According to the cohesive softening model, the material behaves linear elastically until the principal stress reaches the tensile strength of the material, at which point a crack is induced. The linear elastic part of the material response in the numerical simulation is defined by the values for Young's modulus and Poisson's ratio in Table 4-1. For the post cracking behaviour of the material a suitable mathematical softening functions had to be developed. Several different types of post crack cohesive softening functions used for fibre concrete were discussed in Section 2.5. Initially, a simple exponential shape was used for the softening function. Later in the study, the exponential model was replaced by more advanced softening function with crack tip singularity.

A damage function for failure in compression was not included as part of the study. The compressive stresses in the numerical simulation of the flexural tests were monitored to ensure that the compressive stress did not significantly exceed the compressive strength.

5.1.1 Development of exponential tensile softening function

The exponential softening function was developed after completion of the first round of testing. The main advantage of the exponential softening function is that only the tensile strength of the material and the fracture energy need to be known to fully define the shape. Other approaches invariably require tests performed on samples with a range of sizes and a constant geometry, and/or measurement of the crack mouth opening displacement, and/or the use of loading-unloading procedures during the test. This type of detailed information on the post crack behaviour was not available at this early stage of the study. Exponential softening was considered a suitable starting point for the analysis due to the fact that the post crack behaviour of fibre reinforced concrete shows a steep initial drop off in stress followed by a long tail of gradual softening.

The exponential softening functions developed as part of this study for the first four mixes tested, are shown in Figure 5-1. In the numerical simulation, elements respond linear

elastically until the set tensile strength for the material is exceeded, at which point a cohesive crack is formed in the element. After induction of the crack, stress (σ) is transferred across the crack faces following the exponential function of the crack width (w):

$$\sigma = \mathrm{f}(w) = f_t \mathrm{e}^{\frac{-wf_t}{G_f}} \qquad (5.1)$$

The stress transferred over the crack reduces exponentially towards zero with the increase of the crack width. This is an acceptable approximation, as in reality the critical crack width for the total softening function is very large. A situation of zero stress transfer will only be reached when the crack width is equal to half the length of the steel fibres (i.e. ½ x 30 mm) and all fibres in a unit area have been pulled out completely.

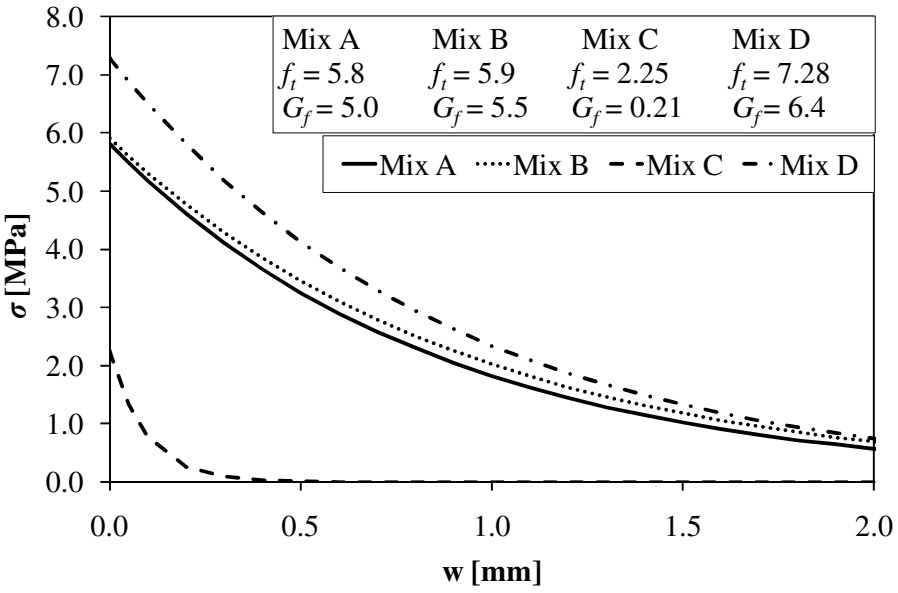

Figure 5-1: Exponential softening functions used for Mix A,B,C,D

The exponential softening function was used to simulate the flexural tests performed on Mix A, B, C and D beam specimens. It was found to be possible to obtain acceptable results from the numerical simulation using the exponential softening function. The results of the numerical simulation in OpenSees for the various specimen sizes are provided in Appendix C. Figure 5-2 shows the results of the numerical simulation with exponential softening for TPB1-A as an example. The figure shows the results for two simulation runs. One (f_t = 6.4)

was performed using the tensile strength obtained from the tensile splitting test, the other (f_t = 5.8) represents a best fit to data determined by means of a parameter study.

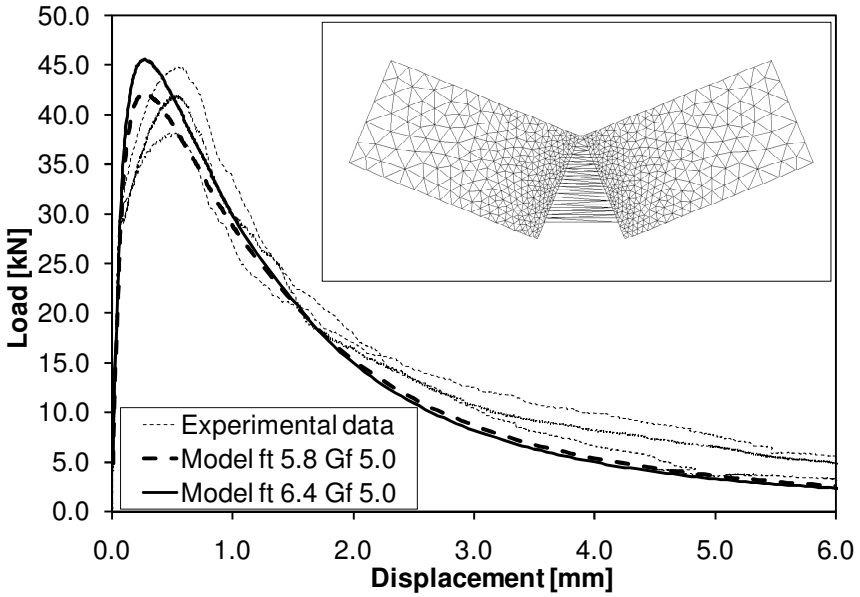

Figure 5-2: Numerical simulation of TPB1-A

With exception of the plain concrete, it was found that simulation using the exponential softening function and the value of f_t from the adjusted tensile splitting test as described in Section 4.4.3 with G_f as determined using the procedure in Section 4.4 leads to overestimation of the flexural capacity of the beams. In the early stages of this study it was not clear whether the error was due to the test method used to determine the fracture properties, or to the shape of the softening function. It was found that a good fit to data could be obtained for the fibre reinforced concrete flexural tests in both TPB and FPB configuration provided the tensile strength was calibrated. The optimized softening functions for the mixes A and B in Figure 5-1 therefore have reduced tensile strengths compared to experimentally determined values. The figures in Appendix C show the results for the numerical simulation using optimized softening functions. The simulation of Mix D tests was performed without calibration. In a publication on the size effect study performed on Mix D by Denneman et al. (2010a) it was simply noted that the exponential softening function leads to an overestimation of the flexural capacity when f_t is used uncalibrated. The simulation of the tests on the plain concrete Mix C specimens also reported in Denneman et al. (2010b) did not require

calibration as the simulation using the experimentally determined fracture properties allowed for acceptable results as shown in Figure 5-3.

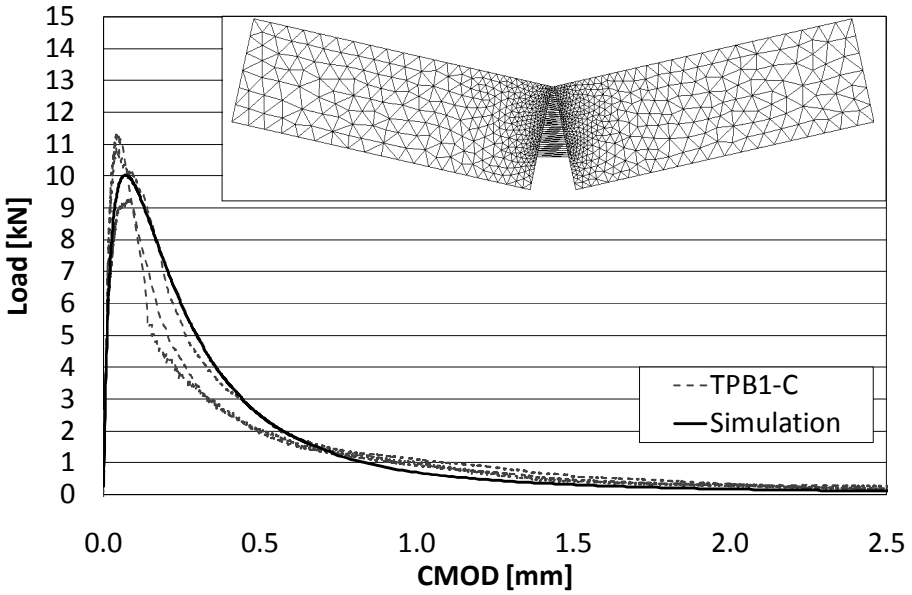

Figure 5-3: Numerical simulation of TPB experiments on plain concrete

Apart from the simulation of experiments performed as part of this study, the EDM with exponential softening function was also applied elsewhere. Wu et al. (2009) used it to model beam tests on asphalt and Denneman et al. (2009) applied it to fracture in concrete specimens. The model was further applied to simulate fracture in disk shaped direct tensile tests on asphalt as reported in Denneman (2010).

The exponential softening function allowed satisfactory simulation of the flexural beams, provided that the model was calibrated for the value of f_t. Through the modelling of the tensile splitting tests (discussed in Section 3.3.2), however it became clear that the simple exponential shape did not replicate the initial part of the softening behaviour of the fibre reinforced material well enough.

5.1.2 Improved exponential softening function with crack tip singularity

As described earlier in Section 2.5.7, Lim et al. (1987) studied the softening behaviour of concrete with a similar type of steel fibres from the same producer as used for this study. The study found that the material behaviour is best simulated using a softening function with an initial spike at high strength followed by a long tail at a lower stress. The rapid drop in stress at crack induction followed by more gradual degradation can be modelled using a crack tip singularity approach. Crack tip singularity is suitable for fibre reinforced composites, as it simulates the initial failure of the matrix followed by the slow pull out of the fibres (Bažant and Planas, 1997, Dupont and Vandewalle, 2004).

To improve on the fit of the numerical simulation allowed by the simple exponential softening function, a slightly more complex softening function with crack tip singularity followed by exponential softening was developed. The material behaviour in tension is shown schematically in Figure 5-4a. Initially the material behaves linear elastically until f_t, is reached. When the crack is introduced in the concrete, the stress drops until the fibres are activated. In the model it is assumed that the stress drops without an increase in crack width w, resulting in a crack tip singularity. The stress at the base of the singularity is the post singularity crack bridging stress (σ_1). After the initial drop in stress, the softening takes an exponential form.

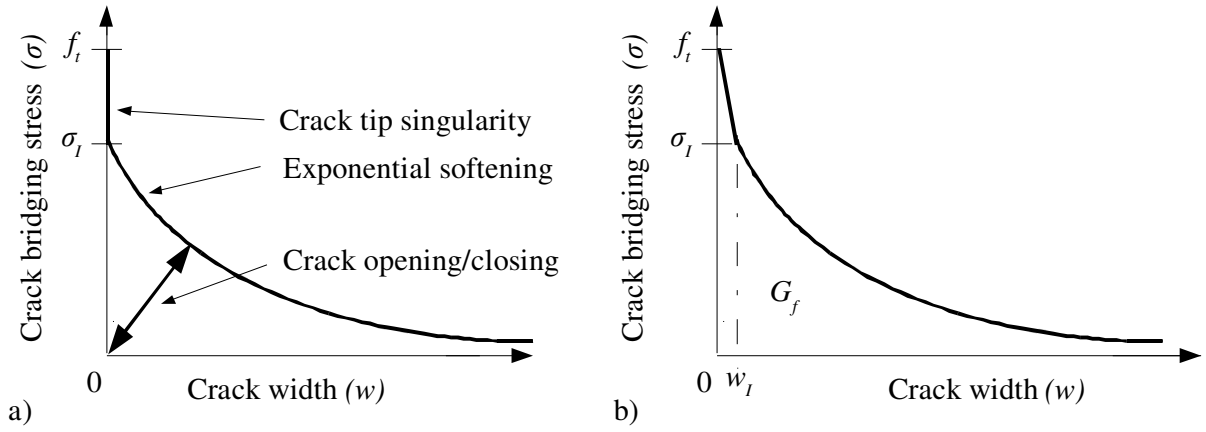

Figure 5-4a: Material behaviour in EDM simulation, b: Softening function as implemented in FEM as part of this study

To achieve the material behaviour shown in Figure 5-4a, a softening function combining a linear and an exponential part was implemented in the EDM code in OpenSees. The function is as shown in Figure 5-4b. When the tensile strength (f_t) of the material is reached a crack is formed, the stress transferred across the crack reduces linearly with an increase in crack width (w) for $0 < w < w_I$ according to:

$$\sigma = f_t\left(\frac{f_t - \sigma_I}{w_I}\right)w \tag{5.2}$$

Once w_1 is reached softening becomes exponential for $w_I < w < \infty$. The exponential softening is defined by value of σ_I and the remaining fracture energy $G_{f,I}$. This is the specific fracture energy G_f less the energy dissipated under the linear softening:

$$G_{f,I} = G_f - \left(\frac{f_t + \sigma_1}{2}\right)w_I \tag{5.3}$$

The exponential part of the softening function is given by:

$$\sigma = \sigma_I e^{(-a_I(w - w_I))} \tag{5.4}$$

With:

$$a_1 = \frac{\sigma_I}{G_{f,I}} \tag{5.5}$$

To create the softening curve with crack tip singularity shown in Figure 5-4a, w_I was initially set to 0 in the above equations for the simulation of flexural beam tests. As G_f is determined from the TPB results and f_t is obtained from tensile splitting tests, σ_I is the only unknown to be calibrated in the model. It was later found that if a small displacement w_I is allowed, a better fit of the model can be obtained for the tensile splitting tests. w_I was set to 0.005 mm, for reasons discussed in detail in Section 5.4. The final calibrated softening curves for the fibre reinforced mixes are shown in Figure 5-5. The curves were developed based on a parameter study to achieve the best fit for both the flexural beam and tensile splitting tests. The difference between the mixes in terms of post cracking stress capacity due to difference in mix composition and importantly fibre content is visible in Figure 5-5. The results of the numerical simulation using the crack tip singularity approach are shown in Appendix D.

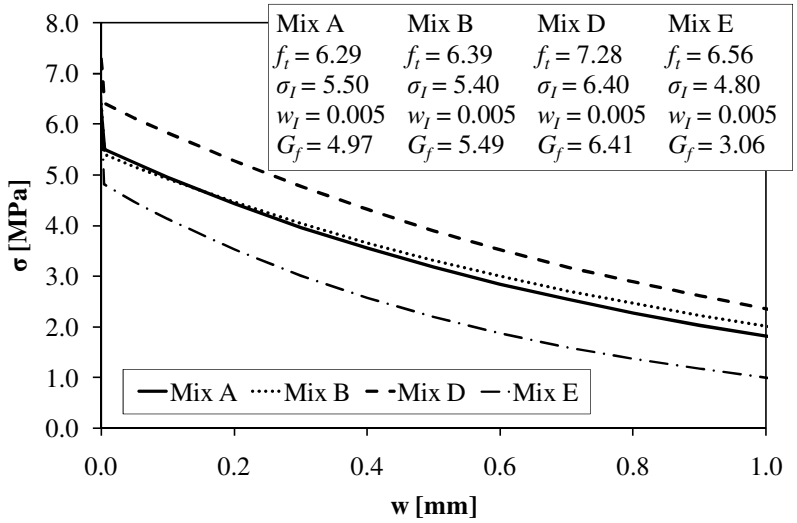

Figure 5-5: Optimized softening functions for studied mixes

5.1.3 Mesh size sensitivity

Researchers often opt for very fine meshes in and around the crack area to avoid issues with mesh size objectivity. In the EDM the crack is not restricted to follow element boundaries and nodal points and this relieves some of the mesh size requirements other FEM crack simulation approaches have. The primary consideration in choosing mesh size for the EDM used in this study is the prevention of crack locking. In the EDM the conditions for cracking and the direction of the crack are calculated at element level. As a result a discrete crack in the beam may lock when an element, typically at the crack tip, forms a crack in the direction perpendicular to the main crack direction. The EDM approach used for the present study includes a technique proposed by Sancho et al. (2007) to avoid crack locking on a local (element) level by allowing the direction of the crack to change and be solved for each analysis step while the crack width is small. Sancho et al. (2007) used crack width values in the range between 0.1-0.2 G_f/f_t as a threshold to fix the direction of the crack. For the present study a value of 0.2 G_f/f_t was applied with good results. Crack locking may still occur, and becomes more likely as the crack approaches the top of the beam. For successful calculations a balance needs to be found between the mesh size, the number of iterations per analysis step, and threshold width for the crack direction. As long as a reasonable number of elements are used in the fracture ligament area the model provides consistent results independent of mesh size. Figure 5-6 shows a comparison between the results of an analysis performed with a mesh size standard for this study (5 mm in the crack area) and an analysis with a very fine mesh (0.5 mm in the crack area). The resulting load-deflection curves are almost identical.

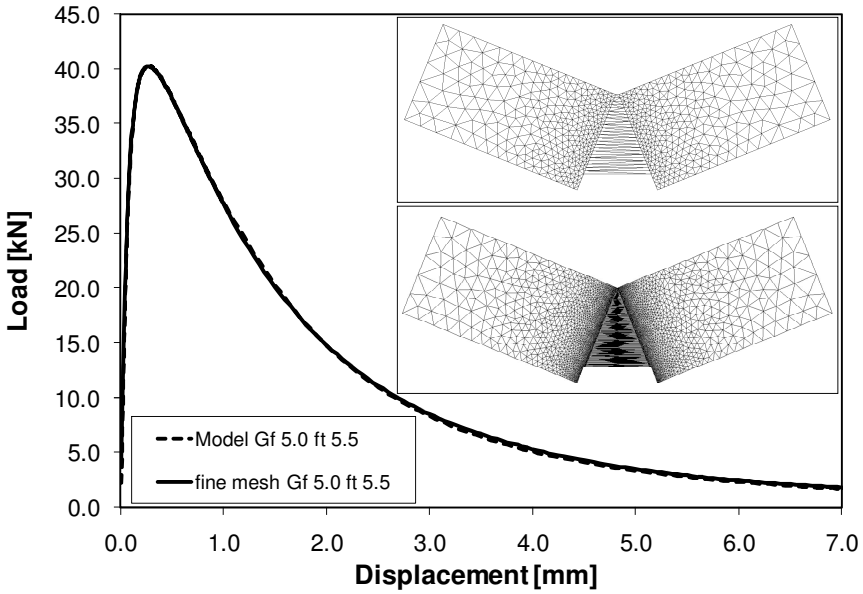

Figure 5-6: Comparison of EDM results using different mesh sizes.

5.1.4 Comparison of OpenSees and Abaqus models

To ensure that the fracture simulation using the Abaqus brittle cracking model with the softening functions developed in this study is equivalent to the results obtained from the EDM in Opensees, both approaches were applied to simulate a TPB test. The results of the numerical simulations of specimen type TPB1-A using the exponential softening function are shown in Figure 5-7.

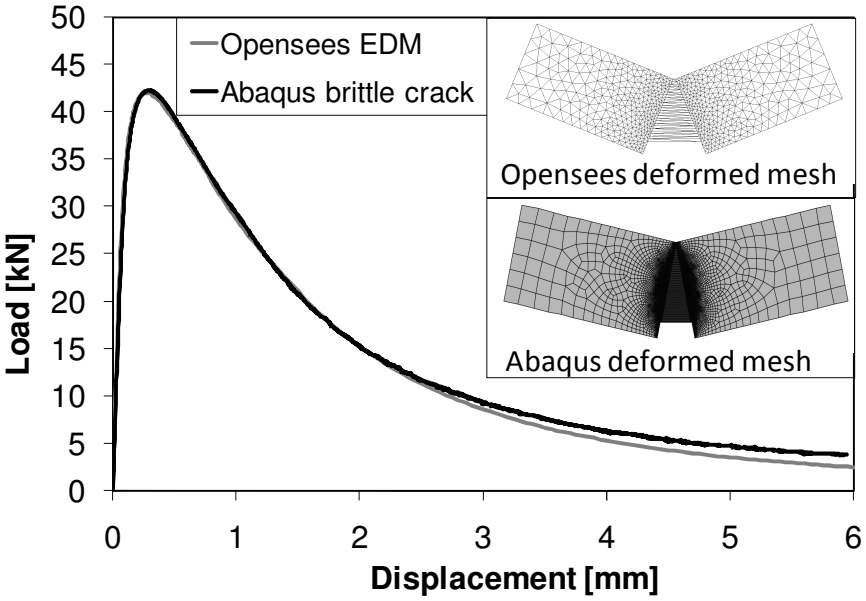

Figure 5-7: Comparison of numerical simulation using Opensees and Abaqus

A characteristic element size of 1 mm was used for both the triangular OpenSees elements and the Abaqus quadrilateral elements in the ligament area above the notch. At the far edges of the mesh, the characteristic size of the elements was set to 25 mm. The results obtained from the simulations are almost equivalent. Only at large displacements do the load displacement curves diverge slightly. This was taken as proof that the Abaqus brittle cracking model was correctly configured, allowing its use for the simulation of the tensile splitting tests and flexural disk tests.

5.2 Size independent simulation of fracture

The most compelling reason for the use of fracture mechanics in the analysis of concrete structures is the occurrence of size-effect. In Section 4.3 it was shown that the high performance fibre reinforced concrete material is subject to significant size-effect. As a result the MOR obtained from laboratory specimens cannot be relied upon to predict the peak load for structural elements of a different size or geometry. The purpose of this section is to demonstrate that the fracture models developed in the previous section can be used to successfully predict the flexural behaviour of elements of various sizes and geometries.

5.2.1 Prediction of size effect in flexural beam tests

In Figure 5-8 a comparison is shown between the average flexural response data obtained from TPB experiments on Mix D specimens and those produced through numerical simulation. Results are plotted in terms of the LE derived nominal stress and the relative deflection of the different sizes of beams as was done earlier for the experimental results only in Figure 4-2b. The numerical simulation was performed in the OpenSees model using the softening function for mix D shown in Figure 5-5. The figure shows the model to provide a close prediction of the change in the material response for the different sizes. The use of LE based design methods would have lead to identical curves for all sizes, which is at odds with reality.

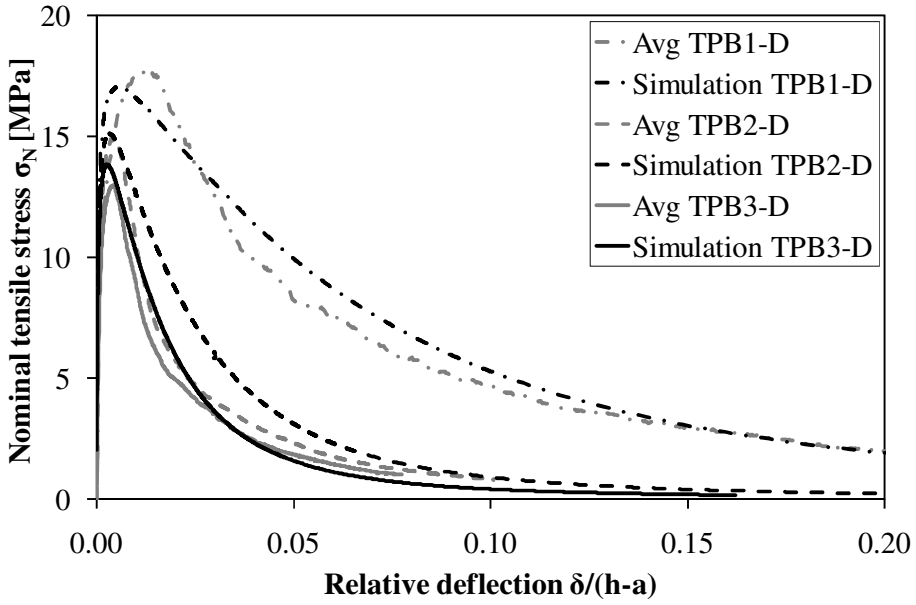

Figure 5-8: Prediction of size effect in TPB tests

The trends in the experimental and predicted σ_{Nu} size-effect for TPB and FPB specimens of mix D are shown in Figure 5-9. To show the numerical trend beyond the two FPB specimen sizes tested, the range of the modelled results was extended by simulating additional fictitious 30 mm, 50 mm and 360 mm high beams maintaining geometry. The numerical simulation provides a satisfactory prediction of the size-effect that occurred in the experiments. The experimental results do show a stronger size-effect than the numerical simulation. This is due to the fact that the numerical simulation predicts fracture mechanics size effect only. Other

sources of size-effects stemming from specimen preparation, e.g boundary layer effect, statistical size effect, hydration heat, etc. are not predicted in the numerical analysis.

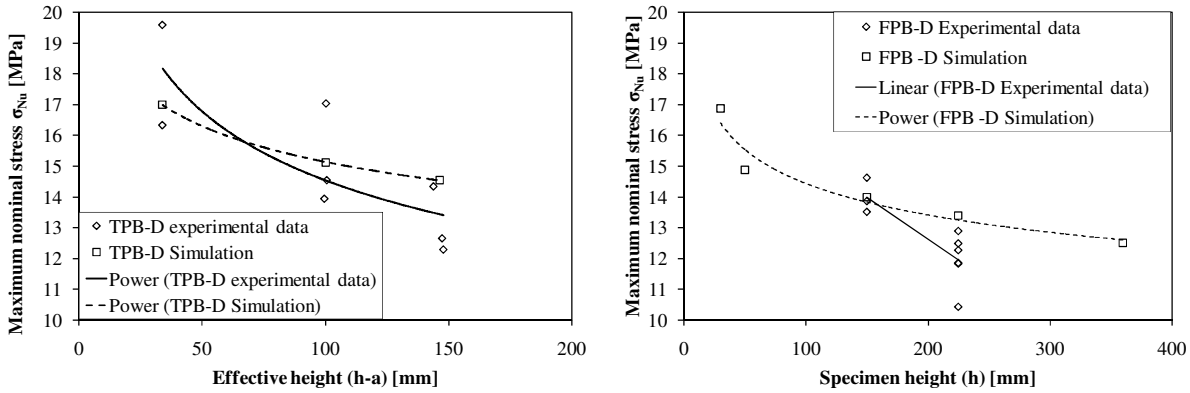

Figure 5-9: Experimental and predicted MOR size-effect trends for TPB and FPB

For the numerical simulation of specimen type TPB3-D, the stress state in the ligament above the notch at peak load is shown in Figure 5-10.

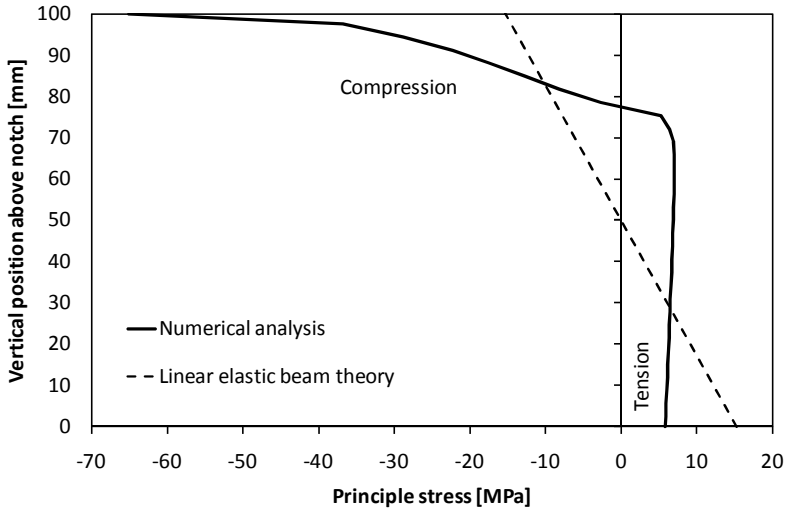

Figure 5-10: Simulated stress state at peak load for specimen TPB3-D

The fracture zone has progressed ¾ of the way up the beam. The figure provides a clear indication of the considerable difference between the proportional tension and compression

stress distribution assumed in LE analysis and the stress state in the fracture mechanics simulation. This difference in stress condition between the two approaches explains why fracture mechanics can be applied to predict the behaviour of different sized elements, while LE analysis cannot.

5.2.2 Simulation of flexural disk tests in Abaqus

The monotonic tests on disk specimens were modelled in Abaqus. A linear elastic (LE) analysis of the tests was run first to compare the results to the assumptions underlying the yield line discussed in Section 4.3.3. The second step was to analyse the disk using the cohesive crack model developed in the previous section. If the numerical simulation proofs successful, this would mean that the fracture mechanics based methodology can be used to predict the flexural behaviour of not only different sized elements, but also elements with different geometry.

In this first simulation, linear elastic material response was assumed, as would normally be done when calculating the carrying capacity of pavement slabs. The mesh for the model is shown in Figure 5-11a. Figure 5-11b shows the principal stress condition in 800 mm diameter disk at the peak load recorded in the experiments.

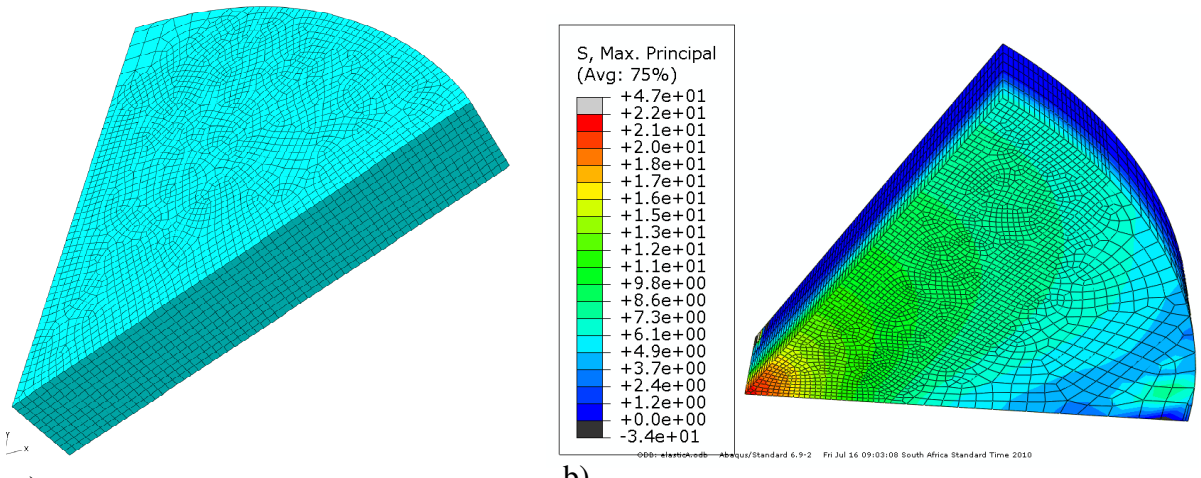

a) b)

Figure 5-11a: Mesh, b: Peak stress distribution LE model

The results indicate that the maximum tensile stresses at peak load condition are in the region of 22-24 MPa, well above MOR strength values for the material presented in Table 4-2. These peak stresses are also well above the σ_N values obtained using yield line theory as discussed in Section 4.3.3. The difference stems from the fact that in the yield line solution the stresses along the failure plane are assumed to be evenly distributed at the experimental peak load. These results indicate that if the MOR was used to predict the peak load condition of the panels, as is done in pavement design, the flexural capacity of the panels would have been underestimated. Since the MOR values for the material are between 11 and 14 MPa, the error in the prediction of the disk capacity would have ranged from approximately 70 to 100 percent.

The model can also be applied to determine whether size effect occurs in the disk test results when analysed under the assumption of linear elasticity. Figure 5-12 shows the nominal tensile stress along the symmetry line midway between two supports from the centre of the disk to the edge. In other words: along the highly stressed edge as seen on the left in Figure 5-11b. Results are shown for the 800 mm and 600 mm diameter disks prepared using Mix A and B material. The distance to the centre is plotted relative to the size of the disk. The models of the different specimen types are loaded to the respective experimental average peak load. The results show the high tensile stress at the centre of the disk. The results further indicate a slight size-effect between the results for the 800 mm and 600 mm diameter disks, with the smaller specimens providing a relatively higher loading capacity.

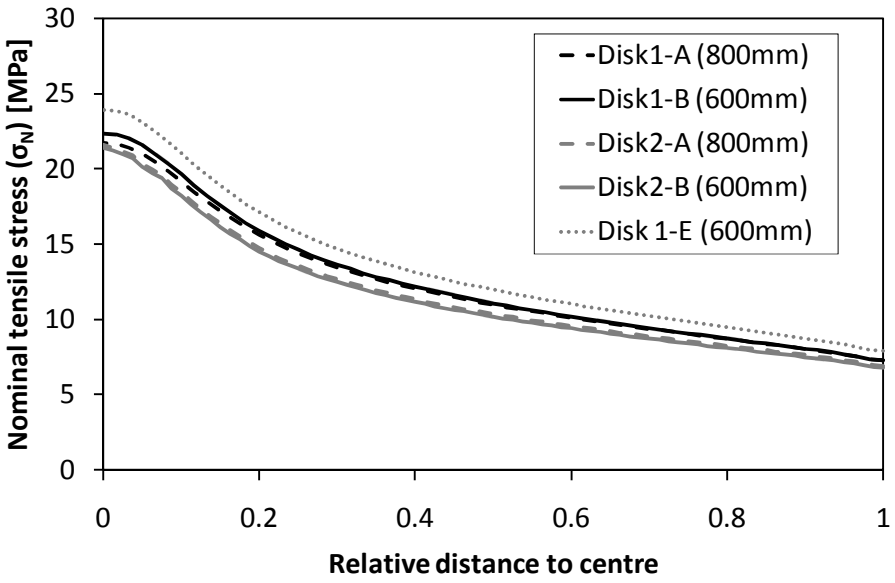

Figure 5-12: Linear elastic stress condition at mid span of disks

The next step is to numerically simulate the disk experiments using the same cohesive crack damage model applied successfully to the beams in the previous sections. The disks are modelled in using the Abaqus software environment as discussed in Chapter 3. The model and mesh for the fracture analysis are as shown in Figure 5-11b. Cohesive elements were used for the entire model, with exception of the area around the support. In this area linear elastic bulk elements were used to prevent cracks forming due to unrealistic stress concentrations.

When the initial cracks form in the model at midspan between the supports stresses redistribute leading to new highly stressed areas. Secondary cracking will occur in these areas, leading to a front of multiple cracks moving away from the main crack. This situation corresponds well to the reality of the experiments in which secondary crack patterns were observed parallel to the principal cracks as can be seen in Figure 5-13. Although the disk eventually breaks into three parts, with the failure plane approximately at the centre between the support, tension cracks have formed over a considerable area around the main cracks.

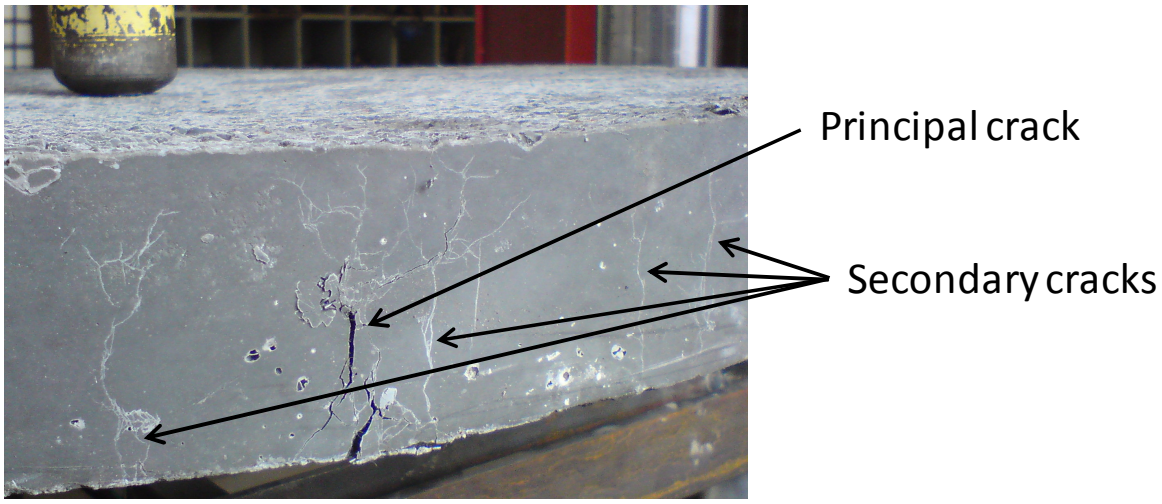

Figure 5-13: Multiple cracks forming in centrally loaded disk test

Appendix E contains the results of the numerical simulation for the different disk specimen types. Figure 5-14 shows the result of the numerical simulation for the 800 mm diameter, 70 mm high disk produced from mix A.

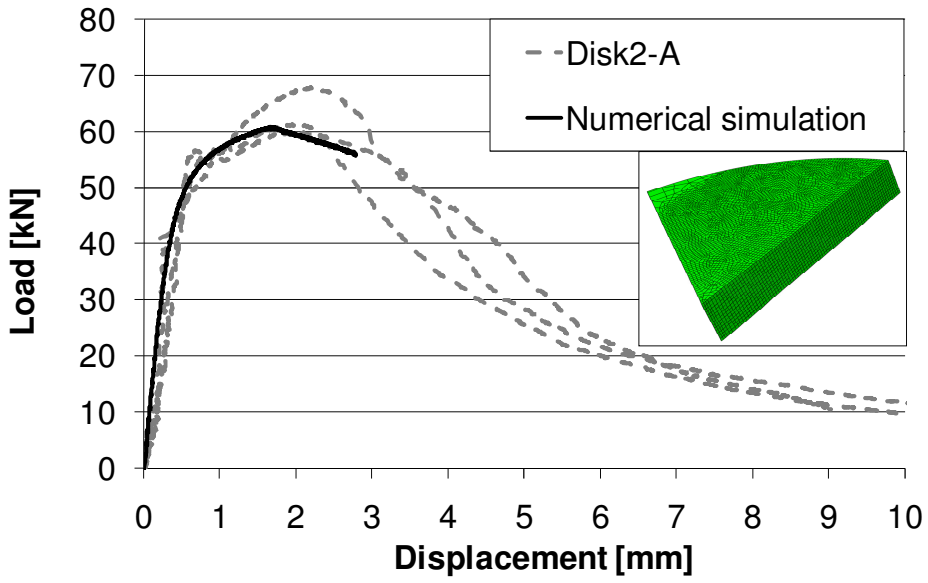

Figure 5-14: Result of numerical simulation Disk2-A

The results provide an accurate prediction of the pre-peak, peak load and early post-peak behaviour for the specimens. At larger deflections the crack tends to get locked, leading to impossibly high stresses in the material. As a result, the load carried by the slab does not decrease at the pace observed in the experiments. The simulation was stopped when crack locking started to occur. The simulation yields satisfactory results in predicting the peak load for the disks however.

The main difference between the LE and the fracture mechanics analysis is the distribution of highly stressed areas. In the LE analysis at the peak load condition recorded in the experiment, an area with unrealistic high stresses, much higher than the tensile strength or even MOR exists at the bottom around the centre of the disk. In the fracture mechanics analysis, the first cracks appear in this area when the stress reaches the tensile strength of the material. The stresses redistribute as the crack grows up and towards the edge of the slab. As the stresses redistribute, elements next to the initial cracked area start reaching the tensile strength as well and the fractured area spreads. The occurrence of additional smaller cracks, besides the three main cracks at mid span between supports, corresponds to the observations made during the experiments.

5.2.3 Summary of results for numerical simulation of unreinforced flexural tests

Table 5-1 shows the accuracy of the numerical models, in terms of the prediction of the peak load obtained in the various flexural experiments. In some cases the error is still considerable, however the prediction is far more accurate than linear elastic analysis would allow.

For some of the experiments, analysis was performed using both the exponential softening curve and the softening function that combines crack tip singularity with exponential softening. Comparing the results of the numerical simulation of beam bending tests obtained using the two softening function types however, serves limited purpose as both were calibrated against these data sets. The softening function with crack tip singularity has the following advantages over the simple exponential function:

- it resembles the documented softening behaviour of fibre reinforced concrete better,
- it allows simulation of the material behaviour observed splitting tests as will be shown in Section 5.4, and

- it allows the unaltered use of the tensile strength as obtained from tensile splitting tests as a material property.

Table 5-1: Accuracy of numerical models in prediction of monotonic peak load.

Specimen ID	P max experimental [kN]	Pmax Exponential [kN]	Error [%]	P max singularity [kN]	Error [%]
TPB1-A	41.7	39.6	4.9%	40.4	3.1%
TPB2-A	42.2	39.4	6.6%	40.5	4.0%
TPB3-A	5.6	6.7	-20.4%	6.9	-22.9%
TPB4-A	6.9	6.7	2.9%	6.9	-0.3%
FPB1-A	102.8	85.7	16.6%	91.4	11.1%
Disk1-A	39.4			39.4	0.0%
Disk2-A	63.0			60.8	3.5%
TPB1-B	43.5	40.3	7.3%	40.0	8.0%
TPB2-B	6.7	6.9	-2.6%	6.8	-1.8%
TPB3-B	7.4	6.9	7.0%	6.8	7.7%
FPB1-B	109.2	109.9	-0.6%	90.4	17.2%
Disk1-B	40.0			40.4	-1.0%
Disk2-B	61.9			61.8	0.2%
TPB1-D	12.6	11.7	7.2%	11.9	5.6%
TPB2-D	30.5	29.5	3.3%	30.4	0.3%
TPB3-D	37.4	40.7	-8.9%	41.2	-10.2%
FPB1-D	107.4	119.9	-11.6%	106.3	1.0%
FPB2-D	137.3	163.3	-18.9%	153.3	-11.7%
TPB1-E	25.5	24.7	2.9%	26.3	-3.3%
FPB1-E	101.5			101.0	0.5%
FPB2-E	49.9			47.3	5.2%
FPB3-E	12.1			12.2	-0.8%
Disk1-E	42.2			45.0	6.6%

5.3 Modelling beams with reinforcement bars

The goal of this study is to help improve the design models for concrete road pavements containing a combination of fibre reinforcement and conventional rebar. Therefore, the test matrices for Mix A and B include TPB tests on concrete beams containing reinforcement bars in addition to fibres. The effect of the rebar on the material response in TPB needs to be provided for in the numerical model for it to fully simulate material behaviour in the bending

tests. The behaviour of the steel reinforcement bars in tension has to be known in addition to the earlier discussed fracture properties of the fibre concrete mixes. A set of direct tension tests was performed on the reinforcement bars to determine elastic and plastic properties. The stress-strain relationship obtained for the rebar is shown in Figure 5-15. The average ultimate tensile strength of the bar is 550 MPa, while Young's modulus (E) was estimated at 2.11E+05 MPa from the slope of the elastic part of the curve. A typical value of 0.28 for Poisson's ratio of steel was selected. The behaviour of the rebar is modelled using the Opensees J2 Plasticity material. The element requires bulk modulus (K) and shear modulus (μ) to be defined for the elastic part of the stress strain behaviour:

$$K = \frac{E}{3(1-2\upsilon)} = 1.60\text{E}05\ \text{N/mm}^2 \tag{5.6}$$

$$\mu = \frac{E}{2(1+\upsilon)} = 8.24\text{E}04\ \text{N/mm}^2 \tag{5.7}$$

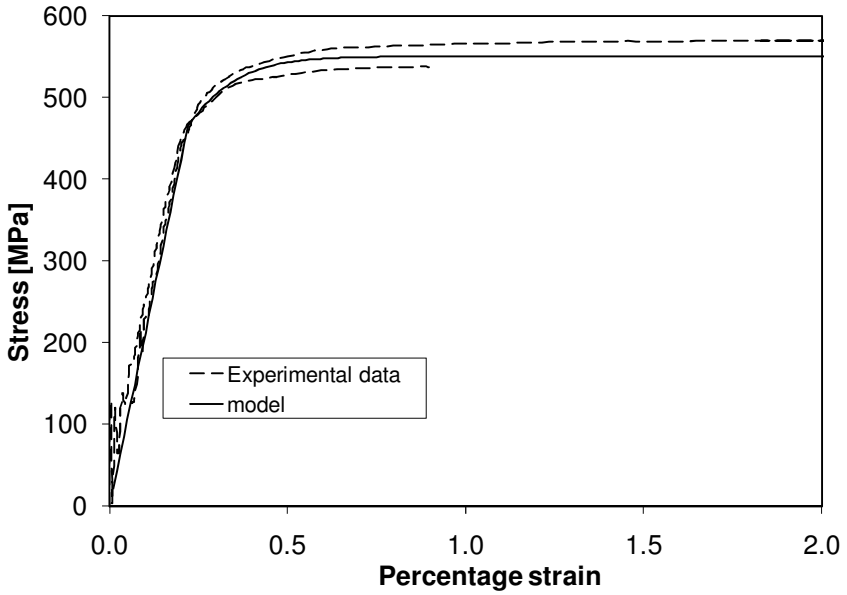

Figure 5-15: Experimental and modelled stress-strain relationship for reinforcement bars

The plastic part of the material behaviour is represented by an initial yield stress, a final yield stress level and an exponential and/or linear hardening parameter. Based on the direct tensile test results for the rebar the initial yield strength was set to 465 MPa and the saturation stress level at 550 MPa. An exponential hardening parameter of 1000 was found to provide the best fit to the test data. The result of a numerically modelled uniaxial test on the rebar with the properties described above is also shown in Figure 5-15.

The reinforcement bars are included in the numerical model as a thin strip of continuum elements. The thickness of the strip was chosen such that the cross-sectional area of the three 5.6 mm diameter reinforcement bars is divided equally over the width of the beam. Figure 5-16 shows an example comparison between the load-deflection curves obtained from the laboratory experiments and from the numerical model.

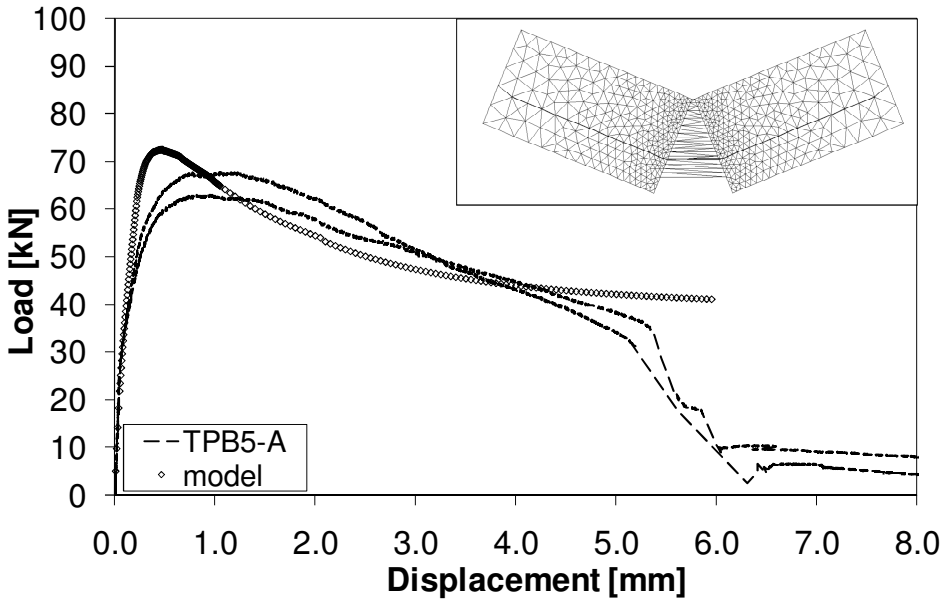

Figure 5-16: Experimental data and numerical simulation for specimen type TPB5-A including rebar

The predicted and experimentally obtained peak loads for beams of different sizes are shown in Table 5-2. The numerical model over-predicts the peak load. One of the reasons for this is the absence of bond slip; unrealistically high shear stresses are transferred to the concrete material surrounding the rebar. It would be possible to further improve the results by including a pull-out model; a number of available methods are described in Bažant and

Planas (1997). Another limitation of the current model is that the eventual tensile failure of the reinforcement bars cannot be covered by the J2 Plasticity material. Therefore, the model does not show the sudden drop in load level that can be identified in the experimental data in Figure 5-16 at approximately 5.5 mm deflection. Notwithstanding these two limitations the model was found to provide a satisfactory prediction of the peak load and the shape of the load-deflection curve. Importantly, this exercise shows that it would be possible to include rebar in the fracture mechanics analysis of concrete pavement structure.

Table 5-2: Comparison between predicted and actual peak loads for beams with rebar

Specimen type (Mix A + 3Y5.6)	**TPB5-A**	**TPB6-A**	**TPB7-A**	**TPB8-A**	**FPB2-A**
P_{max} [kN] Experiment	65.4	64.1	10.5	11.6	116.5
P_{max} [kN] Simulation (G_f = 5.0 N/mm, f_t = 5.8 MPa)	72.3	73.1	13.9	14.0	159.9
Percentage error [%]	10.6%	14.0%	32.4%	20.7%	37.3%
Specimen type (Mix B + 3Y5.6)		**TPB4-B**	**TPB5-B**	**TPB6-B**	**FPB2-B**
P_{max} [kN] Experiment	-	64.4	12.6	13.4	141.2
P_{max} [kN] Simulation (G_f = 5.5 N/mm, f_t = 5.9 MPa)	-	75.6	14.1	14.1	161.3
Percentage error [%]	-	17.4%	11.9%	5.2%	14.2%

5.4 Numerical model of tensile splitting test

The adjusted tensile splitting experiments were simulated using the Abaqus model discussed in Section 3.3.2. The simulated load-transversal deformation response for the different mixes is shown in Figure 5-17. The simulation is successful in predicting the first peak load P_I at which a crack is introduced. If the obtained P_I values are used to back-calculate f_t using Equation 4.19 the results are within 1 percent of the input value. This confirms the need to use the correction for boundary conditions proposed by Tang (1994), on which Equation 4.19 is based. Importantly, the results of the numerical simulation shows a similar trend to the experimental results, after reaching the first peak, the load level stabilizes and then starts to increase again. This phenomenon is caused by the use of the softening function with crack tip singularity.

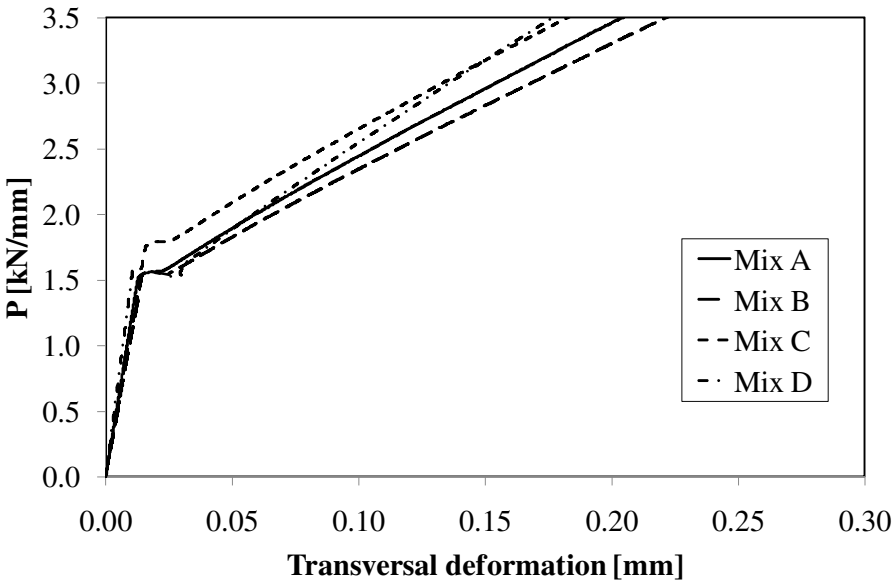

Figure 5-17: Simulated load-transversal deformation response

The numerical analysis allows a study of the stress distribution at the different stages of the test. Figure 5-18a shows the principal stress distribution just before a crack forms at the centre of the specimen. This is the linear elastic stress distribution assumed when calculating the tensile strength from the splitting test using Equation 4.19.

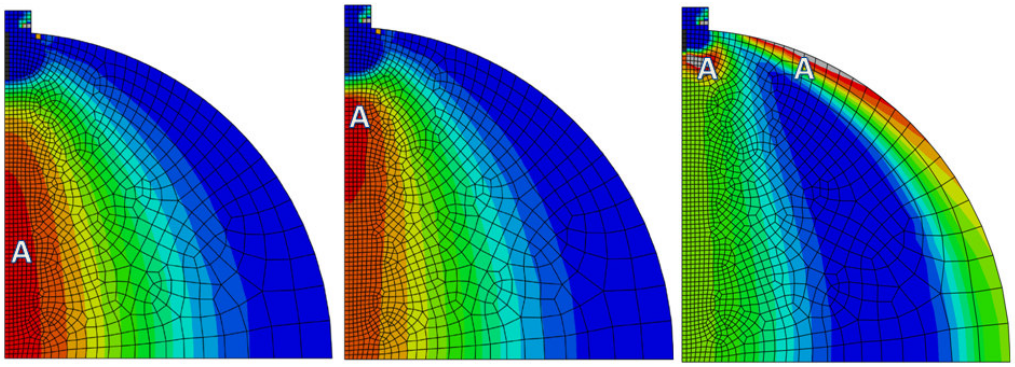

a) b) c)

Figure 5-18: Principal stress distribution in numerical model of splitting test

Highly stressed areas are indicated in the figure with “A”. Once the tensile strength is reached, a crack forms at the centre of the specimen and propagates upward as shown in

Figure 5-18b. The stress redistribution following the initial peak load, shown in Figure 5-18c, sees the relaxation of stresses along the loading axis and the formation of highly stressed areas at the top and the side of the specimen. The stresses in these areas exceed the tensile strength of the material and would lead to secondary cracking as discussed in Section 3.2.6. The model however does not contain fracture elements in these regions and therefore no secondary cracking occurs in the simulation. Consequently, the load- transversal deformation curves in Figure 5-17 do not yield an ultimate load P_u value.

The numerical simulation of the tensile splitting tests confirms that the ultimate peak load is related to secondary cracking mechanisms. The first peak P_I represents the linear elastic limit state and from it a best estimate of the tensile strength material property can be calculated.

5.5 Application of the damage model to simplified pavement structure

The numerical simulation and analysis in this document have so far been confined to laboratory experiments. To further explore the use of fracture mechanics in pavement design, a simple hypothetical pavement structure is analysed. The numerical analysis is run using LE and fracture mechanics material behaviour for the concrete pavement slab. Figure 5-19a shows the boundary conditions of a simplified pavement system. A 50 mm thick slab was modelled using the material properties of Mix E. The slab is supported by a 950 mm thick base with a E value of 200 MPa, on a stiff support. The load case is a classical corner load on the free edge of the slab. The area of the structure is 1.8m x 1.8m, with symmetry boundary conditions on two of the edges of the slab, making the effective size of the model 3.6 m x 3.6 m. The pressure loading is applied on a 100 mm x 100 mm patch using a ramp function. The mesh for the pavement slab consists of two layers of elements with a characteristic size of 25 mm. The elements for the elastic base layer are larger. The model is simplistic and not representative of an in situ pavement, UTCRCP or other, nor is the meshing optimal for analysis of a pavement. This simple model is however deemed suitable to compare the behaviour of a pavement slab with LE material properties and a slab with a cohesive crack damage definition on an elastic support.

Figure 5-19b and Figure 5-19c show a comparison between the results obtained for the simulation of stresses in a slab consisting of LE and for a slab consisting of elements with cohesive fracture damage definition. The pressure load on the LE model was increased until

the tensile stresses in the slab were equal to the MOR value of 13.9 MPa as obtained for the material from FPB tests on beams with a 150 mm x 150 mm cross section (refer Table 4-2). This occurred at a pressure of 3.36 MPa in the loaded area, equal to an external load of 33.6 kN. Coincidentally, this is representative for the load applied by the wheel of a truck steering axle. The resulting stress distribution in the pavement is shown in Figure 5-19b. The stress distribution in the slab with the cohesive crack damage definition under the same loading is shown in Figure 5-19c.

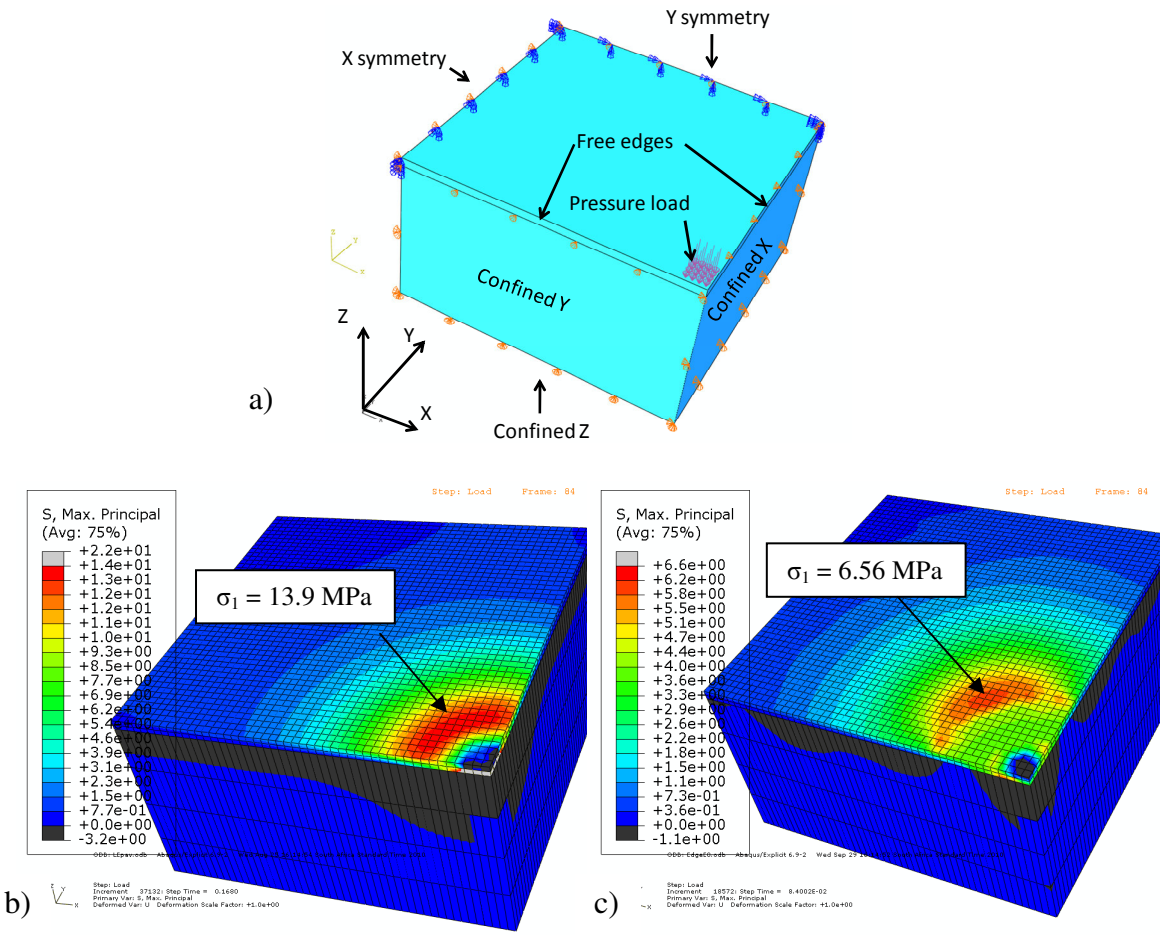

Figure 5-19a: Boundary conditions FRC pavement model, b: Result LE analysis, c: Result fracture model.

Fracture occurs at a tensile stress of 6.56 MPa, the first crack formed in the same area where the highest tensile stress occurs in Figure 5-19b. Further loading results in the cracks forming in elements further away from the slab edge. At the final 33.6 kN load condition, the stress area for which the highest stress occurs in the LE analysis has decreased significantly due to softening in the crack model. The main implication is that at stresses of approximately 50 % of the MOR cracks are introduced to the pavement causing stress relaxation. The comparison

shows that LE analysis leads to unrealistically high stresses that cannot occur in the material. As discussed in Chapter 2, fatigue performance of the pavement is predicted in conventional theory by the ratio of the LE derived stresses in the pavement slab to the MOR of the material. The purpose of this example is to show that the fatigue function is based on an unrealistic analysis of the stresses in the pavement slab.

A third analysis was run to investigate the load needed to completely break the slab under monotonic loading. Figure 5-20a shows the load displacement curve for the fracture mechanics based concrete pavement model. The slope of the load increase will be greatly dependent on the stiffness of the subgrade. The pavement slab fails at a load of approximately 85 kN and a deflection of 10 mm. This can be observed by the change in slope of the graph in Figure 5-20a at 10 mm deflection. The major principal stress condition in the pavement at time of failure of the slab is shown in Figure 5-20b. The principle stresses have dropped below the maximum tensile stress of 6.56 MPa over the entire area. The displacements have been scaled five times in the figure to enhance visibility. This type of analysis may provide a suitable point of departure for fatigue prediction, as it provides an indication of peak load capacity at failure similar to what is recorded in beam bending tests and disk tests.

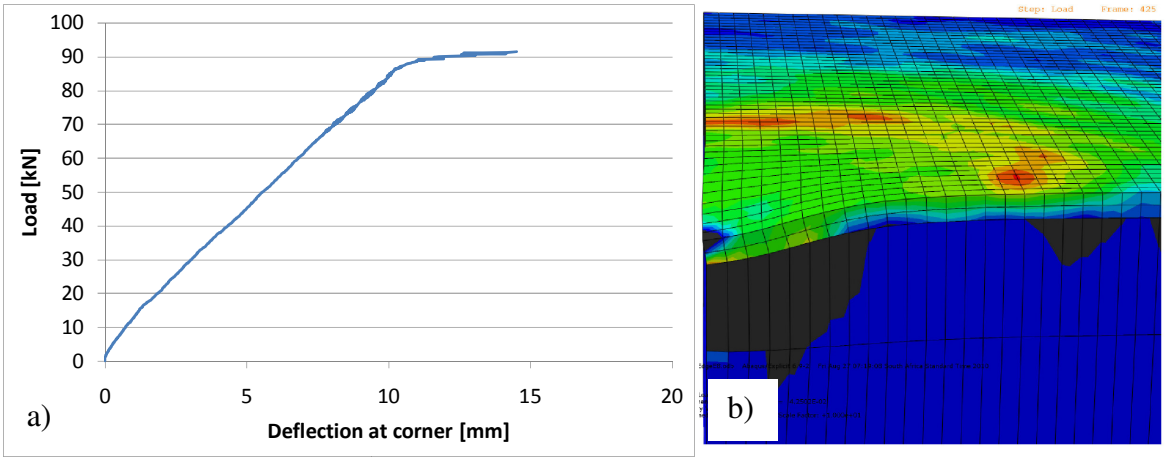

Figure 5-20a: Load-displacement curve for pavement structure, b: Major principal stress condition at failure concrete pavement (displacement scale x5)

For comparative purposes, a similar analysis was run for a plain concrete pavement. The material properties were based on the test results from phase 2 and the softening function developed for this 40 MPa plain concrete material tested at UC Davis. The model is shown in Figure 5-21a. The boundary conditions are the same as for the FRC pavement, but the slab

thickness was increased to 200 mm, which is more representative for plain concrete pavements. The results of the LE analysis of the concrete slab are shown in Figure 5-21b, the results of the fracture mechanics based analysis are shown in Figure 5-21c. As before, a pressure load was applied to the LE model until the principal stresses in the slab reached the nominal maximum stress value of 4.7 MPa determined in the flexural beam experiments. This occurred at a pressure loading of 6.5 MPa on the loading patch, which corresponds to a 65 kN total load. The same pressure load was then applied to the fracture mechanics model. This example again shows the difference in the stress condition calculated using LE analysis and the more advanced fracture mechanics based model. It is proposed that the fracture mechanics model provides a more accurate picture of the stress condition in the pavement and the location of progressive (fatigue) damage formation.

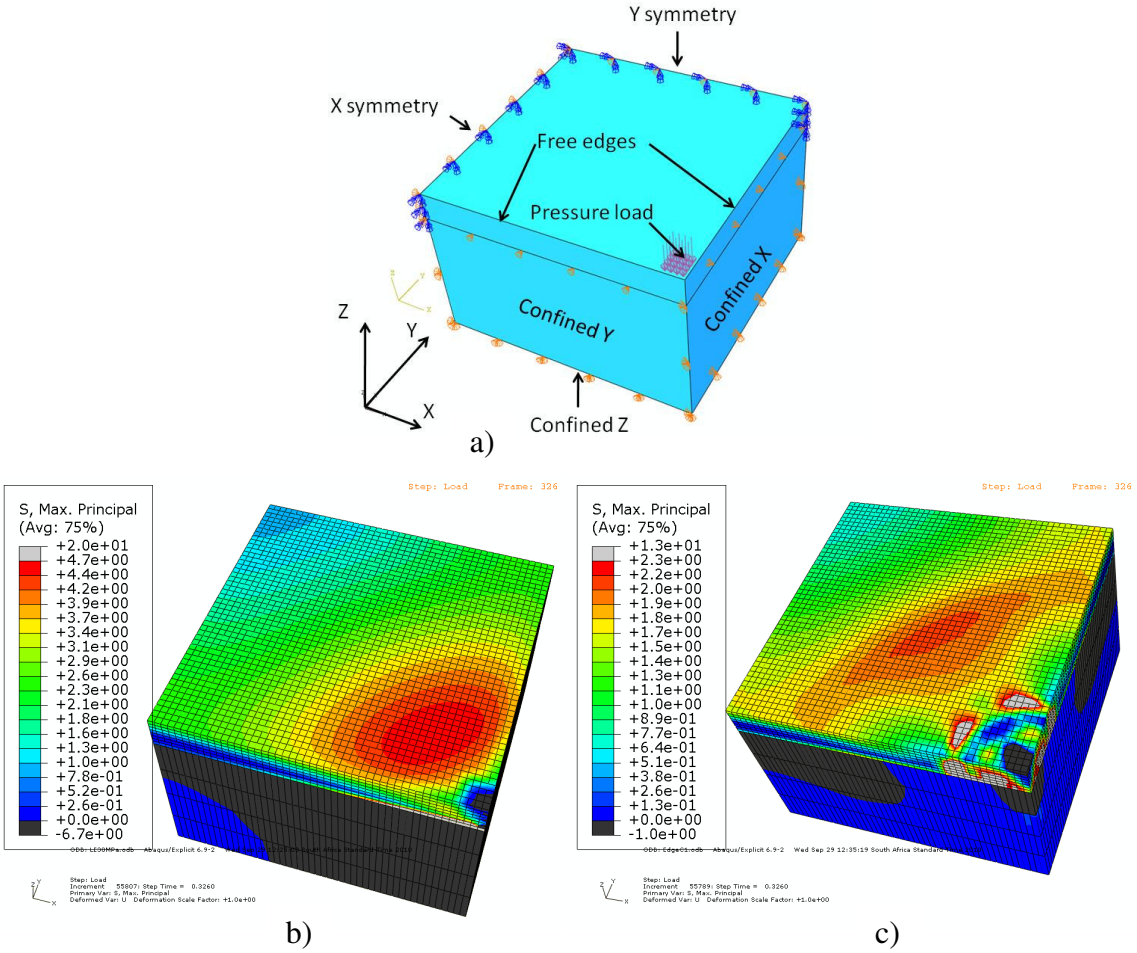

Figure 5-21a: Boundary conditions plain concrete pavement model, b: Result LE analysis, c: Result fracture model.

5.6 Fatigue fracture prediction

In the previous sections it was shown that fracture mechanics concepts can provide a more accurate prediction of the flexural behaviour of high performance fibre reinforced concrete under monotonic loading. The next step is to assess whether fracture mechanics principles can be applied to increase the accuracy and precision of fatigue prediction models. To this aim, a model for the prediction of fatigue is calibrated using the approach applied in conventional pavement design methods. Once this model is defined, alternative models based on fracture mechanics approached are calibrated, to explore whether more precise predictions can be obtained. The fatigue tests on the FPB specimens with 150x150mm^2 cross section are used as the benchmark for calibration. The models are then compared in terms of their predictive performance for the fatigue life recorded in experiments on specimens of different sizes and geometry.

5.6.1 Fatigue prediction using the conventional method

In conventional pavement design, the fatigue life is calculated based on the ratio of the maximum tensile stress (σ_d) in the concrete slab calculated using LE analysis of the pavement structure and the MOR, i.e. the maximum nominal tensile stress (σ_{Nu}) achieved in standardized FPB tests. The form of the fatigue model as used in the current South African concrete pavement design, shown earlier as Equation 2.3, is maintained here:

$$N = a_1\left(\frac{\sigma_d}{MOR}\right)^{b_1} \tag{5.8}$$

The test results for the 150 mm x 150 mm cross section FPBF1-E are shown in Figure 5-22. The power function shown in Equation 5.8 is fitted to the results. The best fit with an R^2 of 0.79 is obtained for a_1 = 2526 and b_1 = 14.21. In the figure the power curve is extrapolated to show the prediction of the model at different stress levels.

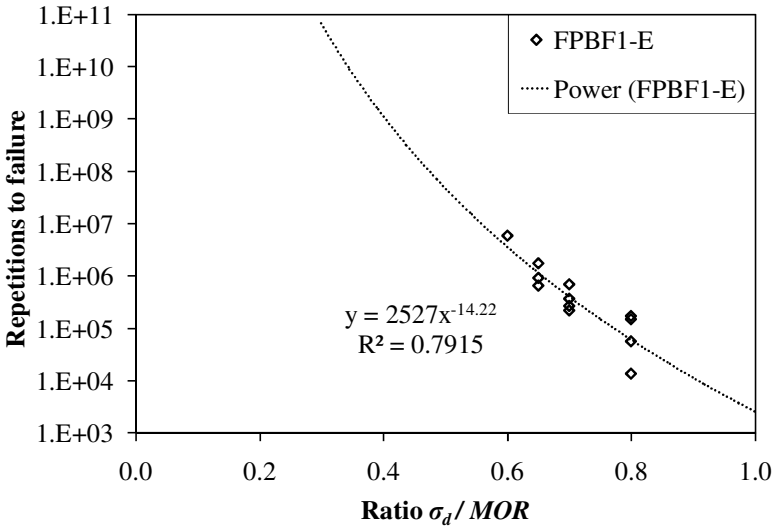

Figure 5-22: Calibration of conventional fatigue model

An interesting point to note here is that many concrete pavement design methods, including the current South African method and the new American method according to NCHRP 1-37 use a power shape to represent the performance of concrete at different stress levels. This in contrast to the logarithmic function that is typically fitted to the data in fatigue studies on concrete, e.g. Lee and Bar (2002). The choice of the shape of the curve is important, because pavement design typically concerns large numbers of load repetitions to failure. This will often involve extrapolating the model beyond the range of experimental fatigue data against which it was calibrated. Such extrapolation will yield significantly different results for power function curves than for logarithmic functions.

The predictive performance of the conventional fatigue model for specimens of different sizes and geometry is Figure 5-23. The vertical axis shows the ratio between the peak stress (σ_d) in the different specimens calculated using LE theory and the peak stress σ_{Nu}. (MOR) from FPB tests on 150 mm x150 mm cross section.

The model performs relatively well in predicting the fatigue life of the 100 mm x 100 mm and 50 mm x 50 mm beam specimens the relationships for which are shown in Figure 5-23a and Figure 5-23b. Note that due to size effect, these specimens failed at a higher peak stress than the 150 mm x 150 mm specimens and since the tests were performed at fixed percentages of the peak load for each beam size, the specimens were therefore tested at a higher stress level compared to the 150 mm x 150 mm specimens.

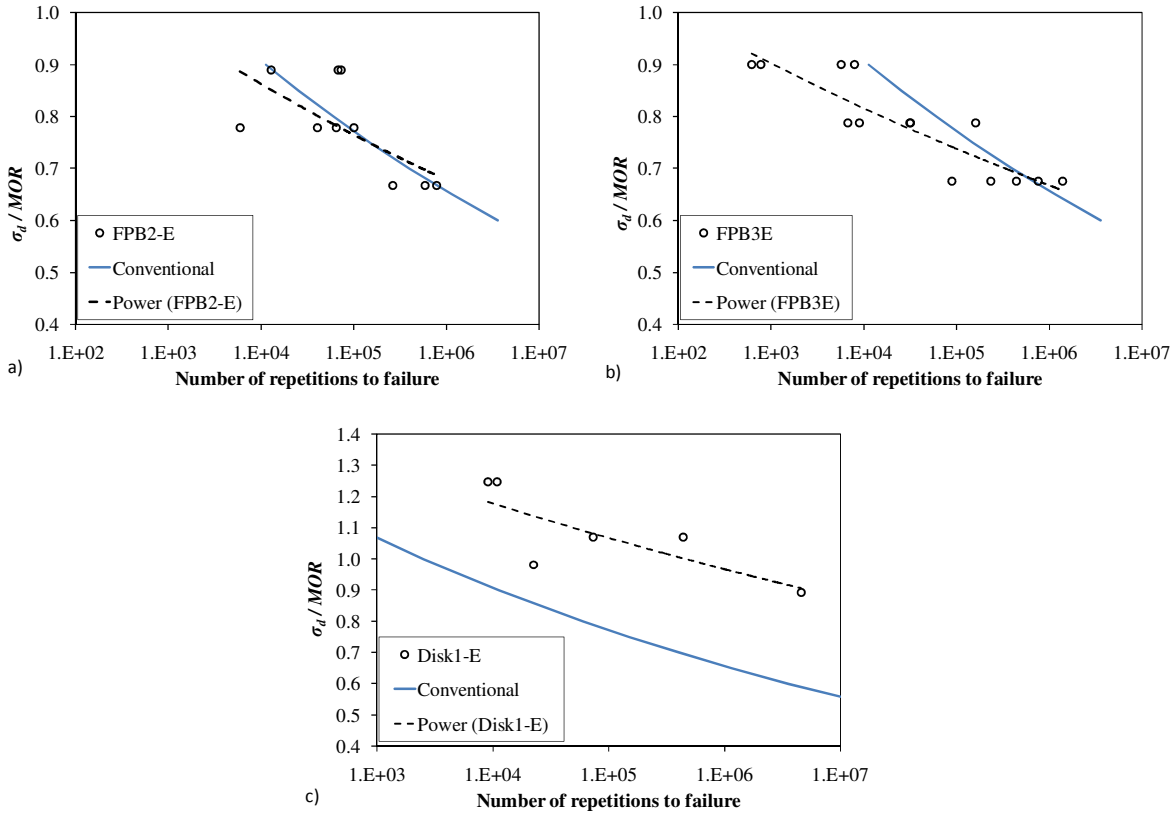

Figure 5-23: Predictive performance of conventional fatigue model for: a) 100 mm high beams, b) 50 mm high beams and c) 600 mm diameter disk specimens

There is some indication from the relative trajectory of the power functions, that at lower stress levels, the model may start to under-predict the fatigue life. The performance of the model for the prediction of the fatigue life of the disk specimen as shown in Figure 5-23c is less than satisfactory. The predicted number of load repetitions to is 100 times smaller than the actual number of load repetitions to failure. The limitations of the MOR as material property combined with LE analysis of the disk become visible here. The disk tests were performed at load levels, which according to LE analysis results in stresses higher than the MOR of the material.

For the calibrated functions used in pavement design the gap between the results predicted by LE theory and the results obtained from large scale experiments or data from actual pavement structures would have been remedied by the use of shift factors. In other words, statistical calibration of Equation 5.8 to fit data from the field, without mechanistically addressing the limitations of LE analysis.

5.6.2 Fracture mechanics based method

For the development of a fracture mechanics based model a number of observations and findings made previously in this study can be used:

- The cohesive crack model developed in the study can be applied to reliably predict the behaviour of the UTCRCP material in monotonic flexure,
- The cohesive crack model can probably also be used to calculate the crack length at different levels of displacement,
- It may be assumed that the stress at the crack tip will be equal to the tensile strength of the material determined from the tensile splitting test.
- The load-displacement envelope of monotonic experiments or monotonic loading fracture mechanics analysis of a structure may provide a good indication of the displacement at failure in the fatigue tests,
- The fatigue tests indicate that the equivalent energy (G_E) dissipated at the time of failure may be constant and independent of specimen geometry for fatigue tests on a material.

The challenge is to find a reliable model for the prediction of fatigue that is practical enough to be used and calibrated for general application in pavement engineering.

5.6.3 Peak load based fatigue prediction model

The point of departure for the development of a first fracture mechanics based fatigue model is that the main limitation to the current fatigue predictions may not lie in the statistical calibration to fatigue data, but instead lie in the simple LE analysis of the stresses in structural elements. The first attempt to develop an improved fatigue model is therefore based on the improved understanding of the stress state in the specimens allowed by fracture mechanics analysis.

Both stress parameters in Equation 5.8 suffer from the assumption that the material behaves linear elastically. As a result, the value of the stress (σ_d) calculated for a pavement structure will be unrealistic in case its value is higher than the tensile strength (f_t) of the material. The other parameter, the MOR is subject to size effect, again as a result of the LE assumption. In reality cracks form well before the peak load in the FPB test is reached and the stress therefore never reaches the MOR value.

An improved model can be devised that draws on the fracture mechanics models developed in this study by simply replacing the LE derived stress parameters in Equation 5.8 by values calculated using fracture mechanics. The use of the stress condition would be complex, because according to the model, once f_t is reached, the stress becomes a function of the crack width, with the possibility of multiple cracks forming in the structural element. Therefore, instead of the stress, the load applied to the element is used. The equation becomes:

$$N = a_1 \left(\frac{P_d}{P_{du}} \right)^{b_1} \tag{5.9}$$

Where P_d is the load total of external loads applied to the element, and P_{du} is the peak load for the element derived through numerical simulation using a fracture mechanics approach.

The model is again calibrated against the fatigue results for the 150 mm x 150 mm cross section FPBF1-E specimens. This of course results in exactly the same fit, as the MOR is the LE stress condition calculated from the P_{du} value on these specimens.

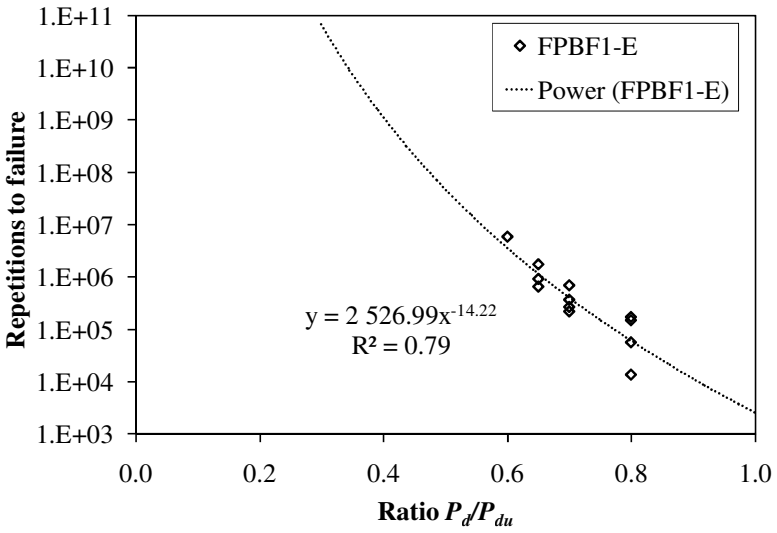

Figure 5-24: Calibration of fracture mechanics based fatigue model

The predictive performance of the fracture mechanics based fatigue model for specimens of different sizes and geometry is shown in Figure 5-25. The figure shows the results based on the value of P_{du} calculated using the cohesive crack model developed in the previous chapter. The cohesive crack model has a high accuracy in the prediction of the peak load however,

there will always be a certain error as was shown in Table 5-2. For comparison purposes the results for the fatigue model are also shown for the optimum situation where there is a 0% error in the prediction of the average peak load from the numerical simulation.

Compared to the results of the conventional model, the prediction of the fatigue life of the 50 mm x 50 mm specimens in Figure 5-25a and of the 100 mm x 100 mm specimens in Figure 5-25b, using the fracture mechanics based approach is less accurate. This is a consequence of the size effect predicted in the numerical simulation, which is not visible in the fatigue test results. As shown in Figure 5-25c, the fracture mechanics based model provides a slightly more precise prediction of the fatigue performance of the disk. The error however is still significant. The predicted fatigue values are about 30 times larger than the actual values. The predictive performance of the equation for specimens of a different geometry is not as encouraging as expected.

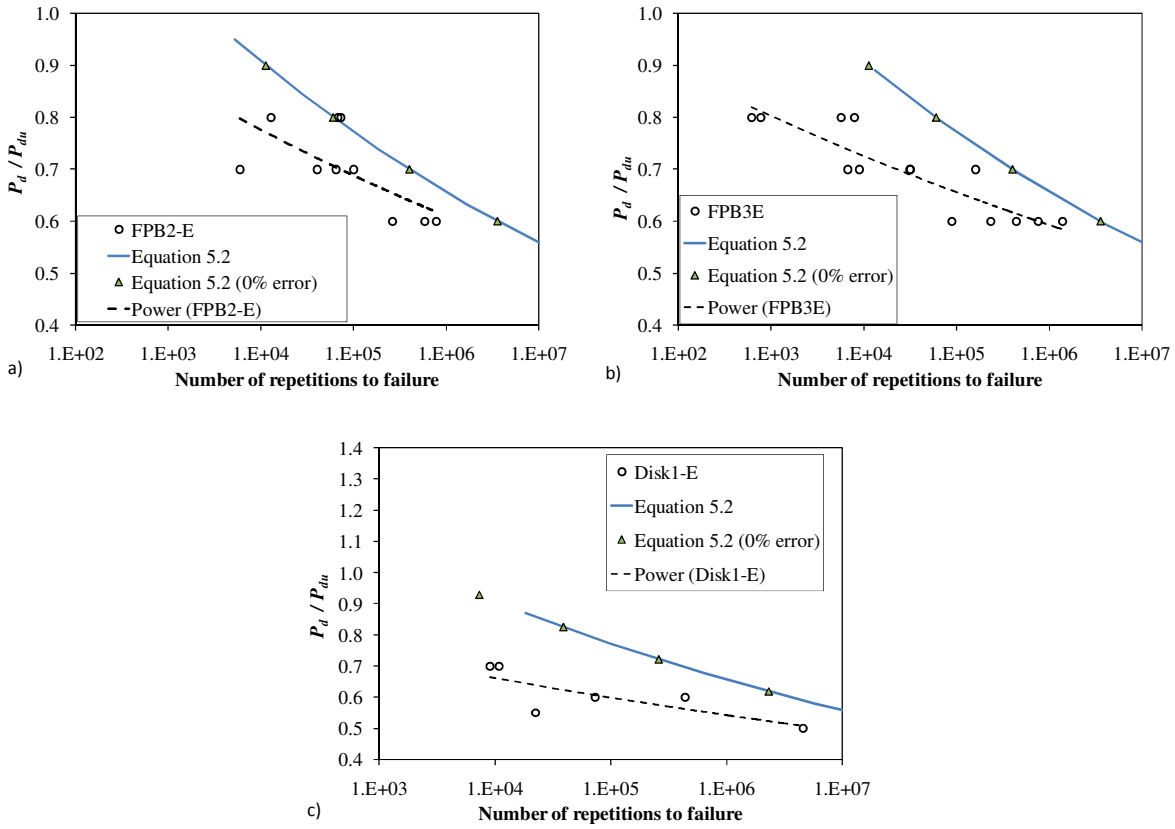

Figure 5-25: Predictive performance of fracture mechanics fatigue model for: a) 100 mm high beams, b) 50 mm high beams and c) 600 mm diameter disk specimens

To apply the predictive fatigue to a full size pavement structure, it would be necessary to separate the load absorbed by the pavement structure from the load absorbed by the slab. The loading required to break the slab representing P_{ud} for the fatigue model. This may be possible by loading the pavement slab to complete failure in the numerical simulation as shown Figure 5-20a and then unloading the structure to obtain the elastic response offered by the substructure.

5.6.4 Deflection based fatigue prediction model

Previous studies have shown that, although the monotonic load-displacement curve is not valid as an envelope for load-displacement response under cyclic loading, it may be applied as such to fibre reinforced concrete. The data from this study seems to support the theory that failure occurs in cyclic testing when the deflection approaches the monotonic envelope.

The next attempt to model fatigue is therefore based on the relationship between the displacement at the peak of the initial load cycle (δ_0) and the displacement at the peak of the final cycle before failure (δ_1). In Figure 5-26, the model is shown schematically for the simulated load-displacement curve for the FPB1-E test. The positions of δ_0 and δ_1 are shown for the case where the cyclic loading is performed at 60 percent of the peak load. The assumption in the model is that the monotonic curve as obtained from fracture mechanics analysis acts as envelope for the displacement in the fatigue tests. Note that this model is equivalent to a model based on comparing the work of fracture applied in the first cycle to the work of fracture dissipated at the last cycle.

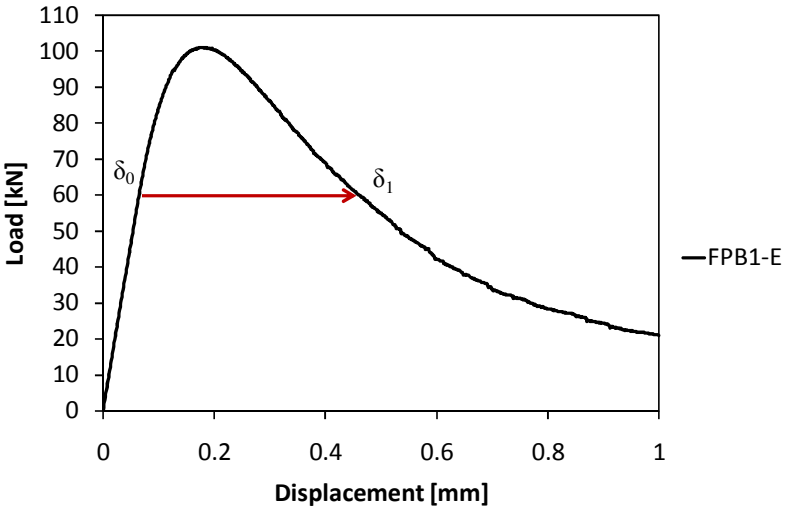

Figure 5-26: Displacement based model

Once again, the familiar power function is calibrated. The displacements at the different load levels are obtained from the load-displacement curves from the numerical simulation of the various specimen types. The fatigue model based on the displacement ratio is shown below. The power function fit to the data for the 150 mm x 150 mm beams is shown in Figure 5-27. Values of 1.098 and -5.1 were found for parameter a_1 and b_1 respectively.

$$N = a_1\left(\frac{\delta_0}{\delta_1}\right)^{b_1} \tag{5.10}$$

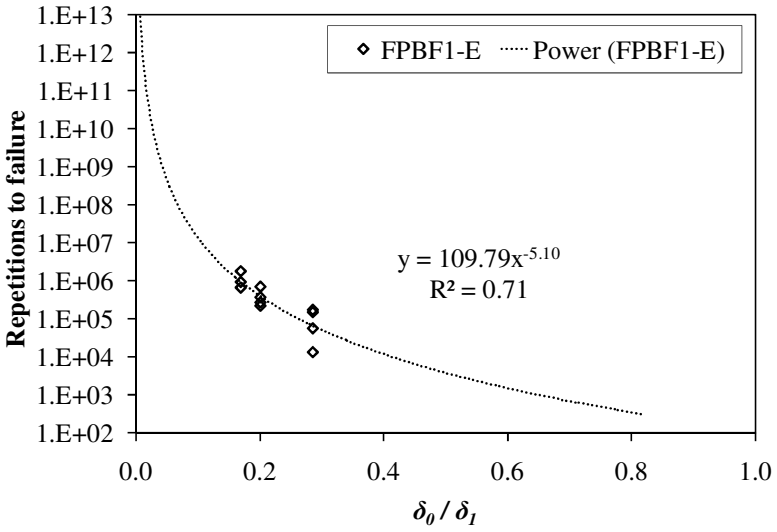

Figure 5-27: Calibration of displacement based fatigue model

Unfortunately, the model shows severe limitations in the prediction of the fatigue life for the 100 mm and 50 mm high beams as well as for the disks as shown in Figure 5-28. The lack of fit may be caused by the difference between the predicted load-displacement envelope and the actual displacement at which failure under cyclic loading occurs. The lack of fit may also indicate that there is little correlation between the relative horizontal distance between δ_0 and δ_1, and the fatigue life. This is opposite to what was expected however, as δ_0 and $\delta 1$ are indicators of W_{ff} and the dissipated energy G_E, which were found to be consistent. The prediction of fatigue based on the dissipated energy or deflection may require a different approach.

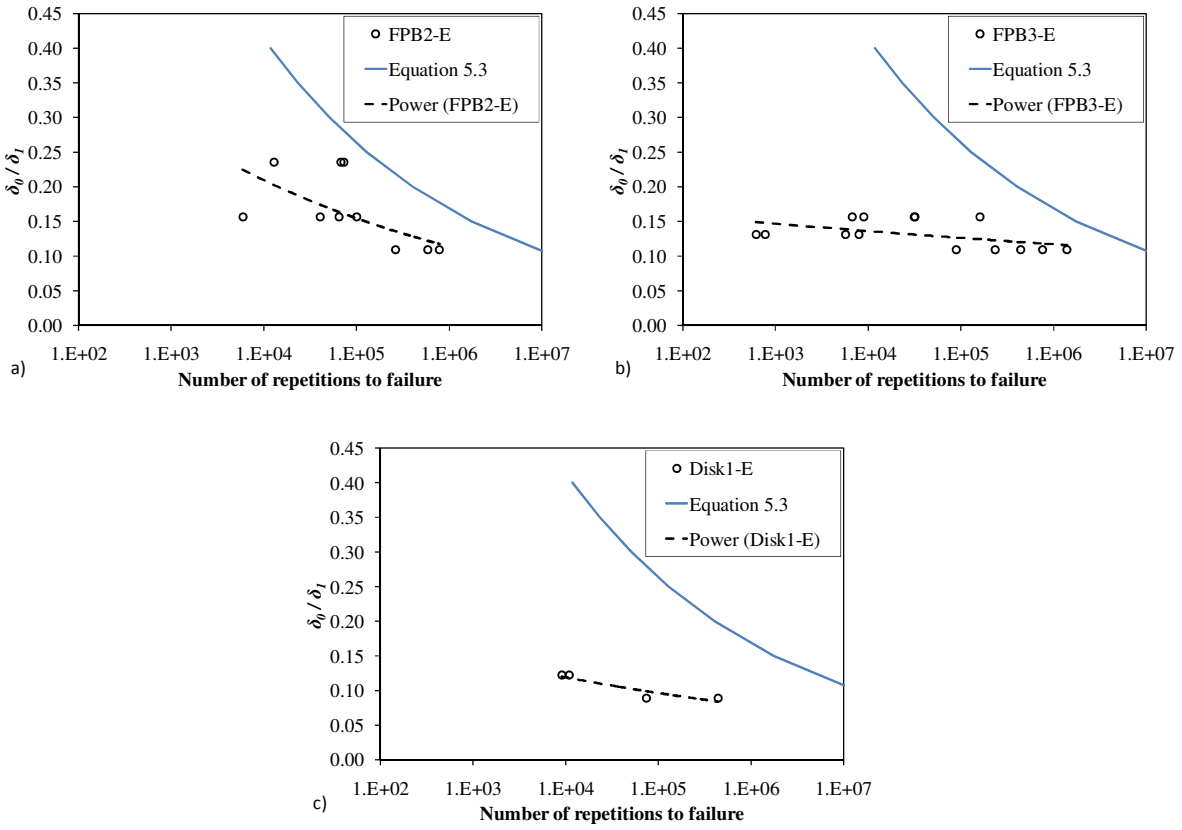

Figure 5-28: Predictive performance of displacement based fatigue model for: a) 100 mm high beams, b) 50 mm high beams and c) 600 mm diameter disk specimens

5.6.5 Model based on crack length

As discussed in Chapter 2, researchers have previously developed methods based on Paris' equation to predict fatigue fracture propagation. For such models data on the increase in crack length per load cycle is required. This data could be compared to the increase in crack length in monotonic tests. It is possible using the numerical simulation models presented in this document to track the effective crack length a in the specimens under increasing monotonic load. Figure 5-29 shows for the different specimen sizes, the crack length (a) relative to the specimen height (h), plotted against the ratio of the applied load (P) and the peak load (P_u).

The effective crack length under cyclic loading can be derived from the load compliance and effective stiffness recorded in cyclic experiments. The measuring equipment and sample rate used in the cyclic experiments in this study however, are not suitable to calculate a precise estimate of the effective crack length development. A predictive model for fatigue behaviour

based on the effective crack length from monotonic tests will only yields a similar result as the model based on deflection unless it can be calibrated against actual crack length data from cyclic tests. The development of a fatigue model based on crack length is therefore not pursued any further as part of this study.

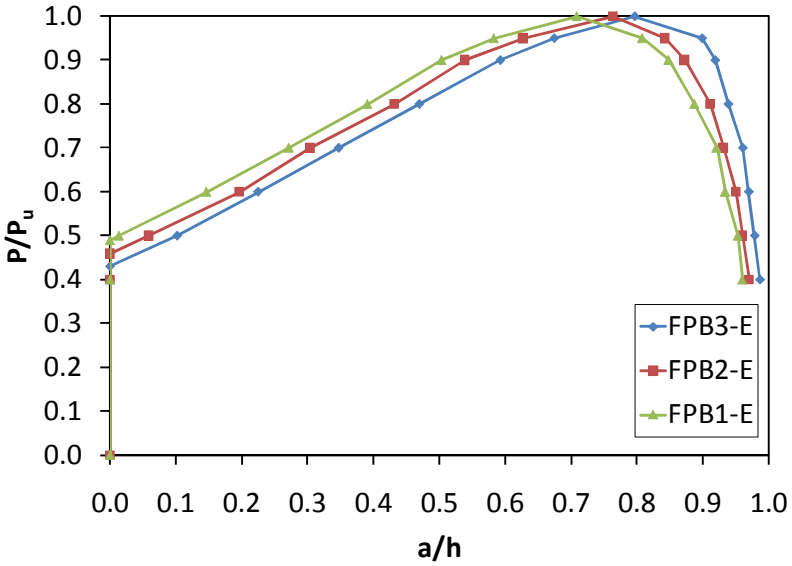

Figure 5-29: Fracture propagation in beams of different sizes.

5.7 Discussion on the numerical simulation of fracture

In this chapter, the fracture properties G_f and f_t determined for the various materials in the previous chapter, were used to define a cohesive crack softening function. The initial simple exponential softening function was completely defined using only the two parameters G_f and f_t. Exponential softening provided satisfactory results for the analysis of fracture in the plain concrete specimens, but it did lead to over-prediction of the peak load for the FRC specimens.

A shape that better suites the softening behaviour of fibre reinforced concrete was constructed by combining crack tip singularity with an exponentially softening tail. It was shown that this model allows for the reliable prediction of the opening mode fracture behaviour of the high performance fibre reinforced concrete material. The shape of the softening function is defined by four parameters, i.e.: Gf, f_t, a standard crack opening width at

which the fibres are activated w_1 and a third parameter σ_1 representing the crack bridging stress at the base of the singularity, which is obtained through calibration. The ability of the method to simulate the fracture behaviour of specimens of different sizes and geometry shows that the calibration of σ_1 is justified.

In essence, it is possible to use the fracture properties obtained from flexural beam experiments and numerically predict the structural capacity of specimens of a different size, different geometry and/or different loading conditions such as the splitting test. The test configuration developed in the chapter, together with the numerical models presented, can be applied with confidence to predict the flexural and tensile capacity of UTCRCP material. This in contrast to the MOR parameter, which because of size effect cannot be used to make reliable predictions.

It was shown in this chapter that the size-effect can to a large extent be predicted through the use of fracture mechanics. The models also provide insight in the cause of size effect, showing that cracks start propagating well before the peak load in a flexural beam test is reached. This clearly shows the error in the assumption that a linear elastic stress distribution exists at the peak load condition in the MOR test. The limitations to LE analysis of structures produced from the high performance fibre reinforced material were also highlighted. If LE analysis combined with the MOR obtained from beams had been used to predict the peak load of the flexural tests on the centrally loaded disk specimens, this would have lead to an underestimation of the capacity of approximately 100%. The analysis of the simplified pavement system showed the LE analysis may result in unrealistic stress conditions. In conventional pavement design, the stresses calculated in this manner are used in the stress/strength ratio for the prediction of fatigue life. The cohesive crack model on the other hand can be used to obtain a more realistic estimate of the stress condition in the pavement.

The precision of the results of the numerical simulation indicate that the methodologies to obtain the specific fracture energy through extrapolation of the TPB load displacement tail and the tensile strength from the adjusted tensile splitting test are fit-for-purpose.

The developed methods could be used for application beyond the scope of the present study. The model with the cohesive crack damage definition could, for instance, be used to predict the crack patterns in the pavement slab by loading the model with a moving load, or simply by putting loads in different positions on the slab. The models may also be used in the design of FRC structural elements for application outside the field of pavement engineering.

At present the fatigue prediction models developed in this chapter are based on the experimental results obtained for a single mix. A laboratory test programme is currently underway which comprises a similar test matrix as used for Mix E, applied to a mix with 80 kg/m^3 fibres and one without fibres. The results of these tests will allow the further development and/or generalization of the models presented here.

Two models were developed, one based on the peak load of the structural element obtained through fracture mechanics analysis, the second based on the deflection of the element as predicted through fracture mechanics analysis. A third model based on the prediction of equivalent crack growth was not pursued further than an initial investigation, due to a lack of suitable data.

The model based on the fracture mechanics derived peak load shows some promise. It could be argued that the precision of the prediction was still poor even though it outperformed the conventional approach. However, in light of the broader findings of this study it is proposed that the model is based on a more accurate description of the fracture mechanism at play. It provides a practical method to relate the improved understanding of crack formation in the material allowed by fracture mechanics to the prediction of fatigue performance. It could be applied to a full size pavement simply by implementing the cohesive softening model for the concrete slab and analysing the response of the system to a static load. It is argued that although the model is not perfect (no model is), it is an improvement to the conventional approach. The model however still relies on statistical calibration for the prediction of fatigue fracture propagation. The mechanism of damage evolution, the gradual tensile softening of the material with the increase in load cycles is not addressed by the method. In essence, the fracture performance of the material in fatigue is related to the fracture performance of the material under monotonic loading through simple calibrated power function.

The model was calibrated using a power function mainly because conventional design methods use this shape. The power function however, results in a very high number of repetitions to failure at low load levels compared to logarithmic functions. This study did not produce data to validate the fatigue performance of the material at low stress levels. In general, due to the practical difficulties in running tests to more than 10^7 cycles, there is little or no data available for fatigue performance of concrete below 50% of monotonic peak load. The results of this study and the literature consulted as part of this study, do not necessarily support the choice for a power function over a logarithmic function. This observation is made

here merely to indicate that in pavement design fatigue is predicted for high cycle applications. Typically the number of load applications carried by a pavement will be at the high end if not beyond the range of the available fatigue data from laboratory experiments. Extrapolation of the available data makes the choice between a power function, or an exponential function an important one.

No matter how many instances of white swans we may have observed, this does not justify the conclusion that all swans are white.

Karl Popper (1959)

6 Conclusions

6 CONCLUSIONS

This study set out to test the thesis that *the accuracy of design models for UTCRCP can benefit from the adoption of fracture mechanics concepts.*

The outcomes of the study support this hypothesis.

The support for the main hypothesis is provided through the validation of the three hypothetical propositions of the study. The high performance fibre reinforced concrete was found to be subject to significant size effect. This finding validates the proposition in this regard as discussed in detail Section 6.1. The conclusions with respect to the implications of the size effect are also described in this section. The second proposition states that in contrast to the MOR, fracture mechanics material parameters can be used to accurately and precisely, predict the peak load and importantly, the post-peak flexural behaviour of elements of a different size and geometry. The results from the numerical simulation performed as part of this study support this proposition as discussed in Section 6.2. According to the third proposition, fatigue prediction models for the material can be improved through the use of fracture mechanics. The findings of this study partially support this hypothesis as explained in Section 6.3. The benefits of adaptation of fracture mechanics in design models for UTCRCP are presented in Section 6.4. In the final section of this document recommendations are provided with regards to the implementation of the methods developed in the study.

6.1 Size effect and its implications for design

As part of this study, purposely designed experiments were performed to quantify size effect in the material. The aim was to test the hypothetical proposition posed in Chapter 1 that: *the high performance fibre reinforced concrete material will exhibit a strong size effect due to its high post crack stress capacity. The size effect will limit the reliability of the Modulus of Rupture (MOR) obtained for a specific specimen size and geometry, as a predictor of the peak load of elements of a different size and or geometry.*

Specimens with identical geometry, but of different sizes were tested. The results showed that the material is subject to significant size effect. The main implication is that the nominal maximum tensile stress (σ_{Nu}) obtained for a certain specimen size cannot be used to reliably predict the peak load for a specimen of a different size. The MOR is σ_{Nu} determined in a standardized four point bending beam test on a specimen with fixed dimensions. The cause of the size-effect lies in the assumption of a Linear Elastic (LE) stress distribution at peak load to calculate the MOR. In reality a crack has formed long before the peak load is reached and the material behaviour is highly non-linear. It was shown that if the MOR is used to predict the peak load in the centrally loaded disk using Linear Elastic (LE) analysis, the error of the prediction is in the order of 70 to 100 percent. The conclusion is that because of the size effect the MOR cannot be expected to yield reliable predictions of the bending capacity of a full size pavement. The size effect hypothesis is therefore supported by the findings of this study.

In the conventional pavement design theory used for UTCRCP, the MOR is treated as the strength of the material in bending. The ratio between the MOR and the tensile stress condition in the pavement calculated using LE theory is used to predict the fatigue performance. It is argued that based on the above, the MOR is not the most suitable parameter to be used in the prediction of the performance of pavements under cyclic loading.

The source of the size effect in the MOR parameter lies mainly in the difference in fracture energy release into the crack front for small and large specimens. A non-linear fracture mechanics approach is required to be able to use the parameters from a single sized specimen to reliably predict the flexural behaviour of specimens of different sizes and geometry.

6.2 Characterization of fracture behaviour under monotonic loading

The development of data analysis methods and numerical models to test the second proposition represent a major part of the work performed for this study. The proposition states that *In contrast to the MOR, fracture mechanics material parameters can be used to accurately and precisely, predict the peak load and importantly, the post-peak flexural behaviour of elements of a different size and geometry.*

Methodologies were developed to determine fracture mechanics properties for the high performance fibre reinforced material. The fracture energy (G_f) for the material is determined from notched Three Point Bending (TPB) experiments. TPB tests on fibre reinforced concrete are invariably stopped before the specimen is fully broken. An extrapolation technique was presented that allows the extension of the load displacement curves and determine the full work of fracture (W_f) required to break the beam specimens completely. A best estimate of G_f can be calculated from the W_f values thus obtained.

A close estimate of the tensile strength (f_t) for the material is obtained from an adjusted tensile splitting test procedure. It was shown in this study that f_t for high performance fibre reinforced concrete may be determined from cylinder splitting tests provided that: measures to reduce size effect are observed, the calculation is corrected for the influence of boundary conditions, and the transversal deformation is measured. The test results for fibre reinforced concrete show two separate peak load conditions. Without the measurement of the transversal deformation, the ductile post crack behaviour of the material will obscure the tensile splitting strength. If only the ultimate peak load is recorded, as is generally done, a tensile strength is calculated that is not related to a linear elastic tensile load condition in the sample. Numerical simulation confirmed that the ultimate peak load is related to secondary cracking mechanisms. The first peak represents the linear elastic limit state and from it a best estimate of the tensile strength material property can be calculated.

The tensile splitting methodology for fibre reinforced concrete proposed in this document provides a relatively simple alternative to the more complex direct tensile testing approach. Direct tensile testing yields more detail on the post cracking behaviour of the composite material, but if only a measure of the tensile strength is required, the presented tensile splitting methodology will suffice.

The fracture parameters G_f and f_t form the basis for the development of a fracture mechanics damage model for the material. The f_t value forms the threshold which, if exceeded leads to the formation of a crack. G_f represents the area under the cohesive softening function. This function defines the relationship between the crack width and the crack bridging stress. In an initial attempt to model fracture, a simple exponential shape of the softening curve was used. In the numerical analysis using the embedded discontinuity approach in OpenSees, this shape was found to overestimate the peak load condition for the specimens.

An alternative shape for the softening curve was chosen that better represents the post crack softening behaviour of fibre reinforced concrete. The improved cohesive softening function combines a crack tip singularity with an exponential tail. Four parameters need to be determined to construct the function. The first two are G_f, f_t obtained as described above. The two other parameters define the shape of the singularity and are determined through calibration against the experimental results, i.e.: the crack width (w_1) and the stress (σ_1) at the base of the crack tip singularity.

This cohesive softening function was implemented in both Abaqus and OpenSees finite element software. It was found to provide satisfactory predictions for the fracture response for different specimen sizes, different specimen geometries, i.e. three and four point bending beam specimens, centrally loaded disks and split cylinder tests. In contrast to the MOR, it can be used to extrapolate the parameters obtained for a certain specimen size, to reliably predict the flexural behaviour of specimens with a different size or geometry. This ability of the method to simulate the fracture behaviour of specimens of different sizes and geometries also shows that the calibration of w_1 and σ_1 is justified. Another advantage of the fracture mechanics approach is that it allows the prediction of non-linear pre- and the post peak flexural behaviour of the material. LE design methods provide a prediction of the peak load condition only.

The numerical simulation of beams containing rebar shows that the models developed in this study can be applied to model the influence of the mesh on the behaviour of UTCRCP.

It is concluded that the findings of the study support the proposition that fracture mechanics parameters can be used to reliably predict the flexural behaviour of the material, whereas the MOR cannot.

It is further concluded that the input required for the definition of the fracture models can be obtained from relatively simple laboratory tests. The fracture energy can be successfully determined from TPB tests using the methodology developed in this study. The tensile strength can be obtained from the adjusted tensile splitting test. It was shown that these methods allow the definition of a softening function that is suitable for the prediction of the flexural behaviour of the UTCRCP material.

6.3 The use of fracture parameters in fatigue life prediction

The last of the propositions of the research states that *the accuracy, and possibly the precision, of fatigue prediction models for the material can be improved through the use of fracture mechanics concepts.*

This proposition is partially supported by the findings of this study. Although the precision of the fatigue life prediction was only nominally improved for the available data, it is argued that fracture mechanics based models are more accurate, because address some of the systematic errors underlying the conventional methods.

The findings of this study showed the limited applicability of LE analysis to the behaviour of the high performance fibre reinforced concrete material. Both of the parameters used as input for conventional fatigue prediction equations, i.e. the maximum tensile stress in the pavement slab and the material strength represented by the MOR, are determined through LE analysis. The numerical analysis performed as part of this study shows that LE analysis of pavement structures may lead to tensile stresses higher than the tensile strength (f_t) of the material. Such stresses cannot exist as they would lead to cracking and stress redistribution. Impossible stresses may be calculated for many design situations since the f_t is generally in the region of 50 % of MOR, which will often be exceeded. The LE assumption underlying the MOR value gives rise to the size effect and disqualifies it as a reliable design parameter as discussed earlier in this chapter.

The fracture mechanics damage models for the material were shown to yield size and geometry independent predictions of the flexural behaviour of the material. By replacing the LE parameters in the fatigue models with parameters determined through fracture mechanics analysis, systematic errors can be eliminated from the predictive equation.

Two fracture mechanics based fatigue prediction models were developed for the material. The first and most promising model requires the ratio between the magnitude of the load at which the cyclic loading is applied and the load at failure of the structural element, as determined through fracture mechanics analysis, as input. This ratio is then used in a statistically calibrated regression equation to predict fatigue life as would be done in the conventional approach. The predictive performance of the model was compared to that of a function calibrated using the conventional approach. Both functions were calibrated against a set of cyclic test results for standard 150 mm x 150 mm beam specimens.

The fracture mechanics peak load model performed slightly better than the conventional model in terms of the prediction of the fatigue life of the centrally loaded disks. Further validation of the method for other mix designs and importantly full scale pavement structures is required.

A second model was developed based on the assumption that the monotonic load-displacement curve provides a suitable envelope for the evolution of the load-displacement response under cyclic testing. This assumption is supported by the comparison of the monotonic and cyclic test data produced as part of this study. An attempt was made to devise a model based on the development of the deflection under cyclic loading. Such an approach can be related to the dissipation of energy in the test. The fatigue data from tests on specimens of different sizes and geometries showed consistency in the amount of energy equivalent dissipated per unit fracture ligament area. Unfortunately the model that was developed performed poorly in terms of the prediction of fatigue.

The fatigue equations developed in this study offer only a limited improvement compared to the conventional approach. The models are based on a mechanistic approach to the prediction of monotonic fracture in the material. This is an important enhancement of the design methodology. The models however, still rely on statistical calibration for the prediction of fatigue fracture propagation. The mechanism of fatigue damage evolution, i.e. the gradual tensile softening of the material with the increase in load cycles is not addressed by the method. A truly mechanistic method that incorporates the softening of the material due to gradual degradation of aggregate interlock and fibre anchorage falls beyond the scope of this study.

6.4 The benefits of the use of fracture mechanics in UTCRCP design

This study has shown that fracture mechanics concepts offer an enhanced description of the fracture behaviour of the high performance fibre reinforced concrete material used in UTCRCP.

The fracture mechanics parameters determined with the methods developed as part of this study are close to true material properties. The use of these parameters will increase the design reliability and decrease uncertainty regarding material specifications. In current practice the MOR tests are sometimes performed on 100 mm x 100 mm beams instead of on beams with a 150 mm x 150 mm cross section. The findings of this study indicate that this would lead to a 10% difference in MOR. Such problems could be remedied through the use of fracture mechanics parameters. The number of tests in the material specifications may also be reduced. Currently the specifications for UTCRCP projects call for both flexural tests on beams to determine the MOR and the centrally loaded disk test to be performed as part of quality control. It has been shown in this study that the performance in the disk test can be predicted from the parameters determined from flexural beam tests, making the disk test redundant.

The determination of fracture mechanics properties during the mix design phase provides additional insight with regards to the fracture toughness of the material. The MOR provides an indication of peak load only, which in addition cannot be reliably generalized beyond the beam specimen for which it was determined. The tensile strength and specific fracture energy can be used to predict the flexural behaviour of a full sized pavement slab and allow optimization of the mix design in terms of fracture softening behaviour.

Fracture mechanics based numerical simulation can be used for the realistic assessment of stresses in the pavement slab. This will assist in identifying the positions where fatigue cracks are likely to develop under different load configurations and how the stresses will redistribute once a crack has formed. Once a crack has been induced, the load response of the damaged slab can be assessed.

The models developed as part of this study can also be applied to predict shrinkage cracking and early age cracking due to warping in concrete pavements. This would require determination of the fracture properties at different ages of the mix. The pavement structure

can then be modelled to assess whether the stresses due to warping and shrinkage exceed the tensile strength of the material at a given time.

Fracture mechanics based fatigue equations, even if these are no more precise for certain cases than the conventional approach, should be more accurate. This implies that they may be applied beyond the data set for which they were developed with more confidence than the conventional approach.

These are some ways in which the fracture models developed in this study can enhance the design methods for UTCRCP. Based on the discussion above and in the previous sections, it is concluded that the findings of this work support the thesis that the accuracy of design models for UTCRCP can benefit from the adoption of fracture mechanics concepts.

6.5 Recommendations for implementation and future research

An immediate improvement of current practice can be achieved by replacing the standard tensile splitting test with the adjusted test procedure developed as part of this study. As discussed in Section 6.2, it was shown conclusively by this study that the standard tensile splitting test method does not provide a measurement of the true tensile strength of fibre reinforced concrete material. It is therefore recommended that the adjusted tensile splitting test is adopted into standard practise.

The fatigue behaviour of a single high performance fibre reinforced concrete mix design as used for UTCRCP was investigated as part of this study. Additional testing is required to assess the influence of mix design variables, such as fibre content, on the fatigue performance of the material. A fatigue study including mixes prepared at a range of fibre contents is currently in progress. This will also allow the assessment of the possible link between the values of the f_t and G_f parameters and fatigue performance.

The fracture mechanics based peak load model developed in this study shows some promise for the available fatigue data. It also represents a logical outcome for the findings from monotonic fracture experiments performed on a range of mixes and specimen types as part of this study. A need exists to validate the methodology for different mix types, which will also be possible once the present laboratory study is completed. If the model proves to be accurate

for the new datasets, the approach still requires further validation for full size pavement systems before it can be implemented in design methods.

The pavement analysis performed in this study involved a simple load case on a simplified pavement system. Further study is required on the application of the fracture mechanics based method to predict crack patterns under moving loads in combination with loss of support over time, shrinkage and warping stresses, etc.

The models developed in this study can be used to analyse the functioning of the mesh in UTCRCP. This is a topic around which there is considerable uncertainty in the industry at present. The Abaqus models can readily be extended to analyse a UTCRCP structure with different mesh configurations.

The limitations of the LE design assumptions highlighted in this study are relevant to plain concrete pavements as well, though possibly to a lesser extent. It is proposed, that certain findings of the study may be of benefit to design methods for plain concrete pavements.

More results from fatigue experiments that are run up to the applicable range of load applications for long life concrete pavement structures (10^7-10^8) are required to determine whether the power function or logarithmic function should be used in fatigue models.

The models developed in this study provide an opportunity to further investigate the modes of failure of UTCRCP both in past heavy vehicle simulator (HVS) experiments and in the field. A need exists to apply the fracture mechanics models to the full pavement structure to gain further insight in the exact role and optimum configuration of the reinforcement mesh, which is currently a topic of much debate. The fracture mechanics models will allow a more accurate assessment of the formation of damage in the structure.

The development of a truly mechanistic approach to the prediction of fatigue fracture development in concrete pavements is required. It is proposed that only a solid mechanics model that covers the mechanism of fatigue damage evolution through gradual softening of the material under cyclic loading can completely overcome the limitations of current design methods.

REFERENCES

ASTM 2005. *ASTM C 1550 - 05 Standard test method for Flexural Toughness of Fiber Reinforced concrete (using centrally loaded round panel)*. ASTM International, West Conshohocken.

ASTM 2008. ASTM C 39 Standard Test Method for Compressive Strength of Cylindrical Concrete Specimens. *Annual book of ASTM standards 2008: section 04.02*. ASTM International.

ASTM 2008. ASTM C469-02. Standard Test Method for Static Modulus of Elasticity and Poisson's Ratio of Concrete in Compression. *Annual book of ASTM standards 2008: section 04.02*. ASTM International.

Abaqus 2009. *Abaqus v 6.9*. Providence: Dassault Systemes Simlia Corp.

BSI 1983. *BS 1881: Testing concrete. Part 116: 1983 Method for determination of comprissive strength of concrete cubes*. British Standard Institute.

Bacon, F. 1605. *The advancement of learning*. www.ebooks.adelaide.edu.au, accessed 1 November 2010

Bache, H., and Vinding, I. 1990. Fracture mechanics in the design of concrete pavements. *2nd international workshop on theoretical design of concrete pavements*. Siguenca, Spain: CROW/PIARC.

Baluch, M., Qureshy, A., and Azad, A. 1987. Fatigue crack propagation in plain concrete. In S. Shah and S. Swartz (eds.), *SEM/RILEM international conference on fracture of concrete and rock* (pp. 64-69).

Barnett, S., Lataste, J., Parry, T., Millard, S., and Soutsos, M. 2010. Assessment of fibre orientation in ultra high performance fibre reinforced concrete and its effect on flexural strength. *Materials and Structures*, *43*, 1009-1023.

Bathias, C. 1999. There is no infinite fatigue life in metallic materials. *Fatigue Fracture in Engineering Materials and Structures*, *22*(7), 559-565.

Bažant, Z.P. 1984. Size effect in blunt fracture: Concrete, rock, metal. *ASCE Journal of engineering mechanics, 110,* 518-535.

Bažant, Z.P. 1994. Discussion of "Fracture mechanics and size effect of concrete in tension." *ASCE Journal of structural engineering*, *120*(8), 2555-2558.

Bažant, Z. P. 2002. Concrete fracture models: testing and practice. *Engineering Fracture Mechanics*, *69*, 165-205.

Bažant, Z. P., and Li, Z. 1995. Modulus of rupture: size effect due to fracture initiation in boundary layer. *ASCE Journal of structural engineering*, *121*(4), 739-746

Bažant, Z. P., and Planas, J. 1997. *Fracture and size effect in concrete and other quasibrittle materials*. CRC Press.

Bažant, Z. P., and Oh, B. 1983. Crack band theory for the fracture of concrete. *Materials and Structures*, *1983*(16), 155-177.

Bažant, Z. P., and Schell, W. 1993. Fatigue fracture of high-strength concrete and size-effect. *ACI Materials Journal*, *90*(5), 472-478.

Bažant, Z. P., and Xu, K. 1991. Size effect in fatigue fracture of concrete. *ACI Materials Journal*, *88*(4), 390-399.

Box, G., and Draper, N. 1987. *Empirical model-building and response surfaces*. Wiley. pp. 424

C&CI. 2009. cncPAVE v4.04. Midrand.

Carpinteri, A., Spagnoli, A., and Vantadori, S. 2006. An elastic-plastic crack bridging model for brittle-matrix fibrous composite beams under cyclic loading. *International journal of Solids and Structures*, *43*(16), 4917-4936.

Dassault Systèmes. 2009 Abaqus 6.9 Documentation collection. Build ID: 2009_04_06-12.43.40 32904.

Denneman, E. 2010. Method to determine full work of fracture from disk shaped compact tension tests on hot-mix asphalt. *Proceedings of the 29th Annual Southern African Transportation Conference*, pp. 465-474

Denneman, E., Wu, R., Kearsley, E.P., and Visser, A.T. 2011a. Discrete fracture in high performance fibre reinforced concrete materials. *Engineering Fracture Mechanics,78* (10), pp 2235-2245.

Denneman, E., Kearsley, E.P., and Visser, A.T. 2011b. Splitting tensile test for fibre reinforced concrete. *Materials and Structures,* DOI 10.1617/s11527-011-9709-x

Denneman, E., Kearsley, E.P., and Visser, A.T. 2010a. Size-effect in high performance concrete road pavement materials. In G. Van Zijl and W. Boshoff (eds.), *Advances in cement-based materials*. London: CRC Press pp. 53-58.

Denneman, E., Wu, R., and Harvey, J.T. 2010b. Fracture behavior of concrete pavement material in bending under monotonic and cyclic loading. *Proceedings of the 2nd international symposium on service life design for infrastructure*. Delft, pp. 1035-1043

Denneman, E., Kearsley, E.P., and Visser, A.T. 2010c. Measurement of size effect in monotonic and cyclic tests on fibre reinforced concrete pavement materials. *7th international DUT - Workshop on fundamental modelling of design and performance of concrete pavements*. Sevilla.

Denneman, E., Wu, R., Kearsley, E. P., and Visser, A. T. 2009. Fracture mechanics in pavement design. *Proceedings of the 29th Annual Southern African Transportation Conference*. Pretoria, pp. 255-265

Du Plessis, L., and Fisher, C. 2008a. *First Level Analysis Report: HVS Testing of phase I of the Ultra Thin Continuously Reinforced Concrete (UTCRCP) test sections at the Traffic Control Centre near Heidelberg, Gauteng: Tests 426A5 to 431A5 1st DRAFT REPORT*. CSIR, Pretoria.

Du Plessis, L., and Fisher, C. 2008b. *First Level Analysis Report: HVS Testing of phase II of the Ultra Thin Continuously Reinforced Concrete (UTCRCP) test sections at the Traffic Control Centre near Heidelberg, Gauteng: Tests 432A5 to 436A5 1st DRAFT REPORT*. CSIR, Pretoria.

Dupont, D., and Vandewalle, L. 2004. Comparison between the round plate test and the RILEM 3-point bending test. *6th RILEM Symposium on fibre-reinforced concretes (FRC) - BEFIB* (pp. 101-110). Varenna, Italy.

Einstein, A. 1922. *Sidelights on relativity*. Jefferey G. and Perrett W. (eds.) Methuen and Co., Ltd, London.

Elices, M., Guinea, G., and Planas, J. 1992. Measurement of the fracture energy using three-point bend tests Part 3-Influence of cutting the P-u tail. *Materials and Structures*, *25*, 327-334.

Elices, M., Guinea, G., and Planas, J. 1997. On the measurement of concrete fracture energy using three-point bend test. *Materials and Structures*, *30*, 375-376.

Elsaigh, W. 2007. *Modelling the behaviour of steel fibre reinforced concrete pavements* (PhD dissertation). University of Pretoria.

Gaedicke, C., and Roesler, J. 2010. Fracture-based method to determine the flexural capacity of concrete beams on soil. *Road materials and pavement design*, *11*(2), 361-385.

Gaedicke, C., Roesler, J., and Shah, S. 2009. Fatigue Crack Growth Prediction in Concrete Slabs. *International Journal of Fatigue*, *31*(8-9), 1309-1317.

Gaedicke, C., Villalobos, S., Roesler, J., and Lange, D. 2007. Fracture Mechanics Analysis for Saw Cutting Requirements of Concrete Pavements. *Transportation Research Record*, *2020*, 20-29.

Gao, L., and Hsu, T. 1998. Fatigue of concrete under uniaxial compression cyclic loading. *ACI Materials Journal*, *95*, 575-581.

Geuzaine, C., and Remacle, J. 2009. Gmsh v2.4.2. www.guez.org/gmsh

Griffith, A. 1921. The phenomena of rupture and flow in solids. *Philosophical transactions of the royal society of London*, *221*(A), 163-198.

Guinea, G., Planas, J., and Elices, M. 1994. A general bilinear fit for the softening curve of concrete. *Materials and Structures*, *27*, 99-105.

Guo, X. H., and Li, H. 1999. Determination of quasibrittle fracture law for cohesive crack models. *Cement and Concrete Research*, *29*(June 1998), 1055-1059.

Hillerborg, A. 1983. Analysis of one single crack. In Wittmann F., *Fracture mechanics of concrete*. Amsterdam: Elsevier Science.

Hillerborg, A. 1986. Determination and significance of the fracture toughness of steel fibre concrete. In S. Shah and A. Skarendahl (eds.), *Steel fiber concrete US-Sweden joint seminar* (p. 257–271). London: Elsevier Applied Science Publishers.

Hillerborg, A. 1990. Fracture mechanics concepts applied to moment capacity and rotational capacity of reinforced concrete beams. *Engineering Fracture Mechanics*, *35*(1/2/3), 233-240.

Hillerborg, A., Modeer, M., and Petersson, P. 1976. Analysis of crack formation and crack growth in concrete by means of fracture mechanics and finite elements. *Cement and Concrete. Research*, *6*.

Holmen, J. 1979. *Fatigue of concrete by constant and variable amplitude loading*. *CEB Bulletin* (79-1., Vol. 79). Trondheim: Division of Concrete structures, NTH.

Hordijk, D. 1992. Tensile and tensile fatigue behaviour of concrete; experiments, modelling and analysis. *Heron*, *37*(1).

Hsu, T. 1984. Fatigue and microcracking of concrete. *Materials and Structures*, *17*(1), 51-54.

Inglis, C. 1913. Stresses in a plate due to the presense of cracks and sharp corners. *Transactions of the Institution of Naval Architects*, *55*, 219-230.

Ioannides, A.M. 1995. Fracture mechanics applications in pavement engineering: A literature review. *Report prepared for U.S. Army Engineer Waterways Experiment Station*, Vicksburg.

Ioannides, A. M. 1997 (a). Pavement fatigue concepts: A historical review. *Proceedings of the sicth international Purdue conference on concrete pavement, 3*, 147-159, Purdue.

Ioannides, A. M. 1997 (b). Fracture Mechanics in Pavement Engineering: The specimen size effect. *Transportation Research Record*, *1568*, 10-16.

Ioannides, A. M. 2005. Stress prediction for cracking of jointed plain concrete pavements, 1925-2000. *Transportation Research Record*, *1919*, 47-53.

Ioannides, A. M. 2006. Concrete pavement analysis: the first eighty years. *International Journal of Pavement Engineering*, *7*(4), 233-249.

Ioannides, A., and Sengupta, S. 2003. Crack propagation in Portland cement concrete beams; Implications for pavement design. *Transportation Research Record*, *2853*, 110-117.

Ioannides, A., Peng, J., and Swindler, J. 2006. Abaqus model for PCC slab cracking. *International Journal of Pavement Engineering*, *7*(4).

Irwin, G. 1957. Analysis of stresses and strains near the end of a crack traversing a plate. *Journal of Applied Mechanics*, *24*, 361-364.

JCI. 1983. *JCI-SF4: Method of tests for flexural strength and flexural toughness of fiber reinforced concrete*. Japanese Concrete Institute.

Jenq, Y., and Shah, S. 1985. A two parameter fracture model for concrete. *Journal of Engineering mechanics*, *111*(4), 1227-1241.

Kannemeyer, L., Perrie, B. D., and Strauss, P. J. 2008. Ultra Thin Continuously Reinforced Concrete Pavement Development in South Africa. *Proceedings of the 9th international conference on concrete pavements* (pp. 995-1018). San Francisco.

Kaplan, M.M. 1961. Crack propagation and fracture of concrete, *Journal of the American Concrete Institute*, *58*(5), 591-609.

Kearsley, E.P. and Elsaigh, W. 2003. Effect of ductility on load carrying capacity of steel fibre reinforced concrete ground slabs. *Journal of the South African Institution of Civil Engineering*, *45*(1), 25-30.

Kearsley, E.P. and Mostert, H.F. 2010. Enabling the effective use of high performance fibre reinforced concrete in infrastructure. In G. Van Zijl and W. Boshoff (eds.), *Advances in cement-based materials* (pp. 53-58). London: CRC Press.

Kellerman, W.F. 1932. Effect of size of specimens, size of aggregate and method of loading upon the uniformity of flexural tests. *Public roads. 13*(11), 177-184

Lappa, E., Braam, C., and Walraven, J. 2006. Bending performance of high strength steel fibre reinforced concrete.pdf. In M. Konsta-Gdoutos (ed.), *Measuring, monitoring and modeling of concrete properties*. Springer.

Lee, M., and Barr, B. 2004. An overview of the fatigue behaviour of plain and fibre reinforced concrete. *Cement and Concrete Composites*, *26*(4), 299-305.

Li, V., and Matsumoto, T. 1998. Fatigue crack growth analysis of fiber reinforced concrete with effect of interfacial bond degradation. *Cement and Concrete Composites*, *20*, 339-351.

Lilliu, G., and Van Mier, J. 2007. On the relative use of micro-mechanical lattice analysis of 3 phase particulate composites. *Engineering Fracture Mechanics*, *74*, 1174-1189.

Lim, T., Paramasivam, P., and Lee, S. 1987. Analytical model for tensile behavior of steel-fiber concrete. *ACI Materials Journal*, *84*, 286-298.

Lindner, C.P. and Sprague, I.C.m 1955. Effect of depth of beams upon the modulus of rupture of plain concrete. *ASTM Procedures, 55,* 1062-1083.

Mentat, V. 2003. MSC.Marc. Santa Ana, California: MSC. Software Corporation.

Miller, K., and O'Donnel, W. 1999. The fatigue limit and its elimination. *Fracture of Engineering Materials and Structures*, *22*(7), 545-557.

Miner, A. 1945. Cumulative damage in fatigue. *Journal of Applied Mechanics*, *12*, A159-164.

NCHRP 1-37A, 2004. *Guide for mechanistic-empirical design of new and rehabilitated pavement structures*. Prepared for: National Cooperative Highway Research Program, ARA Inc, Illinois.

Olesen, J. F., Ostergaard, L., and Stang, H. 2006. Nonlinear fracture mechanics and plasticity of the split cylinder test. *Materials and Structures*, *39*(4), 421-432.

Oliver, J. 1996a. Modelling strong discontinuities in solid mechanics via strain softening constitutive equations. Part 1: fundamentals. *International Journal for numerical methods in engineering*, *39*(21), 3575-3600.

Oliver, J. 1996b. Modelling strong discontinuities in solid mechanics via strain softening constitutive equations. Part 2: numerical simulation. *International Journal for numerical methods in engineering*, *39*(21), 3601-3623.

OpenSees. 2008. *Open System for Earthquake Engineering Simulation v1.7.5*. Berkeley: Pacific Earthquake Engineering Research Center, University of California.

Otter, D., and Naaman, A. 1988. Properties of steel fiber reinforced concrete under cyclic loading. *ACI Materials journal*, 254-261.

Palmgren, A. 1924. The Service Life of Ball Bearings. *Zeitschrift des Vereines Deutscher Ingenieure*, *68*(14), 339-341.

Paris, P., and Erdogan, F. 1963. A critical analysis of crack propagation laws. *Journal of basic engineering*, *85*, 528-534.

Park, K., Paulino, G. H., and Roesler, J. 2008. Determination of the kink point in the bilinear softening model for concrete. *Engineering Fracture Mechanics*, *75*, 3806-3818.

Perdikaris, P., and Calomino, A. 1987. Kinetics of crack growth in plain concrete. In S. Shah and S. Swartz, *SEM/RILEM international conference on fracture of concrete and rock* (pp. 64-69).

Pereira, E. N., Barros, J. A., Ribeiro, A. F., and Camões, A. 2004. Post-cracking behaviour of selfcompacting steel fibre reinforced concrete. *6th International RILEM Symposium on Fibre Reinforced Concrete - BEFIB 2004* (pp. 1-10). Varenna.

Petersson, P. 1981. Crack growth and development of fracture zone in plain concrete and similar materials. Lund.

Popper, K. 1959. *The Logic of Scientific Discovery*. Hutchinson and Co.

Popper, K. 1995. *The Open Universe: An Argument for Indeterminism. From the Postscript to The Logic of Scientific Discovery*. (W. Bartley) (p. 44). New York: Routledge.

RILEM. 2002. RILEM TC 162-TDF: Test and design methods for steel fibre reinforced concrete; bending test. *Materials and Structures*, *35*, 579-582.

RILEM. 2003. RILEM TC 162-TDF: 'Test and design methods for steel fibre reinforced concrete' σ-ε- design method. *Materials and Structures*, *36*, 560-567.

Rashid, Y. 1968. Analysis of prestressed concrete pressure vessels. *Nuclear engineering and design*, *7*(4), 334-335.

Reagel, F., and Willis, T. 1931. The effect of dimensions of test specimens on the flexural strength of concrete. *Public roads*, *12*, 37-46.

Redon, C., Li, V., Wu, C., Hoshiro, H., Saito, T., Ogawa, A. . 2001. Measuring and Modifying Interface Properties of PVA Fibers in ECC Matrix. *Journal of Materials in Civil Engineering*, *13*(6), 399.

Rocco, C., Guinea, G., Planas, J., and Elices, M. 1999. Mechanisms of rupture in splitting tests. *ACI Materials Journal*, *96*, 52-60.

Rocco, C., Guinea, G., Planas, J., and Elices, M. 1999. Size effect and boundary conditions in the Brazilian test: Experimental verification. *Materials and Structures*, *32*, 210-217.

Rocco, C., Guinea, G., Planas, J., and Elices, M. 1999. Size effect and boundary conditions in the Brazilian test: theoretical analysis. *Materials and Structures*, *32*, 437-444.

Rocco, C., Guinea, G., Planas, J., and Elices, M. 2001. Review of the splitting-test standards from a fracture mechanics point of view. *Cement and Concrete Research*, *31*(1), 73-82..

Roesler, J. 2006. Fatigue resistance of concrete pavements. In *6th international DUT - Workshop on fundamental modelling of design and performance of concrete pavements*. Belgium.

Roesler, J., Paulino, G. H., Park, K., and Gaedicke, C. 2007. Concrete fracture prediction using bilinear softening. *Cement and Concrete Composites*, *29*, 300-312.

Roesler, J., Paulino, G., Gaedicke, C., Bordelon, A., and Park, K. 2007. Fracture Behavior of Functionally Graded Concrete Materials for Rigid Pavements. *Transportation Research Record*, (2037), 40-49.

Rosselló, C., Elices, M., and Guinea, G. (2006). Fracture of model concrete: 2. Fracture energy and characteristic length. Cement and Concrete Research, 36, 1345-1353.

Roylance, D. 2001. Introduction to fracture mechanics. Massachusetts Institute of Technology, Cambridge.

Sain, T., and Chandrakishen, J. 2007. Residual fatigue strength assessment of concrete considering tension softening behavior. *International Journal of Fatigue*, *29*(12), 2138-2148.

Sain, T., and Chandrakishen, J. 2008. Probabilistic assessment of fatigue crack growth in concrete. *International Journal of Fatigue*, *30*(12), 2156-2164

Sancho, J., Planas, J., Cendón, D., Reyes, E., and Gálvez, J. (2007). An embedded crack model for finite element analysis of concrete. *Engineering Fracture Mechanics*, *74*, 75-86.

Schlangen, E., Prabowo, H., Sierra-Beltran, M., and Qian, Z. 2010. A model for building a design tool for ductile fibre reinforced materials. In G. Van Zijl and W. Boshoff (eds.), *Advanced cement based materials*. CRC Press.

Selezneva, O., Rao, C., Darter, M., Zollinger, D., and Khazanovich, L. 2004. Development of a mechanistic-empirical structural design procedure for continuously reinforced concrete pavements. *Transportation Research Record*, *1896*, 46-56.

Simo, J., Oliver, J., and Armero, F. 1993. An analysis of strong discontinuities induced by strain-softening in rate-independent inelastic solids. *Computational mechanics*, *12*(5), 227-296.

Slowik, V., Plizzari, G., and Saouma, V. 1996. Fracture of concrete under variable aplitude loading. *ACI Materials Journal*, *93*(3), 272-283.

Smith, E. 1995. A Comparison of the Jenq-Shah Two-Parameter Procedure and the Cohesive Zone Procedure for Predicting the Failure of Large Concrete Structures. *Advanced cement based materials*, *2*, 85-90.

Strauss, P.J., Slavik, M., and Perrie, B.D., 2001. A Mechanistically and risk based method for concrete pavements in Southern Africa. *Proceedings of the 7th International Conference on Concrete Pavements,* Orlando, Florida, USA.

Strauss, P.J., Slavik, M., Kannemeyer, L., and Perrie, B.D. 2007. Updating cncPave: inclusion of ultra thin continuously reinforced concrete pavement (UTCRCP) in the mechanistic, empirical and risk based concrete pavement design method. *Proceedings of the International Conference on Concrete Roads*. Midrand, South Africa.

Subramaniam, K., O'Neil, E., Popovics, J., and Shah, S. 2000. Crack propagation in flexural fatigue of concrete. *Journal of Engineering mechanics*, *126*(9), 891-898.

Subramaniam, K., Popovics, J., and Shah, S. 1998. Monitoring fatigue damage in concrete. *Testing concrete in torsion: Instability analysis and experiments*, *124*(11), 1258-1268.

Subramaniam, K., Popovics, J., and Shah, S. 1999. Fatigue behavior of concrete subjected to biaxial stresses in the C-T region. *ACI materials journal*, *96*(6), 663-669.

Tang, T. 1994. Effects of load-distributed width on split tension of unnotched and notched cylindrical specimens. *Journal of testing and Evaluation*, *22*(5), 401-409.

Tang, T., Shah, S., and Ouyang, C. 1992. Fracture mechanics and size effect of concrete in tension. *ASCE Journal of structural engineering*, *118*(11), 3169-3185.

Timoshenko, S., and Goodier, J. 1970. *Theory of Elasticity* (3rd editio.). McGraw-Hill Book Company.

Walker, S., and Bloem, D.L., 1957.Studies of flexural strength of concrete – part 3: effects of variations in test procedures. *ASTM Procedures. 57,* 1122-1139

Ward, R., and Li, V. 1991. Dependence of flexural behaviour of fibre reinforced mortar on material fracture and beam size. *Construction and Building Materials*, *5*(3), 151-161.

Westergaard, H. 1926. Stresses in concrete pavements computed by theoretical analysis. *Public roads*, *7*(2), 25-35.

Wright, P.J.F., and Garwood, F., 1952. The effect of the method of test on the flexural strength of concrete. *Magazine of concrete research, 11,* 67-76

Wu, R., Denneman, E., and Harvey, J. 2009. Evaluation of Embedded Discontinuity Method for Finite Element Analysis of Cracking of Hot-Mix Asphalt Concrete. *Transportation Research Record*, *2127*, 82-89.

Wöhler, A. 1870. Über die Festigkeitsversuche mit Eisen and Stahl. *Zeitschrift für Bauwesen*, (20), 73-106.

Yankelevsky, D., and Reinhardt, H. 1987. Uniaxial behaviour of concrete in cyclic tension. *ASCE Journal of structural engineering*, *115*(1), 166-182.

Yip, M., Li, Z., Liao, B., and Bolander, J. 2006. Irregular lattice models of fracthre of multiphase particulate materials. *International Journal of fracture*, *140*.

Yoder, E., and Witczak, M. 1975. *Principles of pavement design* (2nd.). John Wiley and Sons.

Zhang, J., and Li, V. 2004. Simulation of crack propagation in fiber-reinforced concrete by fracture mechanics. *Cement and Concrete Research*, *34*(2), 333-339.

Zhang, J., and Stang, H. 1998. Fatigue performance in flexure of fiber reinforced concrete. *ACI Materials journal*, *95*(1), 58-67.

Zhang, J., Stang, H., and Li, V. 1999. Fatigue life prediction of fiber reinforced concrete under flexural load. *International Journal of Fatigue*, *21*(10), 1033-1049.

APPENDIX A: FLEXURAL TEST RESULTS

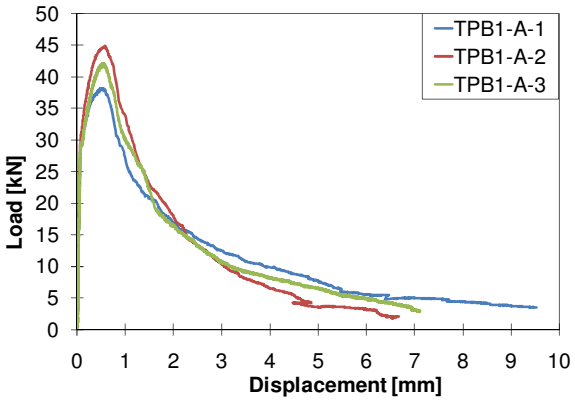

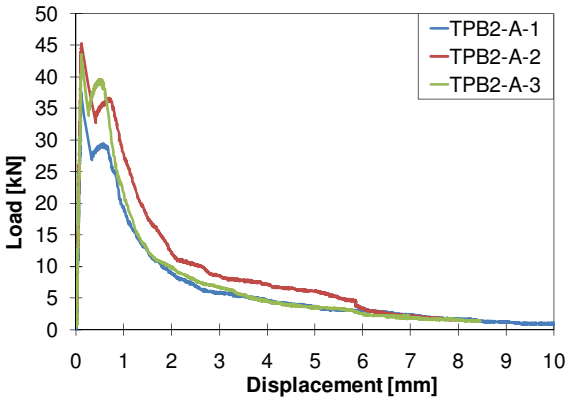

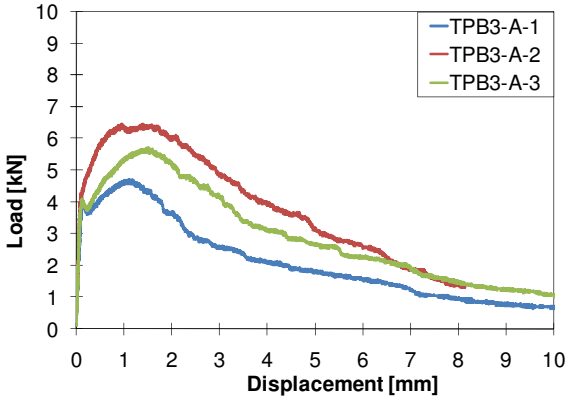

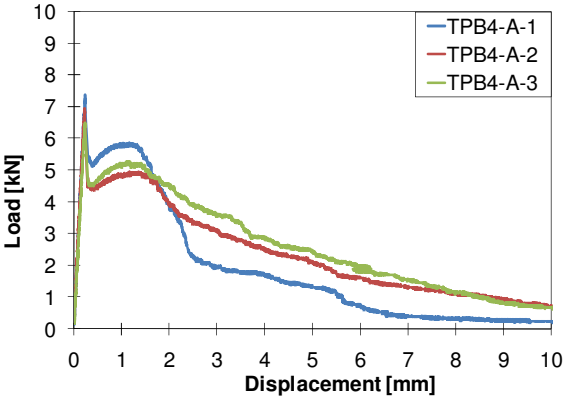

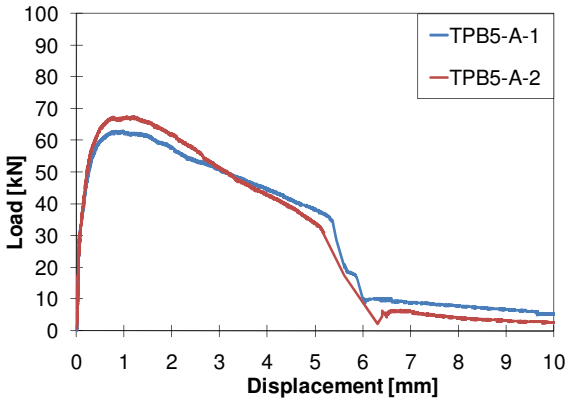

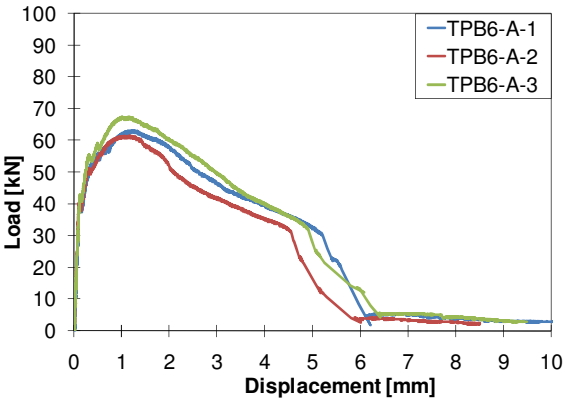

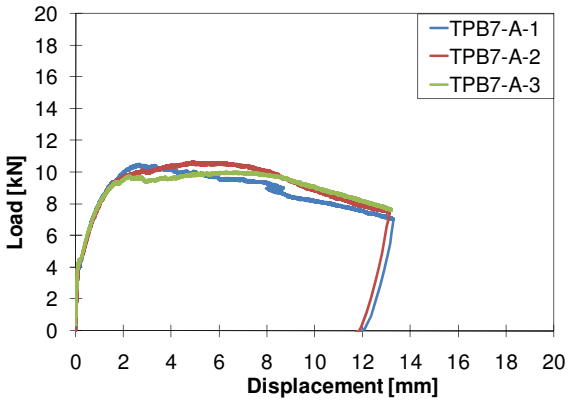

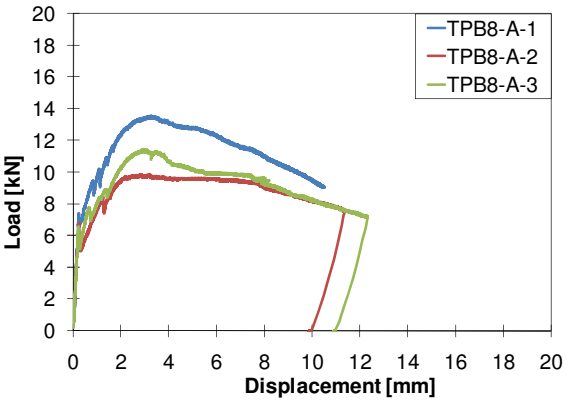

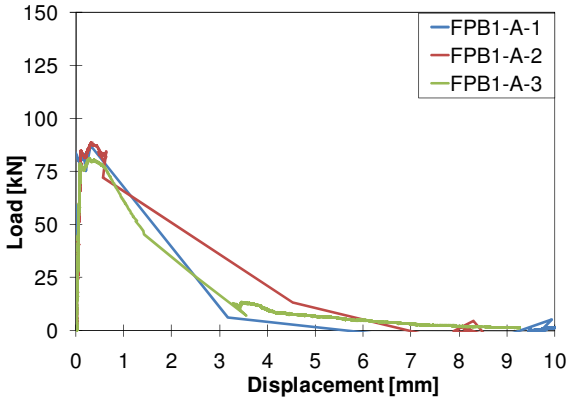
FPB1-A-1
FPB1-A-2
FPB1-A-3
Load [kN]
Displacement [mm]

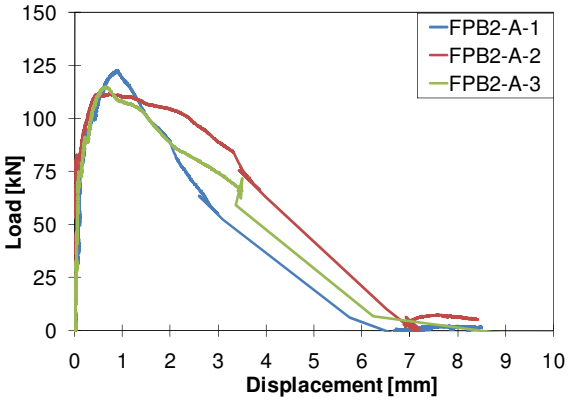
FPB2-A-1
FPB2-A-2
FPB2-A-3
Load [kN]
Displacement [mm]

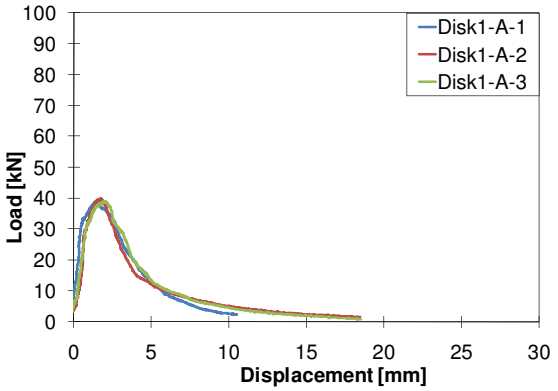
Disk1-A-1
Disk1-A-2
Disk1-A-3
Load [kN]
Displacement [mm]

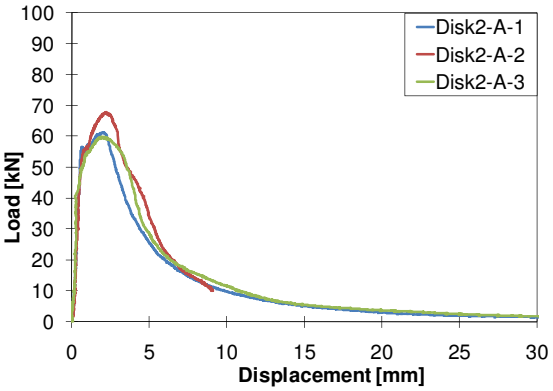
Disk2-A-1
Disk2-A-2
Disk2-A-3
Load [kN]
Displacement [mm]

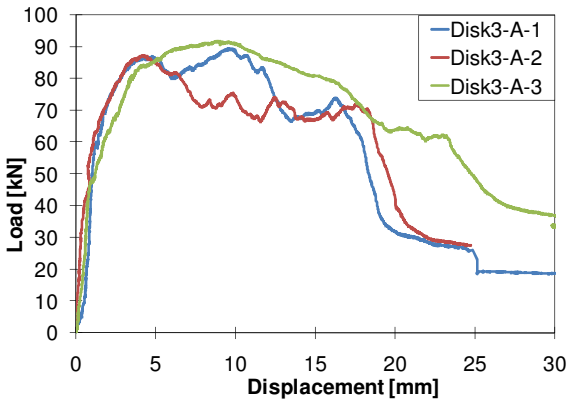
Disk3-A-1
Disk3-A-2
Disk3-A-3
Load [kN]
Displacement [mm]

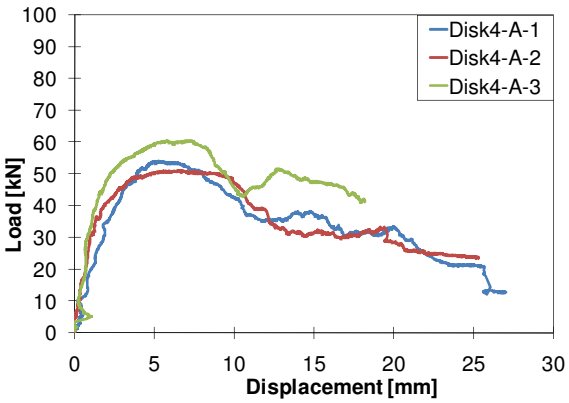
Disk4-A-1
Disk4-A-2
Disk4-A-3
Load [kN]
Displacement [mm]

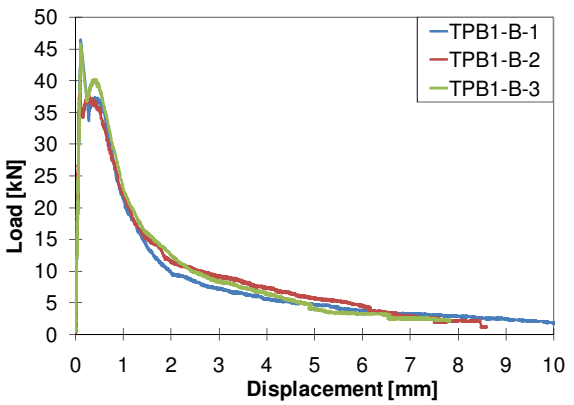
TPB1-B-1
TPB1-B-2
TPB1-B-3
Load [kN]
Displacement [mm]

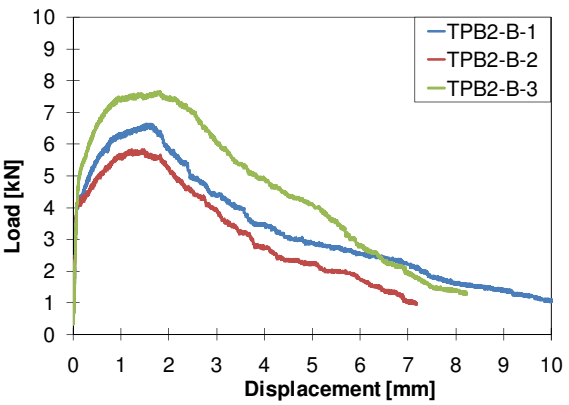
TPB2-B-1
TPB2-B-2
TPB2-B-3
Load [kN]
Displacement [mm]

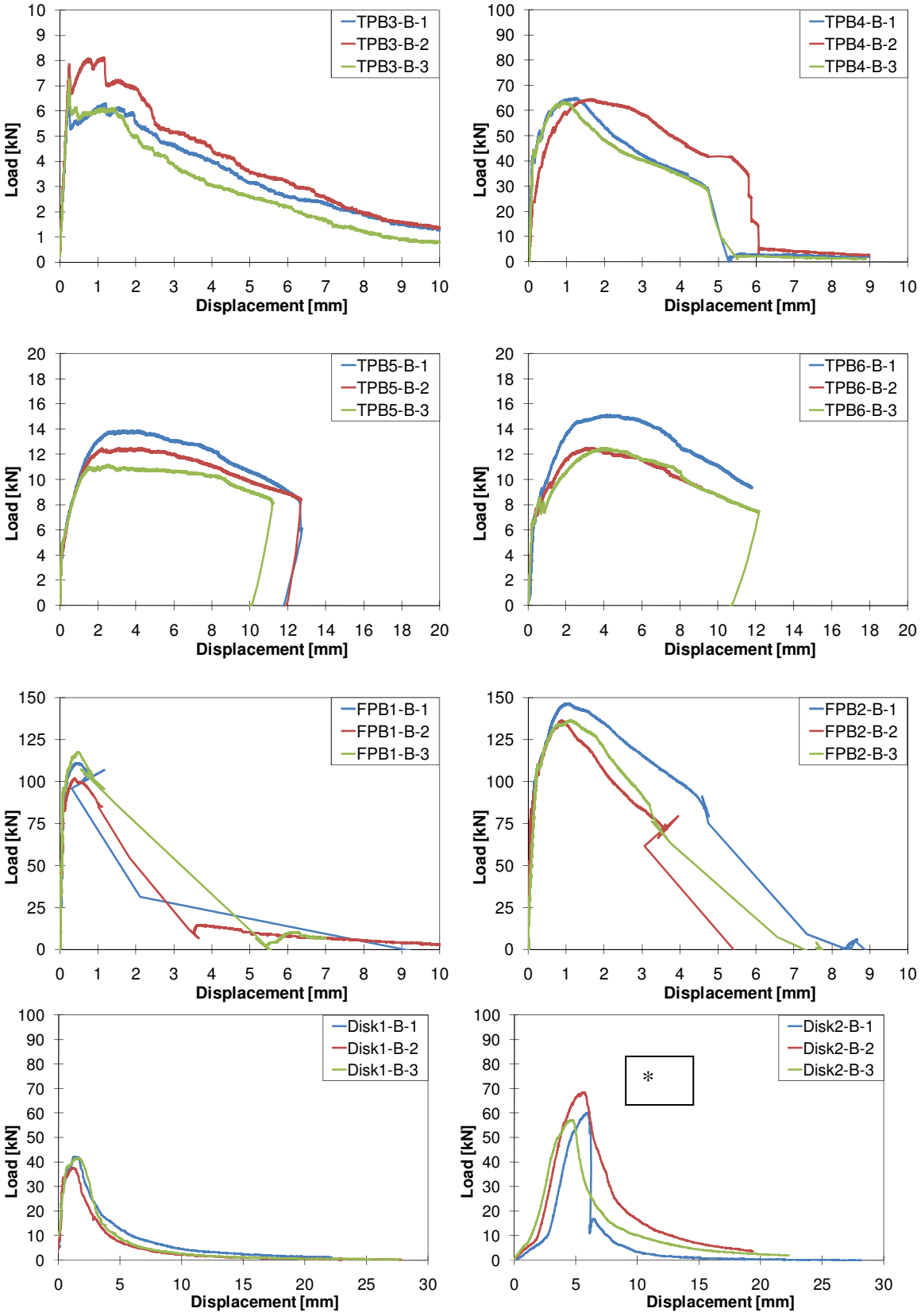

* The LVDT displacement recording malfunctioned during this set of disk tests. The results plotted are the actuator displacement vs .load. The actuator LVDT has limited accuracy, resulting in the aberrant load-displacement curves.

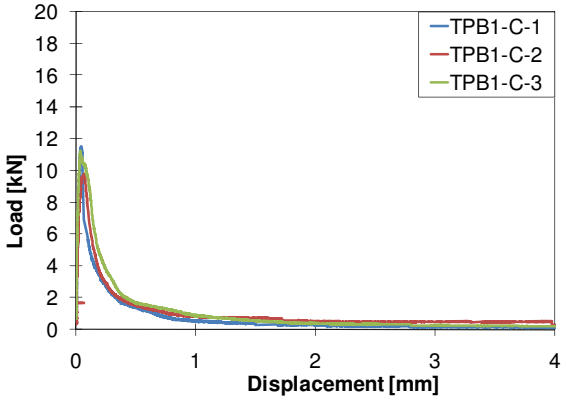
TPB1-C-1
TPB1-C-2
TPB1-C-3
Load [kN]
Displacement [mm]

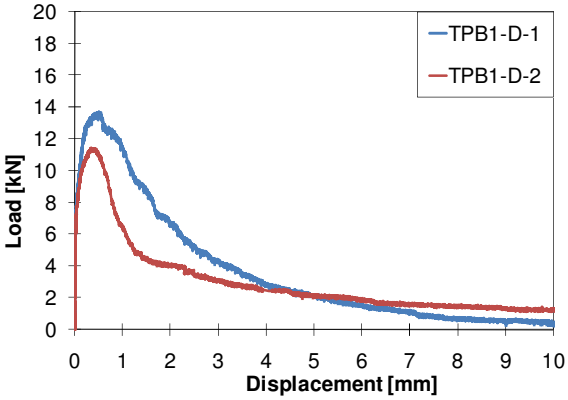
TPB1-D-1
TPB1-D-2
Load [kN]
Displacement [mm]

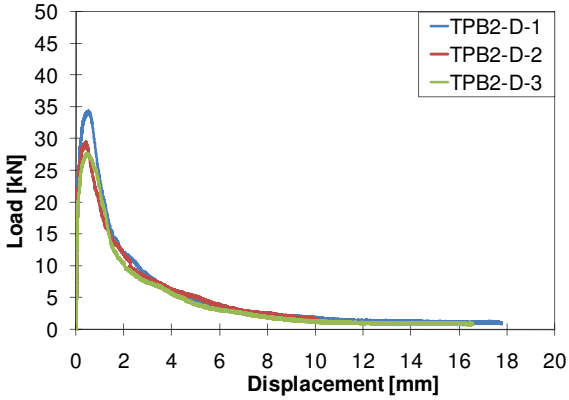
TPB2-D-1
TPB2-D-2
TPB2-D-3
Load [kN]
Displacement [mm]

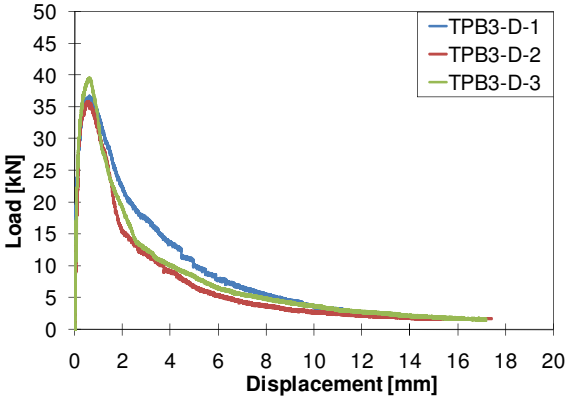
TPB3-D-1
TPB3-D-2
TPB3-D-3
Load [kN]
Displacement [mm]

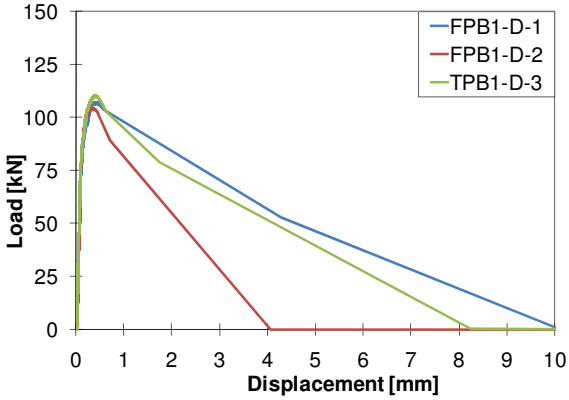
FPB1-D-1
FPB1-D-2
TPB1-D-3
Load [kN]
Displacement [mm]

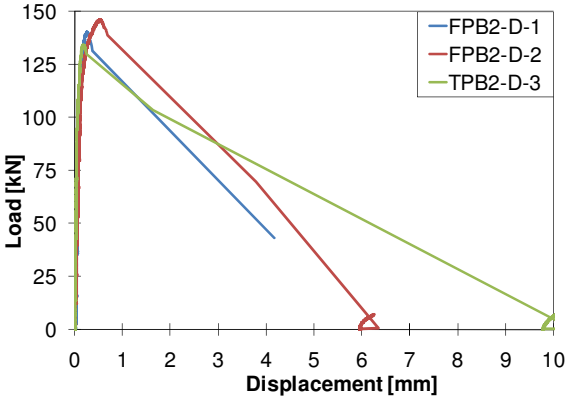
FPB2-D-1
FPB2-D-2
TPB2-D-3
Load [kN]
Displacement [mm]

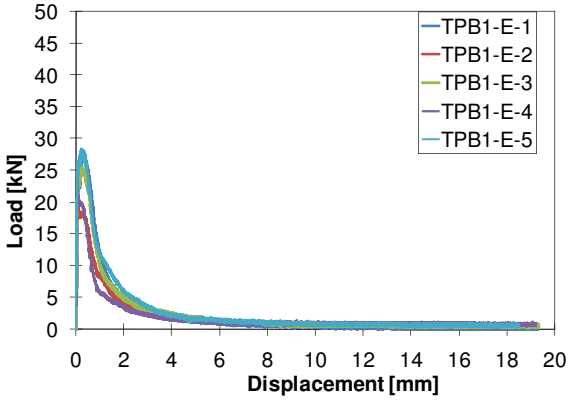
TPB1-E-1
TPB1-E-2
TPB1-E-3
TPB1-E-4
TPB1-E-5
Load [kN]
Displacement [mm]

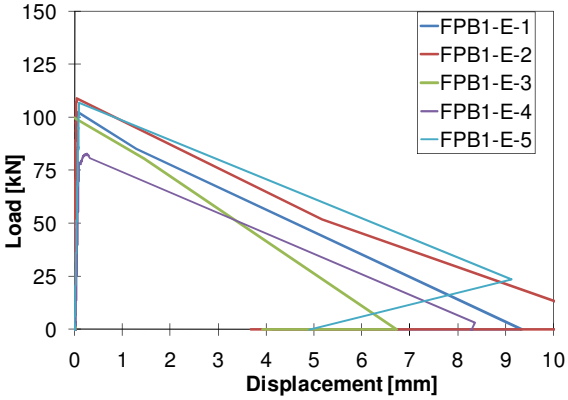
FPB1-E-1
FPB1-E-2
FPB1-E-3
FPB1-E-4
FPB1-E-5
Load [kN]
Displacement [mm]

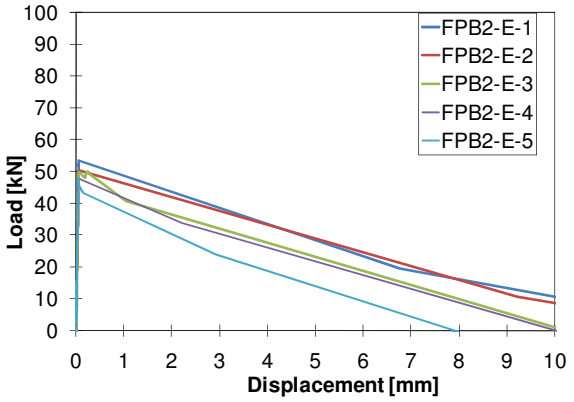

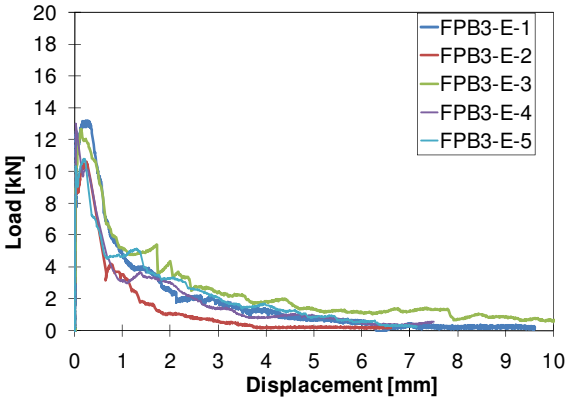

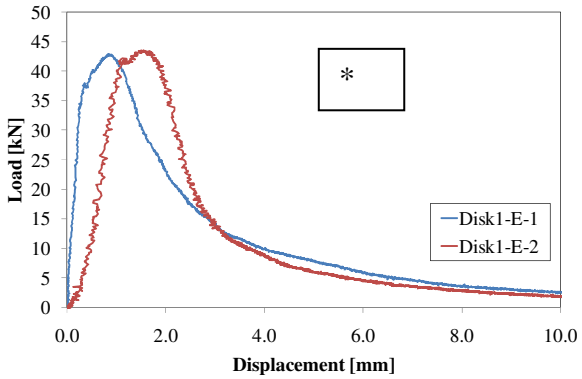

* The LVDT displacement recording malfunctioned during the test on specimen Disk1-E-2. The result plotted for this specimen is the actuator displacement vs .load. The actuator LVDT has limited accuracy, resulting in the aberrant load-displacement curve.

APPENDIX B: CYCLIC TEST RESULTS

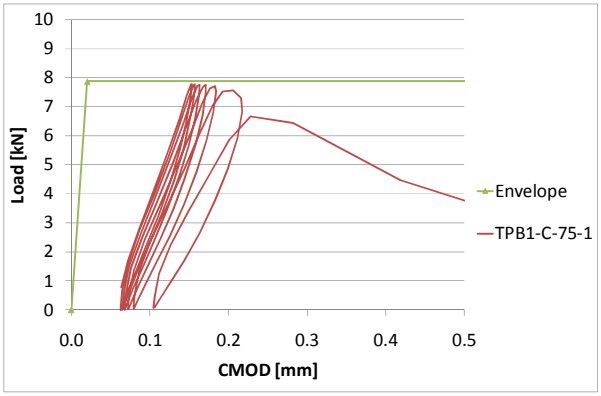

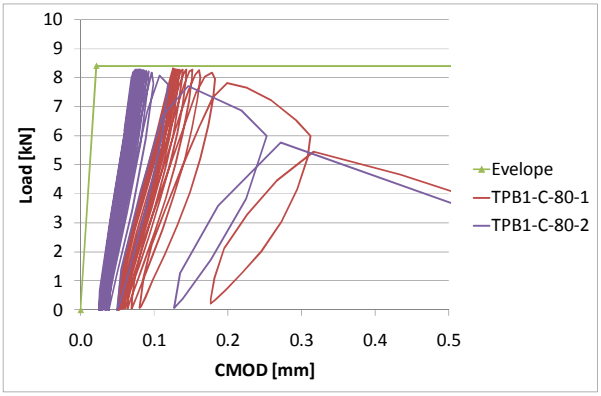

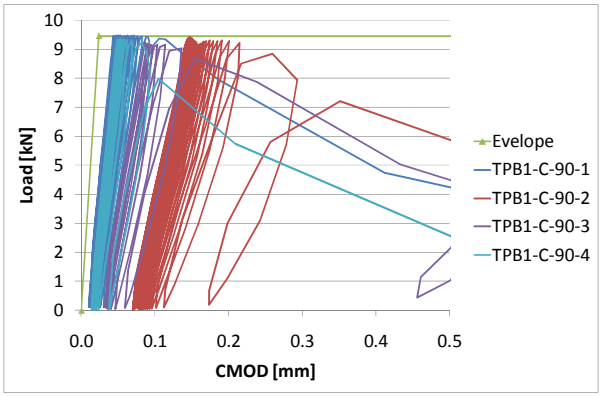

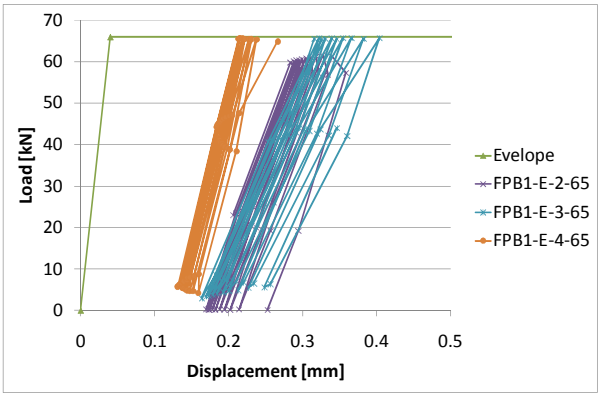

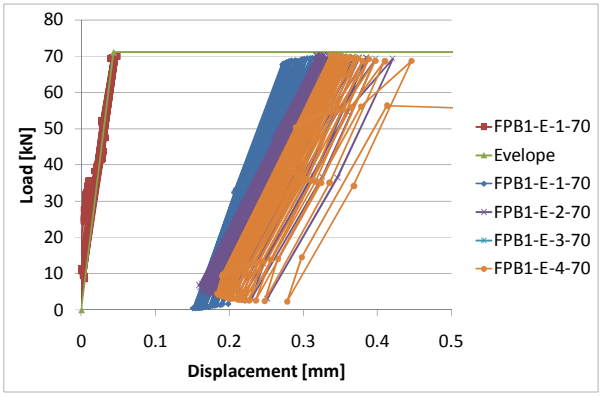

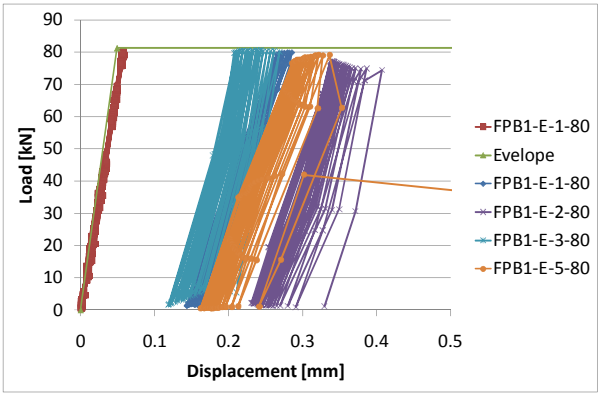

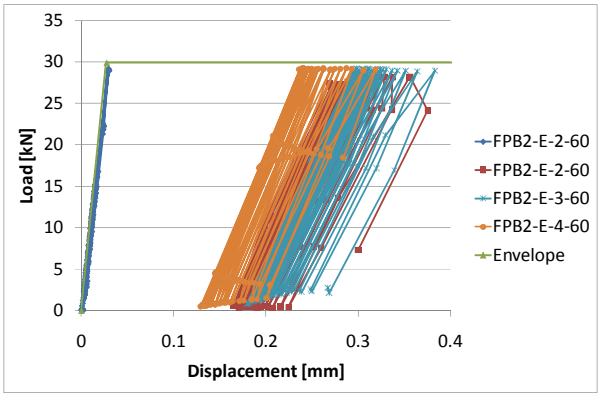

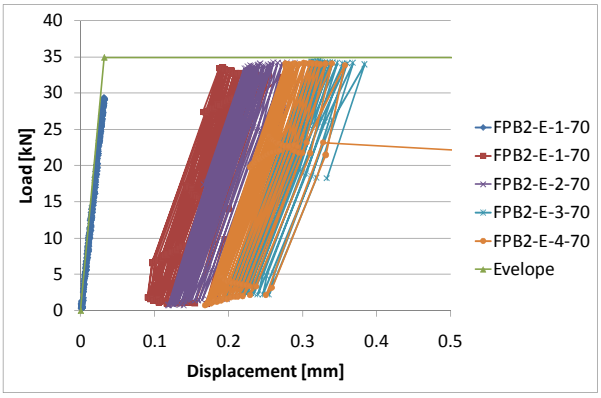

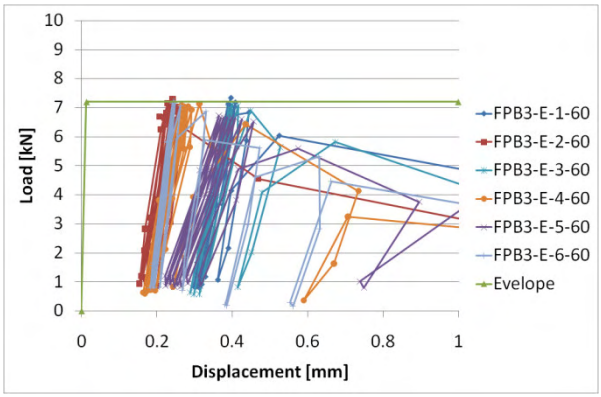
Load [kN]
Displacement [mm]
FPB3-E-1-60
FPB3-E-2-60
FPB3-E-3-60
FPB3-E-4-60
FPB3-E-5-60
FPB3-E-6-60
Evelope

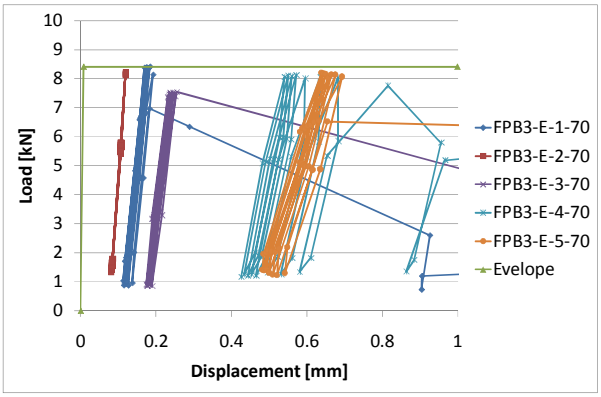
Load [kN]
Displacement [mm]
FPB3-E-1-70
FPB3-E-2-70
FPB3-E-3-70
FPB3-E-4-70
FPB3-E-5-70
Evelope

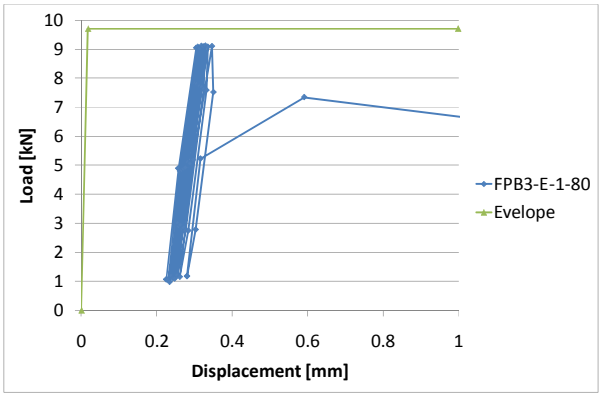
Load [kN]
Displacement [mm]
FPB3-E-1-80
Evelope

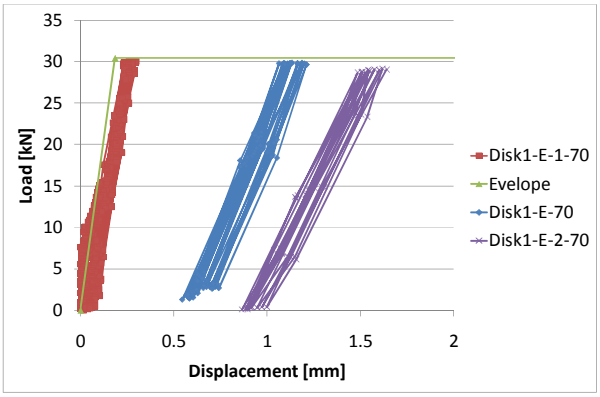
Load [kN]
Displacement [mm]
Disk1-E-1-70
Evelope
Disk1-E-70
Disk1-E-2-70

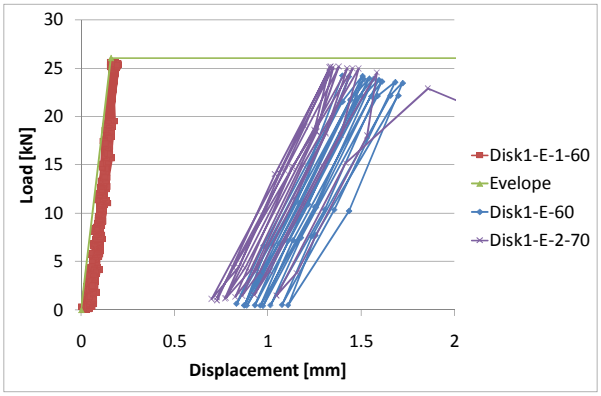
Load [kN]
Displacement [mm]
Disk1-E-1-60
Evelope
Disk1-E-60
Disk1-E-2-70

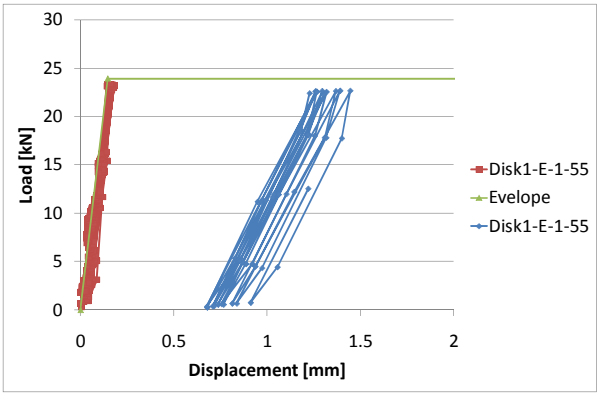
Load [kN]
Displacement [mm]
Disk1-E-1-55
Evelope
Disk1-E-1-55

APPENDIX C: EXPONENTIAL SOFTENING

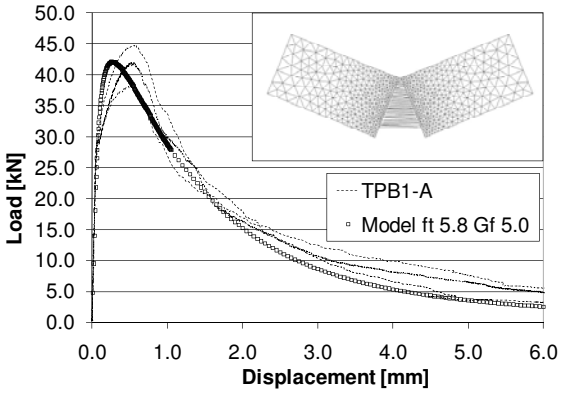

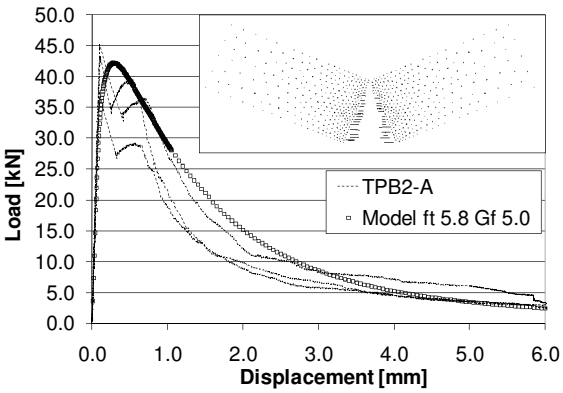

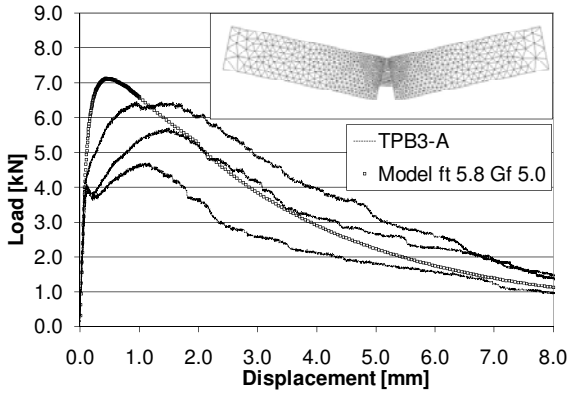

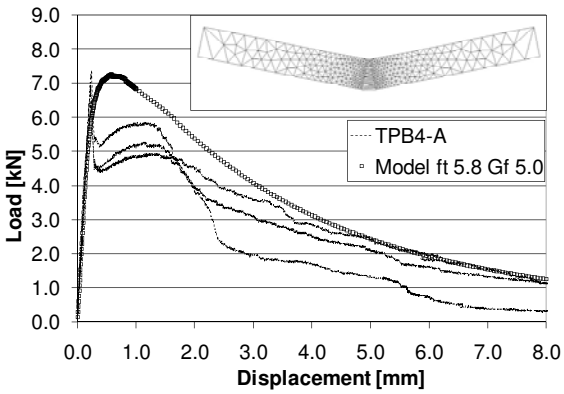

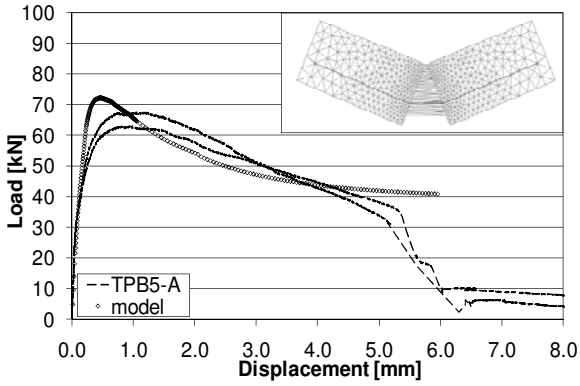

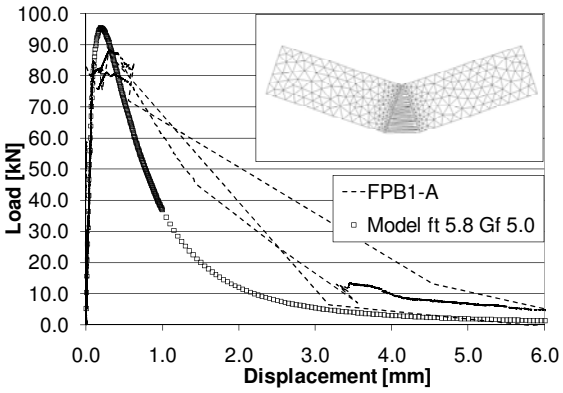

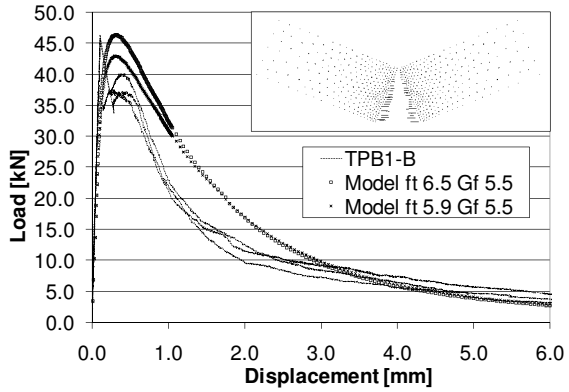

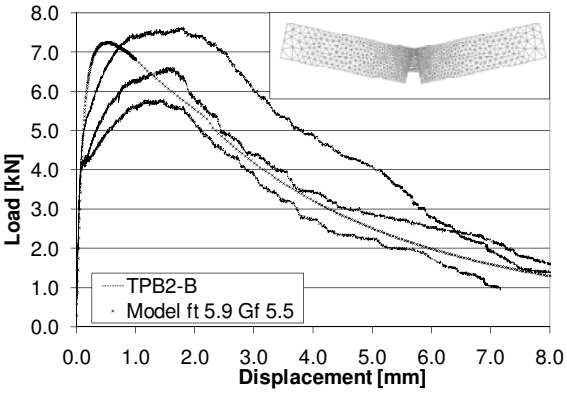

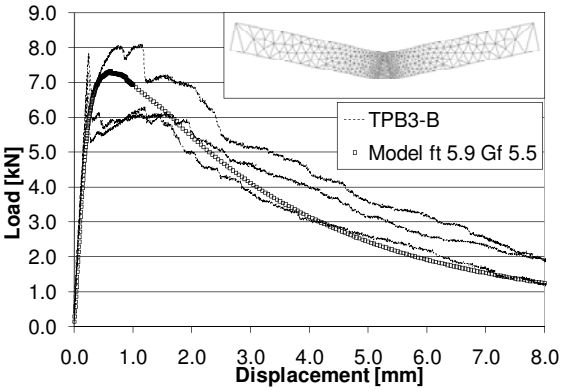
Load [kN]
Displacement [mm]
TPB3-B
Model ft 5.9 Gf 5.5

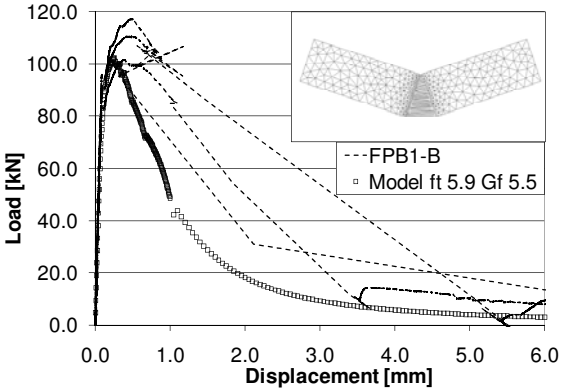
Load [kN]
Displacement [mm]
FPB1-B
Model ft 5.9 Gf 5.5

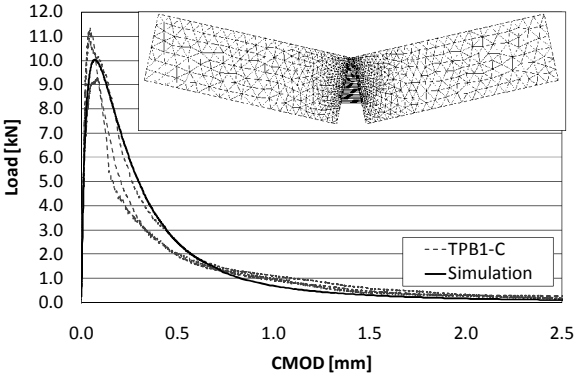
Load [kN]
CMOD [mm]
TPB1-C
Simulation

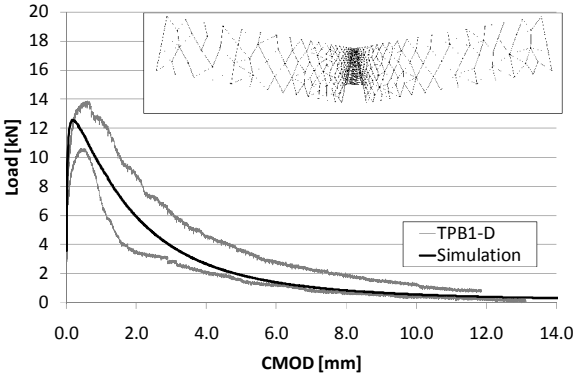
Load [kN]
CMOD [mm]
TPB1-D
Simulation

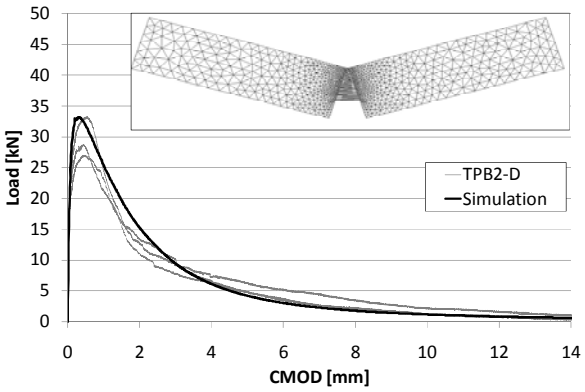
Load [kN]
CMOD [mm]
TPB2-D
Simulation

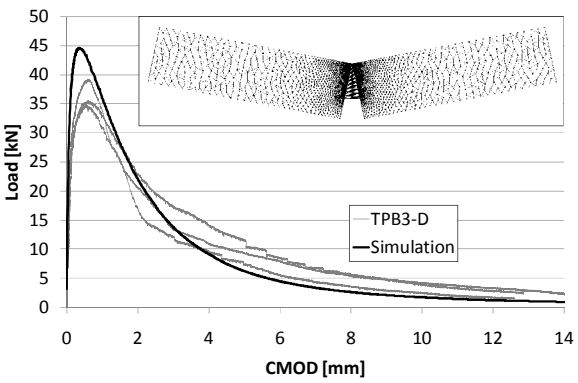
Load [kN]
CMOD [mm]
TPB3-D
Simulation

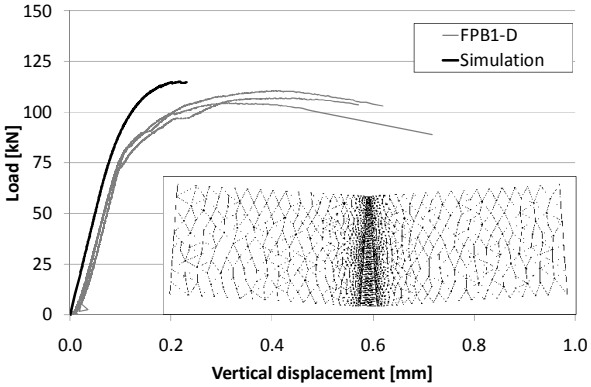
Load [kN]
Vertical displacement [mm]
FPB1-D
Simulation

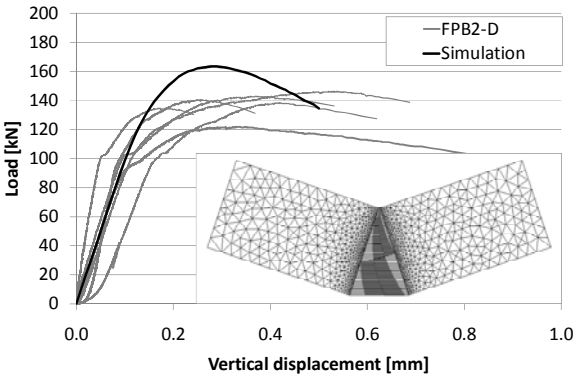
Load [kN]
Vertical displacement [mm]
FPB2-D
Simulation

APPENDIX D: SIMULATION USING CRACK TIP SINGULARITY

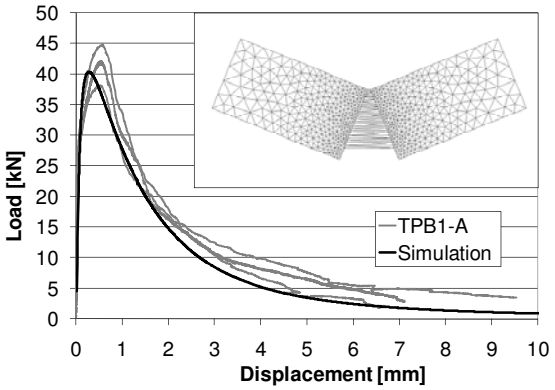

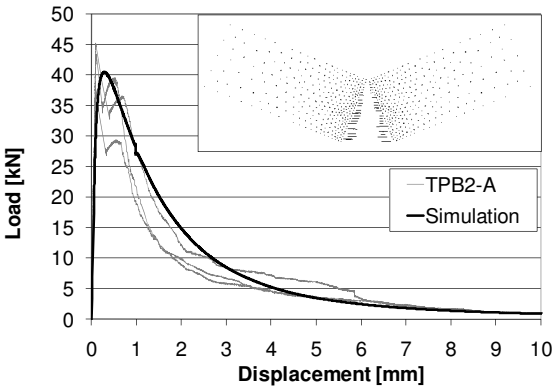

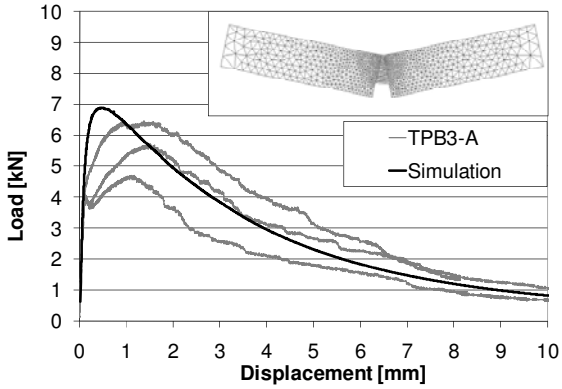

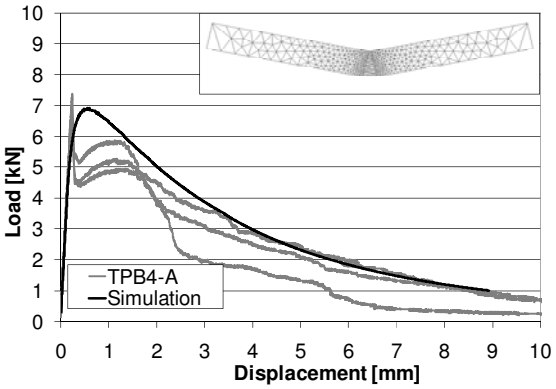

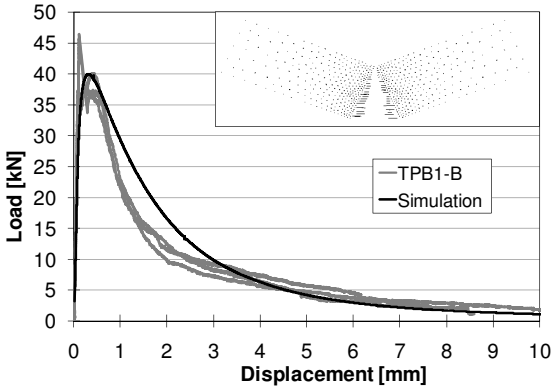

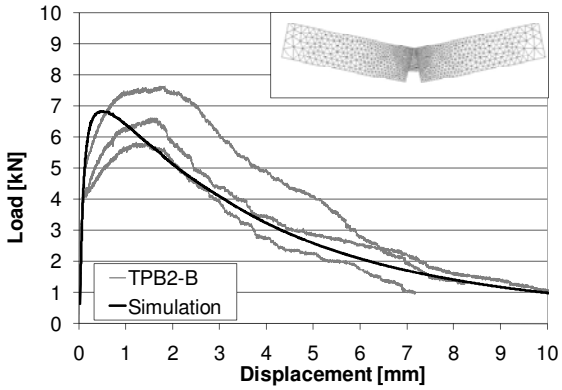

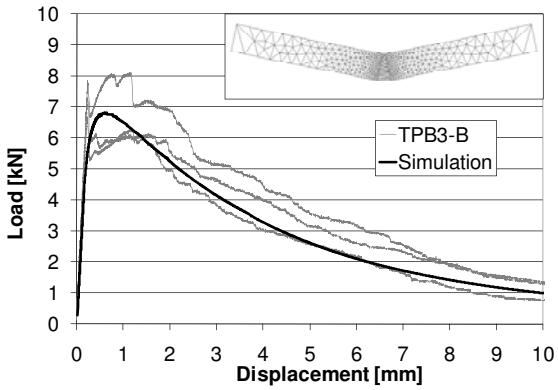

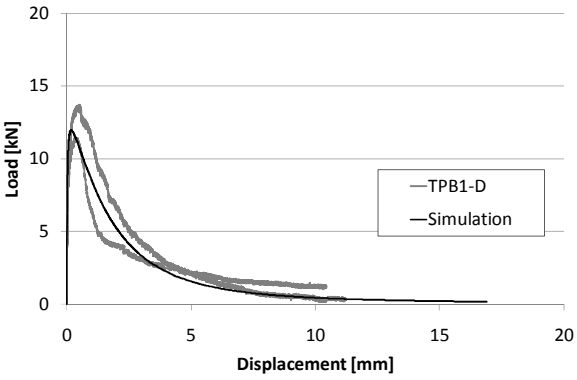

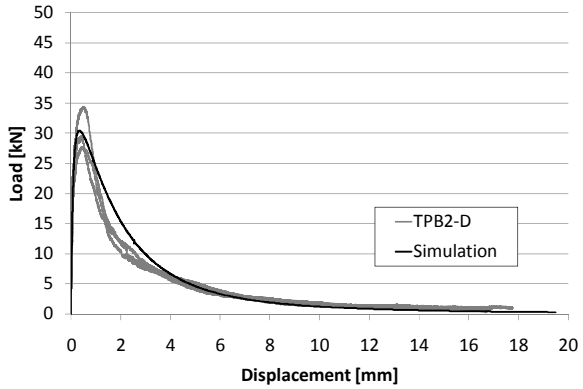
Load [kN]
Displacement [mm]
TPB2-D
Simulation

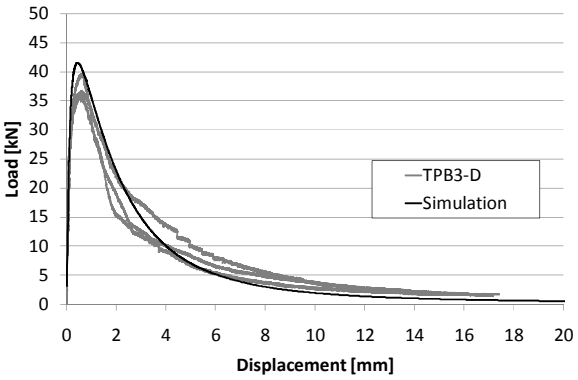
Load [kN]
Displacement [mm]
TPB3-D
Simulation

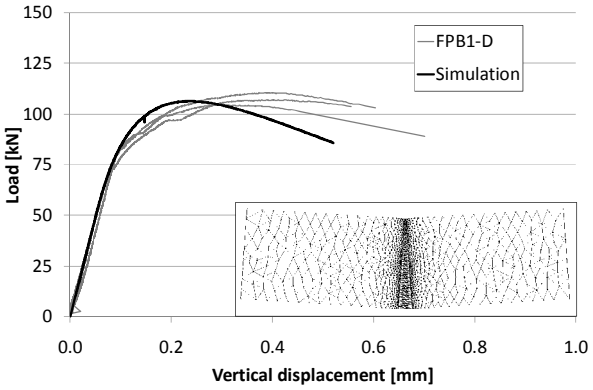
Load [kN]
Vertical displacement [mm]
FPB1-D
Simulation

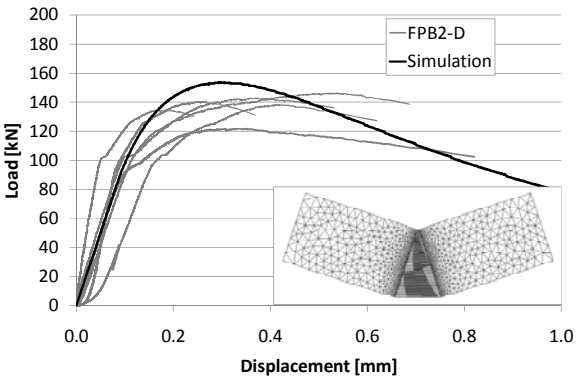
Load [kN]
Displacement [mm]
FPB2-D
Simulation

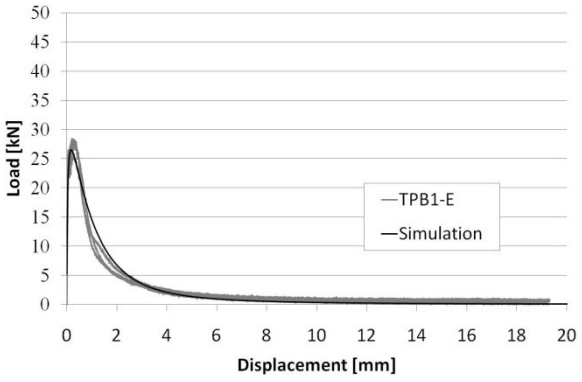
Load [kN]
Displacement [mm]
TPB1-E
Simulation

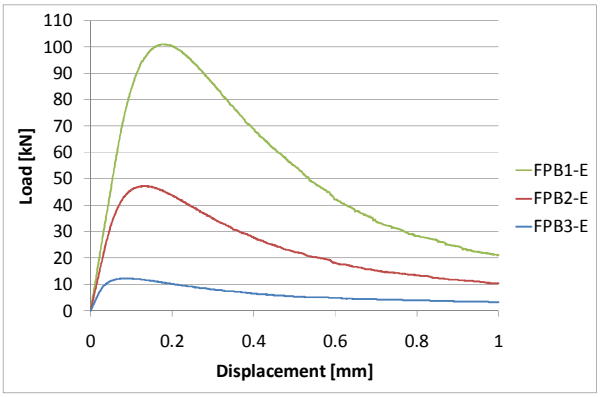
Load [kN]
Displacement [mm]
FPB1-E
FPB2-E
FPB3-E

APPENDIX E: SIMULATION OF FLEXURAL DISKS

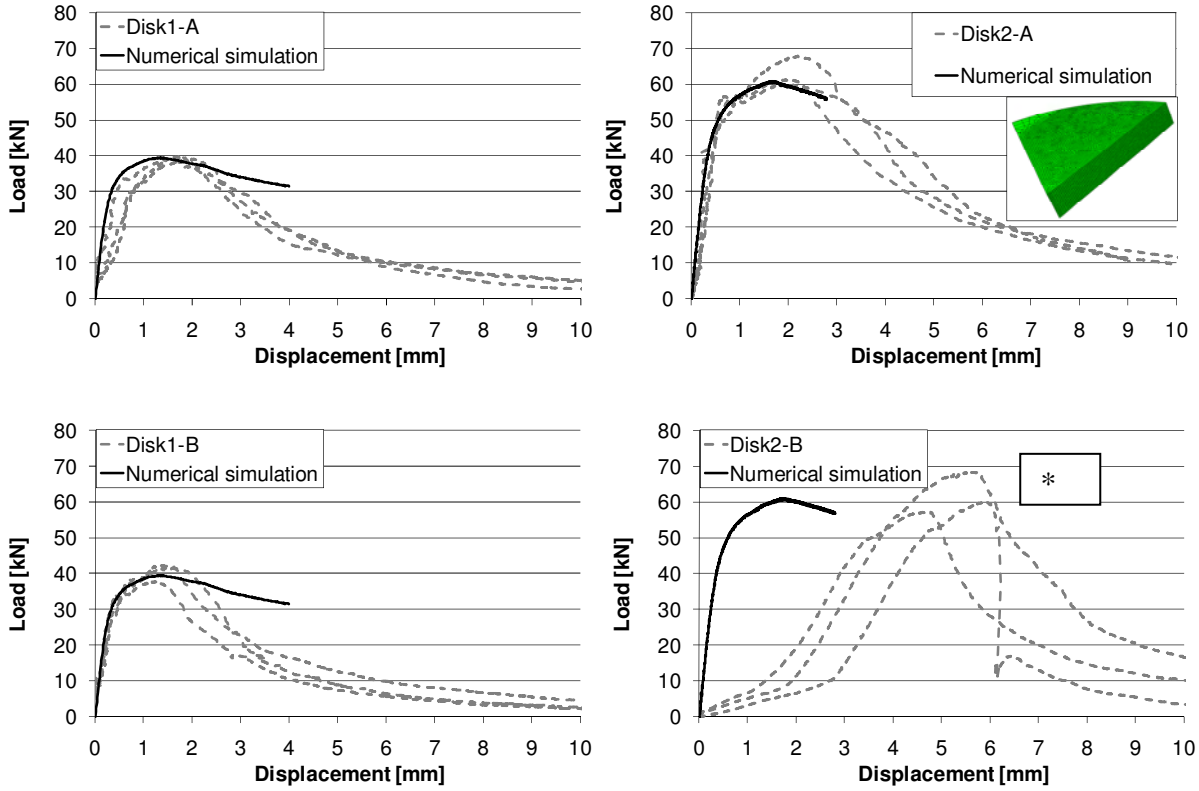

* The LVDT displacement recording malfunctioned during this set of disk tests. The results plotted are the actuator displacement vs .load. The actuator LVDT has limited accuracy, resulting in the aberrant load-displacement curves.